Geophys. J. Int. (2005) **162,** 79–114 doi: 10.1111/j.1365-246X.2005.02651.x

Geomagnetic field intensity during the last 5 Myr: LTD-DHT Shaw palaeointensities from volcanic rocks of the Society Islands, French Polynesia

Y. Yamamoto[1] and H. Tsunakawa[2]

[1]*Institute of Geology and Geoinformation, Geological Survey of Japan, AIST, Tsukuba* 305-8567, *Japan. E-mail: yuhji-yamamoto@aist.go.jp*
[2]*Department of Earth and Planetary Sciences, Tokyo Institute of Technology, Tokyo* 152-8551, *Japan*

Accepted 2005 March 24. Received 2005 February 25; in original form 2004 October 12

SUMMARY

On the basis of the Thellier palaeointensities reported so far it has been thought that the time-averaged virtual dipole moment (VDM) and virtual axial dipole moment (VADM) for the last few million years are almost the same as the present geomagnetic dipole moment ($\sim 8 \times 10^{22}$ A m^2). This estimate has been called into question, however, because recent studies have revealed that the Thellier method occasionally overestimates palaeointensities by as much as twice the true values. In contrast, a recently developed palaeointensity technique, namely the double heating technique of the Shaw method combined with low-temperature demagnetization (the LTD-DHT Shaw method), can yield expected field intensities from samples which give unreliable palaeointensities using the Thellier method. Therefore, we have measured absolute palaeointensities from 0.5–4.6 Ma volcanic rocks from the Society Islands, French Polynesia, mainly using the LTD-DHT Shaw method. As a result, 195 out of 361 samples passed the selection criteria, some of which are compared with additional results obtained with Coe's version of the Thellier method. In the Thellier experiments, 18 out of 40 samples passed the criteria, giving palaeointensities both consistent and inconsistent with the LTD-DHT Shaw results. These samples are characterized mostly by two-segmented Arai diagrams. If we take the LTD-DHT Shaw palaeointensities, 24 reliable site means are available and give a mean VADM of $(3.64 \pm 2.10) \times 10^{22}$ A m^2. This is nearly half of the mean of the 0–5 Ma Thellier data selected from the latest palaeointensity database [$(7.46 \pm 3.10) \times 10^{22}$ A m^2, $N = 458$] as well as the present dipole moment. The LTD-DHT Shaw palaeointensities newly determined in this study suggest that the present-day field is so strong that it may not be typical of the past geomagnetic field.

Key words: French Polynesia, LTD-DHT Shaw method, Palaeointensity, Society Islands, Thellier method.

1 INTRODUCTION

The main geomagnetic field has its origin in the Earth's outer core. Since a dipole component is dominant in the field, information about temporal changes, the average and the deviation of the moment is essential for understanding the evolution of the Earth's deep interior. If we can obtain these values, the long-term evolution of the outer core can be evaluated as well as its current activity. For the period of the last 5 Myr McFadden & McElhinny (1982) estimated a time-averaged virtual dipole moment (VDM) of $(8.67 \pm 3.63) \times 10^{22}$ A m^2, which is almost the same as the present geomagnetic dipole moment ($\sim 8 \times 10^{22}$ A m^2). This conclusion was not greatly changed in a later analysis of a mean VDM of $(7.84 \pm 3.80) \times 10^{22}$ A m^2 for the last 10 Myr by Tanaka *et al.* (1995b) using an updated database (Tanaka & Kono 1994).

However, that database involved a number of palaeointensities obtained by methods other than the Thellier method (Thellier & Thellier 1959). Since many palaeomagnetists regard the Thellier method as the only reliable one (e.g. Selkin & Tauxe 2000; Goguitchaichvili *et al.* 2004), Juarez & Tauxe (2000) questioned the quality of the database. They carefully examined a further updated database (Perrin *et al.* 1998) applying more stringent selection criteria and rejecting data other than the Thellier palaeointensities. Adding their new Thellier palaeointensities from submarine basaltic glasses, they determined the time-averaged virtual axial dipole moment (VADM) for 0.3–5 Ma to be $(5.49 \pm 2.36) \times 10^{22}$ A m^2. This is lower than the both previous values (McFadden & McElhinny 1982; Tanaka *et al.* 1995b) and the present dipole moment.

Since the work of Juarez & Tauxe (2000), a number of researchers have been making efforts to increase the number of absolute palaeointensity data. The latest palaeointensity database (Perrin & Schnepp 2004) contains 3128 items from 215 references. The number of data has almost tripled compared with the 1995 database (1123 items from 83 original papers in Tanaka *et al.* 1995b). Contrary to the conclusion by Juarez & Tauxe (2000), the majority of new measurements by the Thellier method showed high palaeointensities. For example, Laj *et al.* (2000) reported 89 Thellier results from 2.1–3.9 Ma lavas in Oahu, Hawaii, obtaining an average VADM of $(7.0 \pm 2.3) \times 10^{22}$ A m^2. Bogue (2001) gave an average VDM of $(9.38 \pm 2.43) \times 10^{22}$ A m^2 from 25 site mean palaeointensities of 4 Ma lava flows from Kauai, Hawaii. Alva-Valdivia *et al.* (2001) reported palaeointensities from four lava flows erupted between 0.8 and 2.2 Ma in Mexico and the resultant VDMs ranged from 6.4 to 9.1×10^{22} A m^2. Recent statistical analyses by Heller *et al.* (2002) on their own Thellier palaeointensity database revealed that the average VDM for the last 5 Myr resulted in $\sim 8 \times 10^{22}$ A m^2 (Fig. 6 of Heller *et al.* 2002). A comprehensive review by Valet (2003) also concluded the mean VADM for the past 4 Myr volcanic Thellier–Thellier records was $(7 \pm 3.6) \times 10^{22}$ A m^2. These conclusions have been supported by Leonhardt *et al.* (2003). They obtained 42 new Thellier data from 1.8–3.3 Ma Brazilian volcanic rocks that resulted in VADM of $(7.5 \pm 2.6) \times 10^{22}$ A m^2 ($N = 10$). The Thellier method still seems to yield high palaeointensities.

It is possible to say that these high palaeointensities are misreadings of the ancient geomagnetic field, because recent studies have pointed out that the Thellier method occasionally fails in accurate determination of palaeointensity from historical lavas. Biggin & Thomas (2003a) demonstrated that the usual selection criteria of the Thellier method (e.g. $N \geq 4$, $q \geq 5$, where N is the number of data points and q the quality factor of Coe *et al.* 1978) could not discriminate incorrect palaeointensities. Yamamoto *et al.* (2003) showed that the Kilauea 1960 lava in Hawaii yielded systematically higher Thellier palaeointensities (up to twice the expected value). Such bad results have also been reported in conventional Thellier experiments (Tanaka & Kono 1991) and in modern microwave Thellier experiments (Hill & Shaw 2000). In a study of the Kilauea 1970 lava (Oishi *et al.* 2005), two out of seven successful results using the Thellier method showed 46 and 55 per cent higher field intensities than the expected. Anomalous palaeointensities have not been restricted to the Hawaiian lavas. Calvo *et al.* (2002) obtained 25 per cent larger mean intensities from 1910 and 1928 Mount Etna lavas, Italy. From the Oshima 1986 lava in Japan, Mochizuki *et al.* (2004) observed palaeointensities exceeding the expected value by up to about 30 per cent. Although the exact value of the expected intensity is unknown, Böhnel *et al.* (2003) performed both conventional Thellier and microwave Thellier experiments on the AD 330 Xitle lava samples from Mexico, resulting in high palaeointensities up to ~175 and ~155 per cent of the contemporaneous global mean of Yang *et al.* (2000), respectively.

Samples with an intermediate degree of deuteric oxidization have generally been considered to be very suitable for palaeointensity measurements because of their good thermal stability. However, Yamamoto *et al.* (2003), Mochizuki *et al.* (2004) and Oishi *et al.* (2005) showed that samples with an intermediate degree of high-temperature oxidation of titanomagnetites in particular would yield high palaeointensities by the Thellier method. On the other hand, the double heating technique (DHT) of the Shaw method combined with low-temperature demagnetization (LTD) (LTD-DHT Shaw method; Tsunakawa *et al.* 1997; Yamamoto *et al.* 2003) could give correct answers for samples with various degrees of oxidation. By this method, Yamamoto *et al.* (2003), Mochizuki *et al.* (2004) and Oishi *et al.* (2005) obtained averaged palaeointensities of 35.7 ± 3.3 μT ($N = 7$), 46.4 ± 4.7 μT ($N = 6$) and 38.2 ± 2.8 μT ($N = 11$) from the Kilauea 1960, Oshima 1986 and Kilauea 1970 lavas, respectively. They agreed with the expected values (36.2, 45.5 and 35.8 μT) and were better than the Thellier averages of 49.0 ± 9.6 μT ($N = 17$), 51.0 ± 4.1 μT ($N = 15$) and 43.2 ± 8.4 μT ($N = 7$), respectively.

In this paper we retrieve the geomagnetic dipole moments over the last 5 Myr from volcanic rocks of the Society Islands, French Polynesia, to study the palaeosecular variations (PSV). Most of the palaeointensity measurements were done using the LTD-DHT Shaw method. Although there are several variants of the Thellier-type method, Coe's version of the Thellier method (Coe 1967) was additionally applied to selected samples with good thermal stability aimed at a comparison with traditional palaeointensity databases. With careful experiments and analyses we have obtained reliable palaeointensities. We will discuss the VADM variation for the last 5 Myr, especially its average in comparison with the previous ones.

2 SAMPLES AND PREVIOUS PALAEOMAGNETIC STUDIES

The Society Islands consist of 10 volcanic islands and several seamounts. They are of hotspot origin and show a chain-like configuration in a northwest–southeast direction delineating the motion of the Pacific Plate. The present hotspot is located at 18°S, 148°W in the southeastern end of the archipelago (Gripp & Gordon 1990), where several active submarine volcanoes are found. The basaltic volcanism initiated at about 5 Ma (Duncan & McDougall 1976). For these islands, geology, geochemistry and geochronology have been studied by many authors (e.g. Dymond 1975; Duncan & McDougall 1976; Diraison 1991; Duncan *et al.* 1994; Kogiso *et al.* 1997; Blais *et al.* 1997, 2000; Guillou *et al.* 1998; Singer *et al.* 1999). Also about 200 data items on palaeomagnetic direction have been reported (Duncan 1975; Chauvin *et al.* 1990; Roperch & Duncan 1990; White & Duncan 1996).

Regarding palaeointensities, Senanayake *et al.* (1982) obtained 12 Shaw and 18 Thellier data from the Borabora, Raiatea and Tahiti islands. However, the quality of these data is considered to be insufficient because they used a single heating Shaw method and a Thellier method without a check for partial thermoremanent magnetization (pTRM). Roperch & Duncan (1990) applied the Thellier method to 26 samples from Huahine Island but no satisfactory results were obtained. Only Chauvin *et al.* (1990) reported successful Thellier results. Twenty-six out of 48 specimens gave 11 distinct site-mean palaeointensities. Three of them [37.7 ± 1.6 μT ($N = 2$), 27.9 ± 0.8 μT ($N = 2$) and 54.3 μT ($N = 1$)] are from reversely magnetized flows while the others (2.6 ± 0.1 μT to 8.1 ± 1.0 μT) were from samples with intermediate palaeodirections. The main interest of Chauvin *et al.* (1990) was in the transitional geomagnetic field, and thus they did not discuss the long-term variation in the geomagnetic dipole moment from the Society volcanic rocks.

Yamamoto *et al.* (2002) recently reported 130 new palaeomagnetic direction data from seven of the Society Islands: Maupiti, Borabora, Tahaa, Raiatea, Huahine, Moorea and Tahiti. Uto *et al.* (submitted) have measured 52 K–Ar ages for those samples. As some sites suffered from secondary magnetizations, both palaeodirections and K–Ar ages were determined for 46 independent sites. These ages are 4.52–4.61 Ma for Maupiti, 3.21–4.01 Ma for Borabora, 2.57–3.24 Ma for Tahaa, 2.45–2.76 Ma for Raiatea, 2.52–3.19 Ma for Huahine, 1.50–1.62 Ma for Moorea and 0.51–1.12 Ma for Tahiti, ranging between 0.51 and 4.61 Ma. The present palaeointensity measurements have been performed mainly on samples from

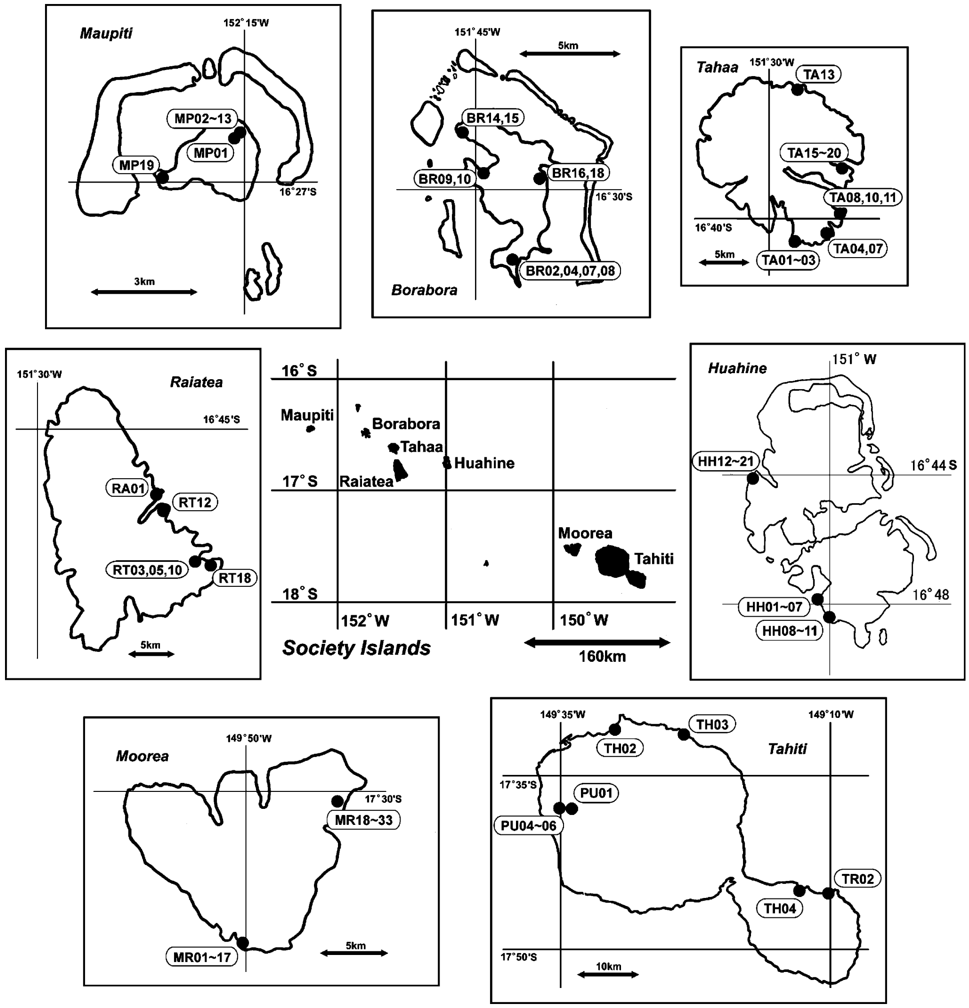

Figure 1. Map showing the sampling sites.

these sites. The studied samples were collected mostly by a portable engine drill. Orientations were made by a magnetic and/or a sun compass (Yamamoto *et al.* 2002). The site localities are illustrated in Fig. 1.

3 ROCK MAGNETIC PROPERTIES

3.1 Thermomagnetic properties

Thermomagnetic analyses were performed on 53 selected samples using a vibrating sample magnetometer (MicroMag 3900 VSM, Princeton Measurement Corporation). The measurements were done in a helium gas flow with a 500 mT DC field. The resultant M_s–T curves could be classified into six types: A, B, C, D, E or F (Fig. 2). Except for type E, they are interpreted as magnetization by titanomagnetites with different Ti contents. All the results are listed in Tables 1 and 2. Curie temperatures (T_c) were evaluated by the so-called 'intersecting tangents method' (Grommé *et al.* 1969).

Type A curves were observed in 21 samples. They show a single phase of Ti-poor titanomagnetite with good reversibility during the heating and cooling cycle, usually resulting in T_c higher than 500 °C. Type B curves were recognized in 12 samples and resembled type A, though a minor phase of Ti-rich titanomagnetite with T_c of 100–400 °C was superimposed. Type C curves were seen in two samples, showing two components of Ti-poor ($T_c \sim 560$ °C) and Ti-rich ($T_c \sim 200$ °C) phases. Type D curves, from five samples, are characterized by a single phase of titanomagnetite with moderate Ti content, the T_c of which ranges between 140 and 260 °C. They show the some amount of increase in the saturation magnetization (M_s) in the cooling stage.

Type E curves are irreversible thermomagnetic curves found in nine samples. They show relatively low-T_c components followed by a small bump of high-T_c ones in the heating curves. Since the high T_cs ranged from 530 to 580 °C, some amount of titanomaghemite might be initially produced by low-temperature oxidation and transformed into Ti-poor titanomagnetites during the laboratory measurements.

Type F curves were found in four samples. They have the weakest magnetization, and some superparamagnetic behaviour is recognized as a relatively large offset in M_s/M_{s0}.

3.2 Low-temperature magnetometry

Low-temperature magnetometry was performed on 45 samples with a low-temperature SQUID susceptometer (Quantum Design MPMS-XL5). Saturation isothermal remanent magnetization (SIRM) was imparted to samples under a 2.5 T field at 300 K, and then their remanences were continuously measured in a nearly zero

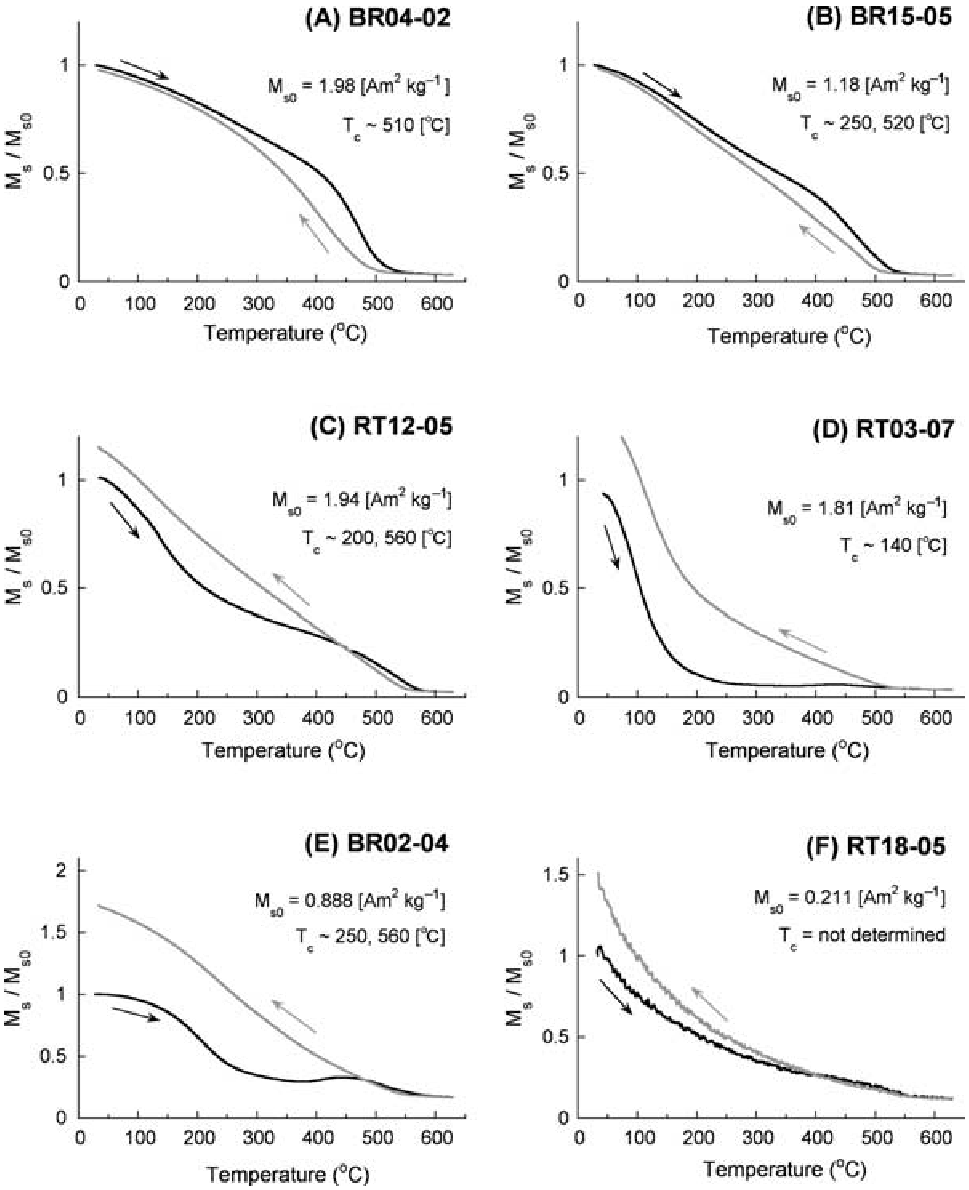

Figure 2. Six types of thermomagnetic curves (black, heating; grey, cooling). All measurements are performed in a helium gas flow with a DC field of 500 mT.

field by cycling temperatures between 300 and 6 K, sometimes 2 K. For 36 of the samples, sister chip samples were subjected to thermomagnetic analyses as described in the previous subsection. The results are grouped into five types: 26 results for Type a, two results for Type b, 13 results for Type c, two results for Type d and also two results for Type e, as shown in Fig. 3. The categorized groups are listed in Tables 1 and 2.

Type a is characterized by loss and partial recovery of SIRM around 100–120 K, implying a presence of nearly Ti-free titanomagnetite because magnetite shows the isotropic point (T_{I}) around 130 K and the Verwey transition temperature (T_{V}) around 120 K (Dunlop & Özdemir 1997). A similar curve is often observed in marine sediments (e.g. Yamazaki *et al.* 2003). Type b also shows the loss and partial recovery in SIRM, but there is a kink around 250 K which can be recognized as a discontinuity in the derivative curves (dotted lines in Fig. 3). Since the Morin transition temperature (T_{M}) of haematite is around 260 K and it is lowered by Ti substitution (Dunlop & Özdemir 1997), and haematite particles of ≤ 0.1 μm in size never show the transition (Bando *et al.* 1965), the present observation suggests the existence of a large amount of haematite associated with a small amount of Ti substitution. As a matter of fact, the corresponding two samples are reddish and contain a lot of heavily deuteric-oxidized olivine phenocrysts which are red in colour. The two Types a and b are yielded from samples with M_{s}–T curves of Types A and B, respectively, indicating consistent magnetic properties between low- and high-temperature magnetometry.

Types c, d and e show a common feature: a continuous decrease of the remanence at temperatures lower than 220 K in the cooling cycle, followed by a consecutive increase in the heating cycle. In Types d and e the curves are almost reversible and there is an additional kink around 220 K in Type e. Since all of them are observed from the samples with M_{s}–T curves of Types C, D, E and F, these low-temperature properties may originate from Ti-rich titanomagnetite phases.

Table 1. Experimental results from the LTD-DHT Shaw method for dykes and single lavas.

Sample ID	HT	LT	NRM_0	$ARM0_0$	B_{rc}/B_c	M_{rs}/M_s	LTD	First heating					Second heating					F_L	F	ΔAIC
							(per cent)	H_L	Slope $_A$	Slope $_N$	f_N	r_N	H_L	Slope $_A$	Slope $_T$	f_T	r_T	(μT)	(μT)	
Maupiti (16.44–16.45°S, 152.25–152.28°W)																				
MP01-02-1	—	—	15.9	138	2.100	0.2484	8.3	20	1.45	0.417	0.793	0.995	0	0.937	1.01	1.00	0.995	10.0	4.17	−1.8
MP01-04-1	A	—	16.7	154	—	—	8.3	30	1.23	0.425	0.475	0.995	5	0.878	0.995	0.898	0.997	10.0	4.25	−2.0
MP01-06-1	—	—	21.3	126	—	—	16.7	25	0.571	0.460	0.249	*0.989*	5	0.822	*1.18*	0.886	*0.987*	10.0	—	—
MP01-07-1	—	—	14.5	134	—	—	16.7	30	0.914	0.374	0.339	0.995	5	0.893	1.03	0.853	0.996	10.0	3.74	−1.9
MP01-09-1	—	—	12.2	108	—	—	25.4	20	0.423	0.396	0.301	*0.980*	0	0.999	0.973	1.00	*0.993*	10.0	—	—
MP01-12-1	—	—	18.2	124	—	—	14.5	25	0.649	0.451	0.291	0.996	0	0.902	1.00	1.00	0.996	10.0	4.51	4.0
MP19-01-2	—	—	92.8	298	—	—	2.9	20	0.231	0.806	0.755	*0.979*	0	1.06	0.997	1.00	0.999	20.0	—	—
MP19-02-1	—	—	91.1	290	1.375	0.5192	2.9	20	0.258	0.754	0.790	0.995	0	1.03	0.994	1.00	0.998	20.0	*15.1*[a]	2.3
MP19-04-2	—	—	68.0	260	—	—	2.9	30	0.165	0.763	0.639	0.995	0	1.06	0.996	1.00	0.999	20.0	*15.3*[a]	−1.7
MP19-05-1	—	—	75.5	283	—	—	3.8	25	0.254	1.12	0.721	0.995	0	1.01	1.01	1.00	0.999	10.0	*11.2*[a]	5.6
MP19-06-1	—	—	69.4	243	—	—	−0.8	25	0.195	0.508	0.580	0.995	0	1.04	0.984	1.00	0.999	20.0	*10.2*[a]	9.9
MP19-07-1	E	c	67.4	226	—	—	4.8	25	0.179	0.662	0.684	0.995	0	1.06	0.997	1.00	0.996	20.0	*13.2*[a]	10.8
Borabora (16.46–16.54°S, 151.73–151.76°W)																				
BR02-04-1	E	c	139	373	1.647	0.2447	6.5	10	0.393	0.999	0.662	0.995	40	1.02	1.04	0.723	0.995	10.0	*9.99*[a]	7.2
BR02-05-1	—	—	138	362	1.648	0.2579	4.8	10	0.404	0.506	0.655	0.998	40	0.934	1.05	0.703	0.997	20.0	*10.1*[a]	−1.7
BR02-06-1	—	—	133	385	1.630	0.2569	4.8	10	0.426	0.844	0.671	0.997	50	0.962	1.03	0.521	0.995	10.0	*8.44*[a]	−1.8
BR02-07-1	—	—	138	396	1.562	0.3050	3.8	10	0.406	0.958	0.998	*0.750*	45	1.04	1.05	0.620	0.995	10.0	*9.58*[a]	0.7
BR08-01-2	—	—	467	255	—	—	2.0	15	0.191	2.44	0.805	0.995	10	1.08	*0.888*	1.00	0.999	20.0	—	—
BR08-02-2w	—	—	767	345	—	—	−0.9	15	0.274	2.64	0.766	0.995	50	1.15	*0.807*	0.724	*0.993*	20.0	—	—
BR08-03-1	—	—	164	190	—	—	6.5	5	0.225	0.849	0.994	*0.984*	0	1.18	*0.869*	1.00	0.998	20.0	—	—
BR08-04-2	—	—	317	244	—	—	1.0	55	0.183	0.816	0.181	0.995	0	1.14	*0.938*	1.00	*0.993*	20.0	—	—
BR08-05-1	—	—	1100	474	—	—	4.8	15	0.446	3.72	0.757	0.998	30	1.09	*1.06*	0.961	0.999	20.0	—	—
BR08-06-1	—	—	985	494	—	—	4.8	15	0.510	3.59	0.723	0.998	0	1.00	*1.10*	1.00	0.998	20.0	—	—
BR08-07-1	—	—	623	293	—	—	3.8	20	0.222	9.39	0.693	*0.992*	0	1.01	0.996	1.00	0.998	10.0	—	—
BR09-03-1	—	—	148	274	—	—	9.1	5	0.885	0.352	0.687	*0.975*	10	0.842	1.00	0.861	0.998	40.0	—	—
BR10-01-1	—	—	65.0	134	1.551	0.5325	7.4	55	0.545	0.248	0.275	*0.991*	0	0.831	1.05	1.00	0.996	20.0	—	—
BR10-01-2	—	—	61.7	125	1.551	0.5325	3.8	65	0.621	0.500	0.232	0.996	0	0.826	1.04	1.00	0.997	10.0	*5.00*[b]	11.7
BR10-02-2	—	—	129	207	—	—	−2.4	40	1.25	1.97	0.486	0.995	0	0.834	*0.913*	1.00	0.995	5.00	—	—
BR10-03-1	D	e	83.3	159	1.825	0.4486	−1.0	10	1.20	0.668	0.341	0.998	0	0.898	0.953	1.00	0.998	10.0	*6.68*[b]	6.7
BR10-03-2	D	e	83.9	146	1.825	0.4486	2.0	55	1.33	0.761	0.403	*0.992*	0	0.852	*0.912*	1.00	0.995	10.0	—	—
BR10-04-1	—	—	149	200	1.548	0.5002	5.7	55	0.972	0.806	0.226	0.996	0	0.834	*1.12*	1.00	0.998	10.0	—	—
BR10-04-2	—	—	131	190	1.548	0.5002	−0.9	65	0.944	0.867	0.196	0.995	0	0.851	1.03	1.00	0.999	10.0	*8.67*[b]	−1.9
BR10-05-2	—	—	114	180	—	—	2.9	50	0.911	1.49	0.365	0.995	0	0.816	*0.908*	1.00	0.997	5.00	—	—
BR10-07-2	—	—	78.1	147	1.615	0.5392	1.0	50	1.18	0.696	0.357	0.995	0	0.878	0.974	1.00	0.999	10.0	*6.96*[b]	17.1
BR16-01-2	—	—	230	348	1.669	0.3168	9.1	25	0.479	1.72	0.205	0.995	5	0.981	0.963	0.926	0.998	10.0	*17.2*[b]	8.0
BR16-02-2	—	—	272	382	1.798	0.3268	4.8	25	0.446	0.765	0.214	0.995	0	0.980	1.03	1.00	0.999	20.0	*15.3*[b]	20.8
BR16-03-1	F	d	269	361	1.882	0.2790	5.7	30	0.424	0.749	0.166	0.997	5	0.960	1.00	0.947	0.999	20.0	*15.0*[b]	2.1
BR16-04-1	—	—	110	297	2.274	0.3203	4.8	30	0.612	0.493	0.286	0.995	20	0.912	1.02	0.786	0.998	20.0	*9.86*[b]	2.1
BR16-05-1	—	—	85.7	232	—	—	16.7	10	0.463	1.22	0.738	0.996	20	0.902	*1.12*	0.883	0.998	10.0	—	—
BR16-05-2	—	—	119	270	—	—	9.1	30	0.290	0.521	0.217	0.995	0	0.970	*1.13*	1.00	0.999	20.0	—	—
BR16-06-1	—	—	255	366	1.705	0.3235	12.3	25	0.462	1.57	0.195	0.995	20	0.965	1.01	0.731	0.999	10.0	*15.7*[b]	16.2
BR16-07-2	—	—	248	351	—	—	9.1	5	0.863	1.04	0.919	0.995	25	1.00	*1.07*	0.738	0.999	20.0	—	—

Table 1. (*Continued.*)

Sample ID	HT	LT	NRM_0	$ARM0_0$	B_{rc}/B_c	M_{rs}/M_s	LTD	First heating					Second heating					F_L	F	ΔAIC
							(per cent)	H_L	Slope $_A$	Slope $_N$	f_N	r_N	H_L	Slope $_A$	Slope $_T$	f_T	r_T	(μT)	(μT)	
Tahaa (16.58–16.59°S, 151.48–151.49°W)																				
TA13-01-1	—	—	111	321	—	—	20.6	20	0.558	0.179	*0.0860*	*0.909*	0	0.844	*0.936*	1.00	0.999	40.0	—	—
TA13-02-1	—	—	139	321	—	—	18.0	20	0.355	0.377	*0.0680*	*0.957*	20	0.945	1.05	0.669	0.996	10.0	—	—
TA13-03-1	—	—	110	369	—	—	16.7	20	0.385	0.461	*0.0860*	*0.934*	20	0.868	0.988	0.708	0.996	10.0	—	—
TA13-06-1	—	—	103	324	—	—	17.4	20	0.441	0.245	*0.0990*	*0.936*	10	0.790	0.952	0.810	0.999	20.0	—	—
TA13-07-1	—	—	139	299	—	—	16.0	20	0.366	0.559	*0.0900*	*0.953*	15	0.877	1.01	0.791	0.996	10.0	—	—
TA13-10-1	A	—	104	262	2.266	0.1503	15.3	15	0.605	1.02	0.351	0.996	0	1.00	0.990	1.00	0.999	10.0	10.2	21.3
TA13-11-1	—	—	101	341	—	—	19.4	20	0.451	0.478	*0.120*	*0.970*	0	0.895	0.976	1.00	0.998	10.0	—	—
Raiatea (16.80–16.92°S, 151.37–151.46°W)																				
RT03-01-1	—	—	276	788	—	—	3.8	20	0.270	0.907	0.401	*0.983*	35	1.03	1.01	0.608	0.995	10.0	—	—
RT03-02-1	—	—	120	577	1.905	0.1924	9.9	20	0.143	0.484	0.429	*0.970*	15	0.948	*1.10*	0.967	0.999	20.0	—	—
RT03-03-2	—	—	94.8	356	—	—	27.5	15	0.382	0.976	0.602	0.995	15	0.808	*1.22*	0.533	0.998	20.0	—	—
RT03-04-2	—	—	49.8	303	—	—	31.5	15	0.317	0.649	0.542	*0.994*	5	0.733	*1.08*	0.701	*0.991*	20.0	—	—
RT03-05-1	—	—	113	380	—	—	20.6	No primary component					5	0.864	1.00	0.888	0.998	20.0	—	—
RT03-06-2	—	—	90.8	354	3.091	0.1532	22.5	20	0.292	1.73	0.537	0.995	5	0.810	1.05	0.756	0.998	10.0	17.3	11.5
RT03-07-1	D	c	67.5	320	2.849	0.1539	31.5	20	0.287	1.49	0.363	0.995	5	0.770	1.02	0.673	0.996	10.0	14.9	5.0
RA01-15-1	—	—	191	502	2.507	0.2892	11.5	20	0.542	0.629	0.563	0.995	0	1.06	1.04	1.00	0.999	20.0	12.6	6.3
Huahine (16.74–16.81°S, 151.00–151.04°W)																				
HH05-01-2w	—	—	137	208	1.476	0.3821	2.0	10	0.340	0.575	0.885	0.995	55	1.24	1.01	0.665	0.997	20.0	*11.5*[a]	12.2
HH05-02-2	—	—	108	181	1.528	0.4280	2.0	10	0.332	1.23	0.911	0.995	45	1.17	1.04	0.842	0.995	10.0	*12.3*[a]	2.4
HH05-03-2w	—	—	166	295	1.413	0.3826	4.8	15	0.239	1.87	0.467	0.998	30	1.11	1.05	0.903	0.995	10.0	*18.7*[a]	−1.9
HH05-05-2w	—	—	228	312	1.616	0.5803	2.0	55	0.323	0.721	0.172	*0.968*	0	1.11	*1.14*	1.00	0.999	10.0	—	—
HH05-06-2	—	—	153	174	—	—	2.0	15	0.276	2.84	0.894	*0.988*	0	1.03	1.04	1.00	0.995	10.0	—	—
HH05-07-2	E	—	134	187	1.392	0.4832	2.9	15	0.296	0.893	0.769	0.997	0	1.06	1.02	1.00	0.998	20.0	*17.9*[a]	4.4
HH06-01-2	E	c	108	487	1.556	0.3563	2.9	10	0.504	0.174	0.779	*0.989*	0	1.25	1.03	1.00	0.998	20.0	—	—
HH06-02-2	—	—	108	406	—	—	0.0	45	0.368	0.255	0.152	0.995	0	1.14	*1.09*	1.00	0.999	10.0	—	—
HH06-03-2	—	—	97.1	485	—	—	2.0	10	0.418	0.251	0.820	*0.989*	0	1.42	1.01	1.00	0.996	10.0	—	—
HH06-04-1	—	—	92.7	411	1.580	0.4146	3.8	0	0.475	0.101	1.00	*0.989*	0	1.04	*1.46*	1.00	0.998	40.0	—	—
HH06-04-2	—	—	94.7	423	1.580	0.4146	2.9	35	0.337	0.212	0.222	*0.986*	0	1.23	*1.11*	1.00	0.997	10.0	—	—
HH06-05-2	—	—	124	419	1.549	0.3709	2.0	15	0.555	0.744	0.693	0.995	0	1.04	1.05	1.00	0.999	10.0	*7.44*[a]	12.2
HH06-06-2	—	—	94.1	385	—	—	2.0	15	0.429	0.522	0.667	*0.991*	0	1.07	1.01	1.00	0.999	10.0	—	—
HH06-06-3	—	—	97.4	372	—	—	−1.9	15	0.446	0.517	0.645	*0.987*	0	1.06	1.02	1.00	0.998	10.0	—	—
HH06-07-2	—	—	118	434	1.559	0.3997	2.9	20	0.439	0.287	0.497	0.995	0	1.11	1.04	1.00	1.00	20.0	*5.74*[a]	94.3
HH07-01-2	—	—	13.5	110	1.672	0.4140	3.8	No primary component					0	1.04	0.978	1.00	0.998	40.0	—	—
HH07-07-1w	—	—	23.6	139	1.519	0.5551	9.1	20	0.094	0.128	0.615	*0.978*	45	1.06	*1.74*	0.755	0.999	40.0	—	—
HH08-01-2	E	c	105	227	1.696	0.2785	9.1	20	0.168	1.19	0.366	0.995	0	1.06	0.990	1.00	0.999	20.0	*23.8*[a]	93.4
HH08-02-1	—	—	104	247	1.815	0.2770	7.4	15	0.560	0.517	0.570	0.998	35	0.818	*3.38*	0.396	*0.986*	40.0	—	—
HH08-02-2	—	—	128	231	1.815	0.2770	8.3	20	0.204	1.40	0.338	0.995	15	1.02	*0.933*	0.958	0.998	20.0	—	—
HH08-03-2	—	—	109	224	1.786	0.2557	6.5	25	0.182	1.21	0.323	0.995	0	1.02	1.01	1.00	0.999	20.0	*24.2*[a]	−0.8
HH08-04-1	—	—	162	294	1.592	0.2793	9.1	10	0.530	0.633	0.675	0.998	30	0.795	*1.85*	0.568	0.995	40.0	—	—
HH08-04-2	—	—	154	280	1.592	0.2793	9.1	20	0.212	1.40	0.350	0.995	10	1.00	0.951	0.978	0.999	20.0	*28.0*[a]	14.3
HH08-04-2-1	—	—	178	286	1.592	0.2793	17.4	20	0.268	0.703	0.404	*0.991*	30	1.13	*0.784*	0.933	1.00	40.0	—	—
HH08-05-1	—	—	122	253	1.872	0.2793	8.3	20	0.214	1.26	0.404	0.995	10	1.01	0.958	0.978	0.999	20.0	*25.2*[a]	20.5
HH08-07-2	—	—	157	277	1.521	0.3216	3.8	15	0.277	1.22	0.455	0.996	0	0.987	1.00	1.00	0.999	20.0	*24.4*[a]	24.2
HH12-01-2	—	—	118	386	1.371	0.4176	4.8	20	0.335	1.01	0.491	0.995	0	1.07	0.985	1.00	0.999	10.0	*10.1*[a]	−1.3
HH12-02-2	—	—	93.9	397	1.426	0.3581	2.0	25	0.222	0.593	0.306	0.996	0	1.15	0.963	1.00	0.997	10.0	*5.93*[a]	2.3
HH12-03-2	—	—	112	437	1.410	0.4260	1.0	25	0.282	0.834	0.552	0.996	0	1.08	1.03	1.00	0.998	10.0	*8.3*[a]	−2.0
HH12-04-1	E	c	136	315	1.509	0.3851	4.8	10	0.468	0.177	0.584	0.998	25	0.999	*1.19*	0.912	0.999	50.0	—	—
HH12-04-2	E	c	139	305	1.509	0.3851	2.0	15	0.381	1.05	0.467	0.998	0	1.02	1.02	1.00	0.999	10.0	*10.5*[a]	9.0
HH12-04-2-2	E	c	153	330	1.509	0.3851	9.9	25	0.311	0.308	0.365	0.997	45	1.22	*0.856*	0.793	0.997	40.0	—	—
HH12-06-2	—	—	120	290	1.523	0.3584	2.0	20	0.273	0.966	0.391	0.997	0	1.14	0.991	1.00	0.999	10.0	*9.66*[a]	−0.1
HH12-07-1	E	—	110	309	1.532	0.3832	5.7	20	0.325	0.182	0.405	0.998	0	1.00	1.02	1.00	0.999	50.0	*9.10*[a]	−0.8
HH12-07-2	E	c	102	287	1.532	0.3832	2.9	20	0.291	0.952	0.426	0.999	0	1.06	1.02	1.00	0.999	10.0	*9.52*[a]	−1.6

Table 1. (*Continued.*)

Sample ID	HT	LT	NRM_0	$ARM0_0$	B_{rc}/B_c	M_{rs}/M_s	LTD	First heating					Second heating					F_L	F	ΔAIC
							(per cent)	H_L	Slope $_A$	Slope $_N$	f_N	r_N	H_L	Slope $_A$	Slope $_T$	f_T	r_T	(μT)	(μT)	
HH13-07-1	—	—	290	440	1.553	0.3622	7.4	35	0.604	0.167	*0.136*	*0.985*	35	0.632	*1.91*	0.427	*0.993*	50.0	—	—
HH14-06-1	D	—	127	135	1.557	0.3585	5.7	15	0.301	0.132	*0.107*	*0.984*	30	0.884	*2.23*	0.708	0.995	40.0	—	—
HH15-02-1	—	—	302	495	1.939	0.1746	16.7	20	0.410	0.140	*0.140*	*0.991*	15	0.920	*2.00*	0.899	0.999	40.0	—	—
HH15-03-1	—	—	341	451	1.878	0.1696	15.3	10	0.379	0.227	0.194	*0.955*	20	0.876	*1.91*	0.720	0.998	40.0	—	—
Tahiti (17.52–17.78°S, 149.17–149.59°W)																				
PU04-01-2	—	—	155	312	1.892	0.2365	13.0	10	0.459	1.09	0.575	0.997	5	0.898	0.998	0.947	0.999	20.0	21.8	0.1
PU04-02-1	F	c	195	335	1.845	0.2200	9.9	15	0.359	0.597	0.400	0.997	5	0.946	0.972	0.955	0.999	40.0	23.9	3.6
PU04-03-2	—	—	165	320	1.747	0.2586	9.9	10	0.495	1.11	0.598	0.995	5	0.911	1.02	0.938	0.999	20.0	22.2	3.3
PU04-06-1	—	—	162	245	1.848	0.2291	31.5	10	0.453	0.557	0.587	0.996	5	0.891	1.02	0.952	0.999	40.0	22.3	11.6
PU04-11-1	—	—	388	224	—	—	9.9	50	1.47	2.48	0.257	*0.991*	0	0.925	*1.39*	1.00	0.999	40.0	—	—
PU04-12-1	—	—	175	351	1.821	0.2331	11.5	10	0.460	1.10	0.573	0.997	5	0.922	0.977	0.944	0.998	20.0	22.0	−0.5
PU05-01-2	—	—	135	483	1.639	0.2708	9.1	15	0.187	0.634	0.342	0.997	0	0.985	1.03	1.00	0.999	20.0	12.7	5.8
PU05-02-1	F	c	116	324	1.904	0.2305	16.0	10	0.451	0.349	0.416	0.995	5	0.859	1.04	0.915	0.999	40.0	14.0	4.2
PU05-03-2	—	—	142	323	2.031	0.2334	13.0	10	0.538	0.865	0.411	0.998	20	0.827	1.02	0.697	0.998	20.0	17.3	13.1
PU05-04-1	—	—	130	316	1.913	0.2260	15.3	10	0.425	0.389	0.410	0.995	5	0.852	1.00	0.908	0.999	40.0	15.6	4.8
PU05-05-2	—	—	190	432	—	—	14.5	15	0.152	1.22	0.199	0.995	0	0.969	*1.11*	1.00	0.995	10.0	—	—
PU05-11-1	—	—	172	346	—	—	16.7	10	0.663	0.574	0.435	0.996	15	0.913	*1.21*	0.572	0.998	40.0	—	—
PU05-12-1	—	—	144	312	2.141	0.2006	11.5	10	0.282	0.799	0.292	0.995	5	0.859	0.985	0.897	0.996	20.0	16.0	10.2
PU06-01-2	—	—	655	271	—	—	3.8	50	1.36	4.32	0.316	*0.979*	0	1.00	1.01	1.00	1.00	20.0	—	—
PU06-04-1	A	a	536	244	1.860	0.3397	−3.1	55	1.09	2.57	0.429	*0.936*	0	1.03	0.973	1.00	1.00	40.0	—	—
PU06-05-1	—	—	794	349	—	—	3.8	55	1.08	1.88	0.226	*0.978*	0	1.03	1.02	1.00	1.00	40.0	—	—
PU06-11-1	—	—	857	342	—	—	5.7	50	1.18	5.27	0.317	*0.988*	0	1.04	1.00	1.00	1.00	20.0	—	—
PU06-21-2	—	—	1310	397	—	—	4.8	25	1.07	3.83	0.879	*0.991*	0	1.02	1.05	1.00	0.999	20.0	—	—
PU06-23-2	—	—	1450	415	—	—	5.7	25	1.04	4.04	0.870	*0.994*	0	1.04	0.987	1.00	1.00	20.0	—	—
PU06-31-2	A	a	1440	450	1.659	0.3973	−7.5	40	0.959	2.22	0.682	*0.972*	0	1.02	1.02	1.00	1.00	40.0	—	—
TR02-01-2	—	—	76.4	412	—	—	21.9	10	0.828	0.432	0.996	*0.979*	5	0.942	*1.08*	0.883	0.999	20.0	—	—
TR02-02-1	—	—	103	397	2.676	0.2039	18.7	10	0.793	0.502	0.832	0.997	0	1.01	1.00	1.00	0.999	20.0	10.0	0.6
TR02-03-2	B	—	60.9	402	3.773	0.2018	24.8	15	0.976	0.790	0.967	0.995	0	0.951	1.02	1.00	0.998	10.0	7.90	−1.0
TR02-04-1	—	—	100	381	2.586	0.2270	22.5	15	0.979	0.483	0.823	0.995	5	0.947	1.05	0.894	0.999	20.0	9.66	1.0
TR02-06-1	—	—	98.1	398	2.586	0.2270	18.0	15	0.904	0.461	0.731	0.996	5	0.946	0.984	0.884	0.998	20.0	9.22	16.3
TH02-01-2	—	—	310	679	—	—	−17.4	15	0.473	0.870	0.583	0.998	10	0.963	*1.09*	0.931	0.999	20.0	—	—
TH02-03-2	—	—	326	765	2.184	0.1648	−2.9	15	0.494	1.30	0.688	0.998	10	0.908	1.04	0.943	0.999	20.0	26.0	5.1
TH02-04-1	A	—	356	742	2.115	0.1759	−15.6	15	0.541	0.736	0.722	0.997	10	1.00	0.958	0.946	1.00	40.0	29.4	−0.4
TH02-13-1	—	—	217	598	—	—	19.4	25	0.545	0.531	0.396	0.995	10	0.942	*1.07*	0.951	1.00	20.0	—	—
TH03-03-2	—	—	36.3	425	2.192	0.1844	16.7	10	0.668	0.191	0.961	0.995	5	1.01	1.04	0.989	0.998	20.0	3.82	1.0
TH03-09-1	—	—	32.9	245	1.946	0.1918	18.7	20	1.03	0.261	0.647	0.995	0	0.985	1.01	1.00	1.00	20.0	5.22	13.1
TH03-12-1	A	—	12.9	322	2.063	0.1881	22.5	5	0.772	0.054	2.10	*0.943*	0	1.03	0.986	1.00	0.999	40.0	—	—
TH03-16-2	—	—	28.8	213	2.291	0.1578	22.5	20	1.04	0.254	0.745	0.995	0	1.01	0.978	1.00	1.00	20.0	5.08	7.0
TH04-03-1	—	—	230	839	—	—	2.0	10	0.330	0.481	0.489	*0.981*	30	0.974	1.03	0.610	0.998	20.0	—	—
TH04-04-1	—	—	229	673	—	—	18.0	10	0.370	0.543	0.575	*0.983*	30	0.986	1.05	0.655	0.998	20.0	—	—
TH04-13-1	B	—	194	638	2.030	0.3313	15.3	10	0.488	0.231	0.798	0.995	20	1.00	0.983	0.954	0.998	40.0	9.24	25.5

HT, LT, classifications of the thermomagnetic and low-temperature cycling curves; NRM_0, $ARM0_0$, initial NRM and ARM0 intensity after LTD (10^{-5} A m^2 kg^{-1}); B_{rc}/B_c, M_{rs}/M_s, core-averaged ratios of remanent coercivity to coercivity and saturation magnetization to remanent saturation magnetization; LTD, LT demagnetized fraction of ARM0 (per cent); H_L, the lowest coercivity force taken for the linear segments; Slope$_A$, slope of ARM spectra ($\geq H_L$) before and after laboratory heating; Slope$_N$, Slope$_T$, slope of the linear segments in the NRM–TRM1* and TRM1–TRM2* diagrams; r_N, r_T, correlation coefficients of the linear NRM–TRM1* and TRM1–TRM2* segments; f_N, f_T, NRM and TRM1 fractions of the linear NRM–TRM1* and TRM1–TRM2* segments; F_L, laboratory induced DC field for TRM1 and TRM2; F, calculated palaeointensity; ΔAIC, AIC difference between linear and quadratic fit (AIC1−AIC2). Note that palaeointensities from specimens with suffix 'w' are calculated with corrections for mass changes.

[a]Not adopted for the calculation of the flow average (because of the possible low temperature oxidation suggested from the M_s–T curve of Type E).

[b]Not adopted for the calculation of the flow average (because of the curved NRM–TRM1* diagram).

Table 2. Experimental results from the LTD-DHT Shaw method for the lava sequences.

Sample ID	HT	LT	NRM_0	$ARM0_0$	B_{rc}/B_c	M_{rs}/M_s	LTD (per cent)	First heating H_L	First heating $Slope_A$	First heating $Slope_N$	First heating f_N	First heating r_N	Second heating H_L	Second heating $Slope_A$	Second heating $Slope_T$	Second heating f_T	Second heating r_T	F_L (μT)	F (μT)	ΔAIC
Maupiti sequence A (16.44°S, 152.25°W)																				
MP13-02-1	—	—	712	697	1.620	0.2870	5.7	5	0.752	1.20	0.417	0.995	10	0.906	0.953	0.851	0.999	20.0	24.0	69.5
MP13-03-1	—	—	397	470	—	—	8.3	15	0.389	2.55	0.349	0.995	10	1.04	*0.946*	0.935	0.996	10.0	—	—
MP13-04-1	—	—	330	436	—	—	10.7	10	0.368	1.18	0.466	0.997	0	1.07	*0.937*	1.00	0.996	20.0	—	—
MP13-05-2	—	—	267	340	—	—	5.7	10	1.04	1.34	0.970	*0.989*	0	1.05	*0.882*	1.00	1.00	20.0	—	—
MP13-06-2	—	—	452	577	—	—	8.3	10	0.543	1.18	0.442	0.998	20	1.01	*0.891*	0.767	0.999	20.0	—	—
MP13-07-1	C	c	392	524	1.601	0.2936	9.9	10	0.482	1.33	0.432	0.995	35	0.751	1.01	0.481	0.995	20.0	26.6	10.1
MP12-02-1	—	—	243	331	—	—	6.5	50	0.737	0.530	0.208	*0.985*	5	0.838	*0.916*	0.962	0.997	20.0	—	—
MP12-03-1	—	—	265	386	1.761	0.3443	8.3	35	0.621	1.28	0.346	0.995	0	0.904	0.981	1.00	0.999	10.0	*12.8*[a]	14.7
MP12-04-1	—	—	299	391	—	—	3.8	15	0.703	1.03	0.639	0.998	10	0.886	*0.926*	0.936	0.998	20.0	—	—
MP12-05-2	—	—	230	463	1.510	0.5070	2.0	10	0.427	0.712	0.753	0.999	0	1.03	1.05	1.000	0.999	20.0	*14.2*[a]	−0.9
MP12-06-2	—	—	231	448	1.372	0.5150	5.7	20	0.319	0.689	0.624	0.998	0	1.02	1.04	1.00	0.999	20.0	*13.8*[a]	−0.6
MP12-07-1	E	d	452	799	1.357	0.5890	0.0	10	0.674	0.932	0.809	0.996	0	1.03	0.997	1.00	0.999	20.0	*18.6*[a]	0.2
MP11-02-1	—	—	618	530	—	—	2.9	20	0.971	1.28	0.672	0.998	0	0.980	*1.07*	1.00	1.00	20.0	—	—
MP11-06-1	—	—	540	549	1.456	0.4238	9.1	15	0.713	1.24	0.835	0.999	0	0.999	1.05	1.00	1.00	20.0	24.8	16.7
MP10-05-1	—	—	497	918	1.864	0.2817	2.9	0	1.11	0.948	1.00	1.00	0	1.03	1.02	1.00	1.00	20.0	19.0	7.4
MP10-07-1	—	—	305	353	—	—	5.7	20	0.481	1.17	0.704	0.998	0	0.980	*1.07*	1.00	1.00	20.0	—	—
MP09-03-1	—	—	518	436	—	—	10.7	15	0.694	1.48	0.864	*0.980*	0	1.02	0.972	1.00	1.00	20.0	—	—
MP09-07-1	—	—	365	411	—	—	9.1	15	0.885	1.33	0.793	*0.991*	0	0.986	0.973	1.00	1.00	20.0	—	—
MP08-03-1	—	—	311	398	—	—	7.4	15	0.883	1.27	0.703	*0.991*	0	1.01	0.992	1.00	1.00	20.0	—	—
MP08-07-1	—	—	270	377	—	—	11.5	20	0.846	1.42	0.636	*0.994*	0	0.998	1.00	1.00	1.00	20.0	—	—
MP07-03-1	—	—	475	480	—	—	5.7	15	1.02	1.55	0.835	0.995	0	1.02	0.989	1.00	1.00	20.0	31.0	34.0
MP07-07-1	—	—	296	355	2.080	0.1797	14.5	20	1.03	1.75	0.722	0.995	0	1.01	0.977	1.00	1.00	20.0	35.0	53.5
MP06-05-1	—	—	388	386	1.986	0.2699	8.3	25	0.973	1.88	0.568	0.995	0	0.997	1.00	1.00	1.00	20.0	37.6	42.6
MP06-07-1	—	—	342	385	—	—	6.5	20	1.07	1.63	0.612	0.996	0	1.01	0.976	1.00	1.00	20.0	32.6	50.7
MP05-05-1	—	—	246	342	2.195	0.1839	12.3	25	0.841	1.67	0.581	0.995	0	0.998	0.995	1.00	1.00	20.0	33.4	45.1
MP05-07-1	—	—	316	420	—	—	2.9	20	0.940	1.52	0.645	0.997	0	1.01	0.960	1.00	1.00	20.0	30.4	16.8
MP04-05-1	—	—	287	263	—	—	13.8	15	0.764	1.60	0.664	*0.988*	0	0.987	*1.06*	1.00	1.00	20.0	—	—
MP04-08-1	—	—	360	369	1.563	0.2697	8.3	15	0.653	1.36	0.621	0.999	0	0.969	1.05	1.00	1.00	20.0	27.2	−0.6
MP03-03-1	—	—	579	553	1.762	0.2651	5.7	25	0.847	1.61	0.593	0.995	0	1.00	0.985	1.00	1.00	20.0	32.2	18.9
MP03-07-1	—	—	371	336	—	—	9.1	35	0.795	1.98	0.339	*0.994*	0	1.00	1.04	1.00	1.00	20.0	—	—
MP02-02-1	—	—	339	416	—	—	7.4	15	0.704	1.19	0.883	*0.992*	0	1.00	1.05	1.00	0.999	20.0	—	—
MP02-03-1	B	a	353	461	1.555	0.4153	4.8	15	0.783	2.22	0.888	0.995	0	1.02	1.05	1.00	0.999	10.0	22.2	9.1
MP02-04-2	—	—	339	449	1.555	0.4200	5.7	20	0.814	0.989	0.813	0.995	0	1.02	1.04	1.00	0.999	20.0	19.8	35.1
MP02-06-1	—	—	366	455	1.491	0.4371	5.7	15	0.703	1.19	0.892	0.995	0	1.05	1.01	1.00	0.997	20.0	23.8	−1.7
MP02-07-1	—	—	320	348	—	—	3.8	25	0.432	1.89	0.667	0.996	0	1.09	*0.947*	1.00	0.996	20.0	—	—
MP02-08-1	—	—	308	337	—		4.8	30	0.359	1.97	0.546	*0.994*	0	1.03	1.03	1.00	*0.980*	20.0	—	—

Table 2. (*Continued.*)

Sample ID	HT	LT	NRM_0	$ARM0_0$	B_{rc}/B_c	M_{rs}/M_s	LTD (per cent)	First heating H_L	First heating $Slope_A$	First heating $Slope_N$	First heating f_N	First heating r_N	Second heating H_L	Second heating $Slope_A$	Second heating $Slope_T$	Second heating f_T	Second heating r_T	F_L (μT)	F (μT)	ΔAIC
Borabora Sequence A (16.54°S, 151.73°W)																				
BR07-01-1	—	—	133	550	1.602	0.2481	11.5	5	0.388	0.549	0.664	0.995	35	0.936	0.959	0.498	0.997	20.0	11.0	30.1
BR07-02-1	—	—	219	515	—	—	16.0	10	0.200	1.89	0.220	*0.982*	0	0.942	*0.767*	1.00	*0.990*	10.0	—	—
BR07-05-1	A	—	156	288	2.501	0.1520	12.3	20	0.696	1.18	0.567	0.998	0	1.01	0.985	1.00	0.999	20.0	23.6	6.3
BR07-06-1	—	—	284	427	2.146	0.2407	14.5	15	0.553	3.55	0.678	0.997	5	0.974	0.979	0.962	0.998	10.0	35.5	24.3
BR04-01-2	—	—	283	364	2.109	0.2006	16.0	10	0.757	0.966	0.777	0.995	0	0.962	0.973	1.00	1.00	30.0	29.0	28.8
BR04-02-1	A	a	269	400	2.113	0.1536	17.4	15	0.658	1.29	0.671	0.996	5	0.913	1.04	0.949	0.999	20.0	25.8	6.4
BR04-03-2	—	—	294	547	1.905	0.3087	15.3	10	0.564	0.739	0.620	0.998	5	0.879	0.989	0.921	0.999	30.0	22.2	30.4
BR04-04-1w	—	—	246	426	—	—	16.0	10	0.524	0.966	0.539	0.999	5	0.848	*0.922*	0.952	0.997	20.0	—	—
BR04-06-2	—	—	337	534	—	—	9.1	15	0.573	1.29	0.640	0.997	0	0.939	*1.16*	1.00	0.999	20.0	—	—
BR04-07-1	—	—	384	550	1.713	0.3425	13.0	10	0.660	1.460	0.785	0.996	0	0.988	0.994	1.00	1.00	20.0	29.2	−1.9
Borabora sequence B (16.47°S, 151.76°W)																				
BR15-01-2	—	—	65.1	267	2.496	0.1304	24.8	20	0.716	0.791	0.420	0.996	0	0.980	0.950	1.00	1.00	20.0	15.8	0.9
BR15-02-1	—	—	66.7	286	2.698	0.1250	23.7	20	0.737	0.699	0.467	0.995	0	0.925	0.984	1.00	0.999	20.0	14.0	11.4
BR15-03-1	—	—	70.7	280	2.620	0.1590	21.3	20	0.729	1.19	0.392	0.995	0	0.915	1.00	1.00	0.998	10.0	11.9	−0.9
BR15-05-1	B	a	75.1	223	2.346	0.1645	22.5	20	0.700	0.730	0.419	0.995	0	0.973	1.01	1.00	1.00	20.0	14.6	7.8
BR15-06-2	—	—	69.9	219	2.448	0.1484	21.3	15	0.654	1.45	0.519	0.995	0	0.924	1.01	1.00	0.998	10.0	14.5	32.2
BR15-07-1	—	—	82.4	211	2.330	0.1464	20.6	20	0.607	1.61	0.414	0.995	0	0.947	1.02	1.00	0.999	10.0	16.1	−0.6
BR14-06-1	—	—	264	519	2.183	0.1652	12.3	15	0.821	0.503	0.591	0.999	0	0.922	0.980	1.00	1.00	40.0	20.1	0.9
Borabora sequence C (16.50°S, 151.73°W)																				
BR18-01-1	—	—	271	389	—	—	8.3	15	1.07	0.867	0.611	0.998	0	1.03	*0.944*	1.00	1.00	20.0	—	—
BR18-02-1	—	—	242	362	2.199	0.1827	9.1	15	1.01	0.870	0.628	0.998	0	1.01	1.01	1.00	1.00	20.0	17.4	6.6
BR18-04-2	—	—	214	325	—	—	9.9	15	0.942	0.804	0.572	1.00	0	0.966	*1.11*	1.00	1.00	20.0	—	—
BR18-06-1	A	a	233	332	2.114	0.1764	10.7	15	1.02	0.843	0.593	0.999	0	0.992	1.03	1.00	1.00	20.0	16.9	0.3
BR18-07-1	—	—	250	358	2.076	0.1860	9.1	15	1.12	0.819	0.599	0.999	0	0.973	1.04	1.00	1.00	20.0	16.4	−0.1
BR18-08-1	—	—	304	407	2.217	0.1886	9.1	15	1.11	1.90	0.647	0.997	0	1.00	0.984	1.00	1.00	10.0	19.0	2.1
Tahaa sequence A (16.68°S, 151.48°W)																				
TA03-02-1	—	—	301	359	—	—	11.5	20	0.330	0.291	*0.046*	*0.966*	15	0.941	1.04	0.908	0.999	10.0	—	—
TA03-06-1	—	—	360	418	—	—	2.0	20	0.249	0.352	*0.032*	*0.978*	15	1.02	1.02	0.955	0.997	10.0	—	—
TA02-08-1	—	—	79.5	424	—	—	7.4		No primary component				25	0.833	0.954	0.705	0.998	40.0	—	—
TA01-05-1	—	—	57.9	420	—	—	22.5		No primary component				15	1.03	*1.21*	0.590	0.999	40.0	—	—
TA01-07-1	—	—	47.4	433	—	—	20.0		No primary component				25	0.868	*1.29*	0.439	0.998	40.0	—	—
Tahaa sequence B (16.68°S, 151.45°W)																				
TA07-07-1	—	—	35.0	128	—	—	13.0	15	1.09	0.223	0.392	0.996	0	1.01	0.973	1.00	0.999	20.0	4.46	9.3
TA04-01-1	—	—	84.2	486	—	—	10.7	10	0.445	0.159	0.269	*0.969*	15	0.991	0.969	0.863	0.996	20.0	—	—
TA04-08-1	—	—	61.5	324	—	—	18.0	20	0.337	0.657	0.543	*0.972*	0	1.03	0.975	1.00	0.997	10.0	—	—
Tahaa sequence C (16.66°S, 151.44°W)																				
TA11-01-2	—	—	1500	288	1.846	0.3266	11.5	30	1.03	1.07	*0.071*	0.995	0	0.956	1.01	1.00	0.999	20.0	—	—
TA11-02-2	—	—	940	191	—	—	17.4	20	0.848	3.47	*0.132*	*0.979*	0	0.983	1.02	1.00	0.996	10.0	—	—
TA11-04-1	—	—	601	124	—	—	16.7	20	0.842	4.23	*0.118*	*0.989*	0	1.02	0.975	1.00	0.999	10.0	—	—
TA11-05-1	B	a	468	279	1.868	0.3072	11.5	20	0.822	1.12	0.279	0.998	5	0.987	0.981	0.981	0.999	20.0	22.4	−1.1
TA11-06-2	—	—	264	191	2.581	0.1567	15.3	25	0.910	1.15	0.244	0.995	0	0.982	0.986	1.00	0.999	20.0	23.0	−0.1
TA11-07-1	—	—	415	261	1.875	0.3062	12.3	20	0.832	2.39	0.303	0.996	0	1.02	0.966	1.00	0.999	10.0	23.9	−1.8
TA10-06-1	—	—	153	247	—	—	22.5	30	0.850	0.492	*0.135*	*0.987*	10	0.931	0.951	0.753	0.999	40.0	—	—
TA08-01-1	A	a	79.7	382	2.416	0.1452	13.0	25	0.871	1.48	1.14	0.997	0	1.02	0.969	1.00	0.999	20.0	29.6	31.5
TA08-02-2	—	—	149	349	2.379	0.1322	18.7	30	0.801	1.10	0.281	0.996	0	1.01	0.980	1.00	1.00	20.0	22.0	19.5
TA08-03-2	—	—	156	333	2.280	0.1447	19.4	35	0.776	1.22	0.227	0.995	0	1.00	0.979	1.00	1.00	20.0	24.4	7.4
TA08-04-1	—	—	211	385	—	—	12.3	15	0.991	1.03	0.548	*0.987*	0	1.00	0.990	1.00	0.999	20.0	—	—
TA08-05-1	—	—	301	354	2.346	0.1475	18.0	30	0.970	0.516	*0.143*	*0.990*	0	0.998	0.972	1.00	1.00	40.0	—	—
TA08-05-2	—	—	260	386	2.346	0.1475	13.0	35	0.921	1.21	0.170	0.995	0	1.01	0.999	1.00	1.00	20.0	24.2	23.4
TA08-06-1	—	—	260	308	2.703	0.1379	14.5	25	0.849	0.949	0.189	0.995	0	0.985	1.03	1.00	1.00	20.0	19.0	28.8
TA08-07-2	—	—	289	321	2.428	0.1395	18.0	40	0.757	1.33	*0.102*	0.995	0	1.01	0.963	1.00	1.00	20.0	—	—

Table 2. (*Continued.*)

Sample ID	HT	LT	NRM_0	$ARM0_0$	B_{rc}/B_c	M_{rs}/M_s	LTD	First heating					Second heating					F_L	F	ΔAIC
							(per cent)	H_L	$Slope_A$	$Slope_N$	f_N	r_N	H_L	$Slope_A$	$Slope_T$	f_T	r_T	(μT)	(μT)	
Tahaa sequence D (16.64°S, 151.44°W)																				
TA20-01-1	—	—	95.6	293	—	—	9.1	15	0.945	0.236	0.716	0.999	0	0.990	*0.915*	1.00	1.00	40.0	—	—
TA19-05-1	—	—	85.1	308	1.593	0.3529	6.5	15	0.611	0.224	0.683	0.999	25	0.794	1.05	0.697	0.999	40.0	8.96	1.5
TA17-02-2w	—	—	28.0	264	—	—	5.7	20	0.290	0.387	0.647	*0.989*	0	1.04	0.953	1.00	0.996	10.0	—	—
TA17-04-1w	—	—	35.0	235	2.194	0.2801	5.7	30	0.233	0.650	0.532	0.995	0	1.10	0.972	1.00	0.998	10.0	6.50	−0.7
TA17-05-1	B	—	42.5	246	2.154	0.2615	5.7	15	0.407	0.485	0.633	0.995	20	0.985	0.982	0.932	0.997	10.0	4.85	9.3
TA17-06-1w	—	—	34.1	243	—	—	5.7	20	0.168	0.267	0.274	*0.895*	0	0.985	0.989	1.00	0.997	10.0	—	—
TA17-07-1w	—	—	45.2	263	—	—	10.7	20	0.165	0.107	0.321	*0.978*	0	0.973	*0.928*	1.00	1.00	40.0	—	—
TA16-03-2	—	—	105	378	—	—	9.1	20	0.707	0.271	*0.113*	*0.973*	0	1.00	0.980	1.00	0.997	10.0	—	—
TA16-04-1	—	—	61.0	229	2.035	0.2468	10.7	20	0.683	0.339	0.173	0.995	0	1.00	1.00	1.00	0.999	10.0	3.39	−1.8
TA16-05-1	A	a	59.1	225	1.987	0.2539	13.8	15	0.717	0.333	0.216	0.996	0	0.999	1.02	1.00	0.998	10.0	3.33	−1.5
TA16-06-1	—	—	17.1	218	1.726	0.3126	9.9	20	0.983	0.275	0.802	0.995	0	1.02	1.02	1.00	0.999	10.0	2.75	−2.0
TA16-07-1	—	—	21.6	224	1.707	0.3147	10.7	20	0.962	0.260	0.603	0.995	0	1.02	1.01	1.00	0.999	10.0	2.60	−1.0
TA15-01-1	—	a	81.7	275	2.247	0.2045	7.4	10	0.866	0.768	0.934	0.995	5	0.983	0.998	0.980	1.00	10.0	7.68	18.5
TA15-02-2	—	—	87.3	278	2.193	0.2081	4.8	20	0.699	0.897	0.825	*0.988*	0	1.02	*1.06*	1.00	1.00	10.0	—	—
TA15-02-3	—	—	91.0	276	2.193	0.2081	9.1	10	0.873	0.844	0.942	0.995	0	1.02	0.999	1.00	1.00	10.0	8.44	21.1
TA15-05-1	—	—	92.9	284	2.270	0.2043	7.4	20	0.778	0.445	0.634	*0.984*	0	1.03	1.01	1.00	1.00	20.0	—	—
TA15-05-2	—	—	93.7	299	2.270	0.2043	6.5	5	0.996	0.714	0.988	0.995	0	1.01	1.05	1.00	0.999	10.0	7.14	26.5
TA15-06-1	A	a	74.3	315	2.464	0.1589	7.4	5	1.18	0.669	0.991	0.998	0	1.04	1.00	1.00	1.00	10.0	6.69	40.3
TA15-07-1	—	—	85.0	289	2.279	0.1925	4.8	5	1.07	0.686	0.995	0.995	0	0.984	1.03	1.00	1.00	10.0	6.86	23.1
Raiatea sequence A (16.85°S, 151.37°W)																				
RT05-06-1	—	—	43.2	337	2.056	0.1975	10.7	20	0.536	0.260	0.621	0.995	0	1.01	0.969	1.00	0.999	20.0	5.20	14.4
RT10-01-2w	—	—	73.7	457	1.837	0.3167	9.1	15	0.312	0.384	0.479	0.995	0	0.990	1.01	1.00	0.999	10.0	3.84	23.1
RT10-01-3	—	—	24.9	409	1.837	0.3167	9.9	20	0.261	0.324	0.737	*0.962*	0	0.990	1.03	1.00	0.998	10.0	—	—
RT10-02-1	—	—	32.7	409	—	—	14.5	20	0.261	0.332	0.488	*0.964*	0	1.01	1.05	1.00	0.999	10.0	—	—
RT10-03-1	B	—	104	434	1.648	0.2840	9.1	25	0.225	0.577	0.330	0.995	0	0.996	0.953	1.00	0.997	10.0	5.77	−1.3
RT10-03-2	B	—	41.7	424	1.648	0.2840	9.1	15	0.327	0.308	0.661	0.995	0	0.993	1.02	1.00	0.997	10.0	3.08	18.4
Raiatea sequence B (16.81°S, 151.39°W)																				
RT12-01-1m	—	—	147	398	2.349	0.2723	13.0	10	0.426	0.707	0.536	0.995	0	0.990	1.04	1.00	0.998	20.0	14.1	11.5
RT12-02-1m	—	—	130	331	1.899	0.2372	16.7	15	0.342	1.78	0.502	0.996	0	1.02	1.01	1.00	0.999	10.0	17.8	−2.0
RT12-03-2	—	—	113	455	2.234	0.2576	13.8	15	0.357	0.822	0.310	0.996	0	0.990	1.02	1.00	0.995	10.0	8.22	−1.5
RT12-04-1	—	—	92.8	460	2.000	0.2567	16.0	10	0.347	0.857	0.469	0.995	0	1.02	1.00	1.00	0.997	10.0	8.57	−1.9
RT12-04-2	—	—	92.2	417	2.000	0.2567	15.3	15	0.325	1.05	0.422	0.995	15	1.06	0.987	0.907	0.996	10.0	10.5	2.4
RT12-05-1	C	c	102	458	1.982	0.2405	13.8	10	0.446	0.913	0.523	0.997	10	1.00	0.998	0.927	0.998	10.0	9.13	15.3
RT12-06-2	—	—	110	436	1.903	0.2269	18.0	15	0.409	0.792	0.335	0.995	0	0.971	1.05	1.00	0.998	10.0	7.92	11.9
RT12-07-2	—	—	128	425	2.071	0.2405	17.4	30	0.473	0.768	0.217	0.997	10	0.982	1.05	0.930	0.999	10.0	7.68	4.5
Raiatea sequence C (16.85°S, 151.36°W)																				
RT18-02-2	—	—	137	364	1.500	0.3532	7.4	15	0.465	1.99	0.601	0.995	0	0.866	1.04	1.00	0.995	5.0	10.0	10.8
RT18-03-1	—	—	48.1	202	2.235	0.3721	5.7	20	0.681	0.331	0.506	*0.990*	0	0.835	*0.912*	1.00	0.999	20.0	—	—
RT18-05-1	F	e	74.6	215	1.760	0.3726	9.9	35	0.472	0.748	0.312	0.995	0	0.744	1.02	1.00	0.998	10.0	7.48	5.5
RT18-06-2	—	—	103	287	1.668	0.3494	14.5	10	0.442	0.924	0.764	0.996	25	0.940	1.01	0.788	0.999	10.0	9.24	16.1
RT18-07-1	—	—	79.1	253	1.942	0.3163	–	15	0.559	1.89	0.767	0.996	0	0.838	0.995	1.00	0.996	5.0	9.45	22.6
RT18-07-2m	—	—	218	462	1.942	0.3163	6.5	15	0.493	1.37	0.695	0.995	0	0.944	1.05	1.00	0.999	10.0	13.7	−2.0

Table 2. (*Continued.*)

Sample ID	HT	LT	NRM$_0$	ARM0$_0$	B_{rc}/B_c	M_{rs}/M_s	LTD	First heating					Second heating					F_L	F	ΔAIC
							(per cent)	H_L	Slope$_A$	Slope$_N$	f_N	r_N	H_L	Slope$_A$	Slope$_T$	f_T	r_T	(μT)	(μT)	
Huahine sequence A (16.80° S, 151.01° W)																				
HH01-02-2w	—	—	227	251	1.884	0.2350	9.9	40	0.692	4.47	0.320	*0.992*	0	1.01	1.04	1.00	1.00	10.0	—	—
HH01-03-2	—	—	206	183	—	—	11.5	40	0.714	4.62	0.291	*0.981*	0	1.01	1.04	1.00	0.999	10.0	—	—
HH01-04-2w	—	—	209	237	1.865	0.2316	10.7	35	0.666	1.46	0.343	*0.986*	0	1.02	1.04	1.00	1.00	30.0	—	—
HH01-06-1	—	—	237	275	1.887	0.2351	9.9	55	0.825	1.31	0.237	*0.991*	25	0.967	*1.62*	0.603	0.999	40.0	—	—
HH01-06-2	—	—	247	270	1.887	0.2351	8.3	30	0.774	1.28	0.481	0.996	0	0.99	1.02	1.00	1.00	30.0	38.4	28.8
HH01-07-2w	—	—	253	270	—	—	9.1	35	0.745	2.06	0.366	*0.990*	0	0.990	1.05	1.00	0.999	20.0	—	—
HH04-05-1w	—	—	207	249	1.819	0.2989	3.8	20	1.05	0.655	0.640	*0.991*	0	1.02	1.03	1.00	1.00	40.0	—	—
Huahine sequence B (16.81° S, 151.00° W)																				
HH11-01-2	—	—	222	520	—	—	9.1	15	0.800	0.592	0.209	0.995	0	0.828	*0.737*	1.00	0.998	30.0	—	—
HH11-02-2	—	—	206	527	1.629	0.2391	11.5	15	0.394	0.751	0.216	0.995	20	0.814	1.02	0.703	0.995	20.0	15.0	19.5
HH11-03-2	—	—	192	486	1.608	0.2613	13.0	10	0.498	0.568	0.447	0.995	20	0.872	1.04	0.744	0.997	30.0	17.0	53.9
HH11-04-2	D	c	239	663	1.608	0.2506	6.5	15	0.496	0.668	0.263	0.995	25	0.893	1.02	0.694	0.997	20.0	13.4	18.6
HH11-04-2-2	D	c	297	717	1.608	0.2506	6.5	15	0.649	0.310	0.273	*0.984*	35	0.782	*1.24*	0.523	0.996	40.0	—	—
HH11-05-2	—	—	228	633	1.574	0.2596	13.0	15	0.480	0.585	0.294	0.995	25	0.861	1.02	0.668	0.997	25.4	14.9	9.7
HH11-06-2	—	—	218	435	—	—	9.9	10	0.446	0.617	0.369	*0.986*	25	0.860	1.01	0.633	0.997	30.0	—	—
HH11-07-1m	D	—	206	482	1.600	0.2368	9.9	10	1.17	0.710	0.426	0.995	0	0.909	0.955	1.00	0.998	40.0	28.4	21.0
HH11-07-2	D	—	221	599	1.600	0.2368	4.8	15	0.667	0.538	0.294	0.995	20	0.610	*0.859*	0.622	0.996	30.0	—	—
HH10-01-1	—	—	114	361	1.785	0.2229	14.5	10	0.270	0.401	0.504	0.996	20	0.974	*1.63*	0.919	0.998	40.0	—	—
HH09-01-2	—	—	363	454	—	—	5.7	10	1.12	0.976	0.892	0.998	0	1.08	*1.06*	1.00	1.00	20.0	—	—
HH09-03-2	—	—	422	474	1.647	0.3349	2.9	10	1.12	0.961	0.903	0.998	0	1.05	1.05	1.00	1.00	20.0	19.2	8.7
HH09-04-1	—	—	367	393	1.735	0.3368	6.5	5	1.33	0.912	0.980	0.997	0	1.10	1.01	1.00	0.999	20.0	18.2	11.9
HH09-05-1	—	—	420	428	1.667	0.3413	3.8	0	1.31	0.367	1.00	0.998	0	1.09	*1.10*	1.00	1.00	50.0	—	—
HH09-05-2	—	—	394	407	1.667	0.3413	2.0	5	1.33	0.853	0.976	0.998	0	1.08	1.02	1.00	1.00	20.0	17.1	0.0
HH09-06-1	A	a	391	411	1.714	0.3390	3.8	0	1.24	0.480	1.00	0.998	0	1.10	*0.866*	1.00	1.00	50.0	—	—
HH09-06-2	A	a	370	396	1.714	0.3390	1.0	0	1.42	0.853	1.00	0.998	0	1.08	1.05	1.00	1.00	20.0	17.1	3.1
HH09-06-2-1	A	a	378	400	1.714	0.3390	2.9	0	1.43	0.424	1.00	0.998	0	1.05	*1.10*	1.00	0.999	40.0	—	—
HH09-07-2	A	a	366	417	1.706	0.3346	2.0	0	1.42	0.860	1.00	0.998	0	1.06	1.05	1.00	0.999	20.0	17.2	13.4
Huahine sequence-C (16.74° S, 151.04° W)																				
HH16-01-2-2	B	a	304	275	1.603	0.2871	11.5	20	0.436	0.956	0.540	0.998	0	1.06	1.01	1.00	0.999	40.0	38.2	4.2
HH16-02-2	—	—	405	317	1.493	0.3320	5.7	20	0.634	1.20	0.550	0.999	0	0.991	1.05	1.00	1.00	30.0	36.0	10.4
HH16-03-1	A	—	402	311	1.692	0.2443	9.1	15	0.700	1.12	0.636	0.998	30	1.08	1.05	0.494	0.996	30.0	33.6	4.1
HH16-06-1	—	a	405	338	1.967	0.1992	9.1	10	0.917	0.988	0.824	0.998	30	1.08	1.04	0.446	0.998	30.0	29.6	7.2
HH16-07-2	—	—	381	317	1.921	0.2026	9.9	10	0.894	1.06	0.815	0.998	0	1.00	1.05	1.00	1.00	30.0	31.8	17.0
HH17-03-1	—	—	428	330	1.659	0.3589	7.4	15	0.602	1.03	0.652	0.999	30	0.993	*1.71*	0.996	*0.639*	40.0	—	—
HH17-07-1	—	—	476	279	1.801	0.2355	10.7	15	0.845	0.973	0.623	0.997	0	1.02	*1.08*	1.00	1.00	40.0	—	—
HH18-01-1	—	—	304	273	2.002	0.1789	13.8	15	0.802	0.785	0.313	0.999	0	0.949	*1.16*	1.00	0.999	40.0	—	—
HH20-01-1	—	—	460	274	1.851	0.2241	13.8	10	0.602	0.952	0.594	0.999	0	1.03	1.05	1.00	1.00	40.0	38.1	14.9
HH20-02-2	—	—	475	270	—	—	11.5	15	0.532	1.91	0.413	0.997	30	1.01	*1.08*	1.00	1.00	20.0	—	—
HH20-03-1w	A	a	490	265	1.784	0.2466	12.3	15	0.659	1.18	0.392	*0.992*	0	0.922	*0.930*	1.00	*0.992*	40.0	—	—
HH20-03-2	A	a	501	281	1.784	0.2466	13.0	10	0.625	1.58	0.570	0.999	25	1.05	1.05	0.566	0.999	25.4	40.1	13.7
HH20-03-2-1	A	a	505	295	1.784	0.2466	9.1	20	0.306	1.36	0.304	0.989	45	1.62	*0.638*	0.230	*0.993*	40.0	—	—
HH20-04-1	—	—	474	265	—	—	13.0	15	0.510	3.99	0.409	0.998	0	1.01	*1.08*	1.00	0.999	10.0	—	—
HH20-05-1w	—	—	463	262	1.823	0.2400	9.1	15	0.592	0.887	0.393	0.999	0	0.974	1.05	1.00	1.00	40.0	35.5	1.6
HH20-05-2	—	—	455	263	1.823	0.2400	12.3	15	0.555	1.02	0.420	0.999	0	0.987	*1.09*	1.00	1.00	40.0	—	—
HH20-06-2	—	—	497	264	1.811	0.2177	12.3	15	0.497	3.98	0.394	0.997	20	1.05	1.04	0.756	0.997	10.0	39.8	−1.2
HH20-07-2	—	—	497	270	—	—	9.9	10	0.638	1.90	0.541	1.00	0	1.01	*1.09*	1.00	1.00	20.0	—	—
HH19-03-1	—	—	399	307	1.882	0.2228	10.7	15	0.812	0.946	0.540	0.998	35	0.997	*1.52*	0.223	0.997	40.0	—	—
HH19-06-1	—	—	428	284	1.913	0.2078	10.7	15	0.867	0.951	0.578	0.997	20	0.974	*1.20*	0.580	0.999	40.0	—	—
HH21-01-1	—	—	358	437	1.746	0.3369	12.3	35	0.805	0.518	0.220	0.996	5	0.953	*1.15*	0.962	0.999	40.0	—	—

Table 2. (*Continued.*)

Sample ID	HT	LT	NRM_0	$ARM0_0$	B_{rc}/B_c	M_{rs}/M_s	LTD	First heating					Second heating					F_L	F	ΔAIC
							(per cent)	H_L	$Slope_A$	$Slope_N$	f_N	r_N	H_L	$Slope_A$	$Slope_T$	f_T	r_T	(μT)	(μT)	
Moorea sequence A (17.59°S, 149.84°W)																				
MR01-01-2	—	—	100	226	2.253	0.1751	14.5	10	0.696	0.692	0.791	0.998	0	1.01	0.997	1.00	1.00	20.0	13.8	6.3
MR01-02-1	—	—	97.6	207	2.174	0.1791	16.0	10	0.772	0.352	0.829	0.996	0	0.939	1.05	1.00	1.00	40.0	14.1	12.9
MR01-03-1	—	—	135	301	2.094	0.2359	15.3	10	0.465	0.790	0.592	0.998	5	0.931	1.05	0.963	0.999	20.0	15.8	5.0
MR01-04-1	B	a	124	285	2.128	0.2418	16.7	10	0.482	0.396	0.634	0.999	0	0.956	1.01	1.00	0.999	40.0	15.8	−1.8
MR01-06-2	—	—	108	280	1.981	0.2226	14.5	10	0.444	0.777	0.676	0.997	0	0.978	1.01	1.00	0.999	20.0	15.5	−1.5
MR02-03-1	—	a	82.3	259	—	—	5.7	0	1.08	0.755	1.00	0.995	0	1.02	1.04	1.00	0.999	10.0	7.55	20.4
MR02-07-1	—	—	213	207	—	—	6.7	0	1.01	1.90	1.00	*0.988*	0	1.01	1.03	1.00	1.00	10.0	—	—
MR03-01-1	—	—	134	151	—	—	3.8	5	0.882	1.97	0.992	*0.971*	0	1.02	0.951	1.00	0.999	10.0	—	—
MR04-01-1	—	a	73.4	131	—	—	9.9	0	0.968	1.14	1.00	0.995	0	0.992	0.995	1.00	0.999	10.0	11.4	11.4
MR04-06-1	—	—	103	159	—	—	8.3	0	1.09	1.47	1.00	*0.993*	0	0.978	0.987	1.00	1.00	10.0	—	—
MR05-02-1	—	—	57.7	151	—	—	8.3	0	0.943	1.06	1.00	*0.963*	0	1.00	*0.800*	1.00	0.970	10.0	—	—
MR06-01-2	—	a	106	371	1.545	0.3310	9.9	0	1.00	0.859	1.00	0.996	0	1.03	1.02	1.00	0.996	10.0	8.59	11.8
MR06-02-1	—	—	68.9	197	1.764	0.2429	12.3	0	1.06	0.472	1.00	0.999	0	0.990	0.989	1.00	0.999	20.0	9.44	−1.9
MR06-03-1	—	—	101	343	—	—	9.9	0	1.01	0.181	1.00	*0.983*	5	1.01	1.02	0.982	1.00	40.0	—	—
MR06-04-2	—	—	71.6	183	1.870	0.2184	13.8	5	1.14	0.899	0.983	0.995	0	0.992	1.02	1.00	0.999	10.0	8.99	1.1
MR06-05-1	—	—	83.0	273	1.689	0.2552	12.3	15	1.26	0.386	0.839	0.997	0	0.991	1.01	1.00	0.999	20.0	7.72	9.5
MR06-06-1w	A	a	101	318	1.687	0.2699	11.5	5	1.01	0.221	0.990	0.995	0	1.00	0.999	1.00	1.00	40.0	8.84	29.2
MR09-04-1	—	a	316	347	—	—	9.1	20	0.827	1.33	0.436	0.995	0	1.01	0.985	1.00	1.00	20.0	26.6	−1.2
MR09-05-1	—	—	40.9	44.2	—	—	5.4	20	0.569	0.832	1.00	*0.994*	0	0.985	1.05	1.00	1.00	20.0	—	—
MR10-01-1	—	—	450	469	—	—	0.0	15	1.10	1.46	0.619	*0.989*	0	1.01	1.01	1.00	1.00	20.0	—	—
MR11-03-1	—	—	417	563	—	—	2.9	15	1.24	2.16	0.697	*0.992*	0	0.986	1.04	1.00	0.999	10.0	—	—
MR12-01-1	—	b	348	503	—	—	5.7	15	1.07	2.06	0.506	0.995	0	1.01	1.02	1.00	1.00	10.0	20.6	−0.3
MR13-01-1	—	—	360	304	—	—	13.8	45	0.522	4.97	0.257	*0.885*	0	0.993	0.981	1.00	1.00	10.0	—	—
MR14-03-1	—	b	294	293	—	—	4.8	10	1.51	2.76	0.838	0.995	0	1.01	0.993	1.00	0.999	10.0	27.6	1.3
MR14-07-1	—	—	246	280	—	—	17.3	0	0.779	1.30	1.00	*0.946*	0	1.01	*0.941*	1.00	1.00	20.0	—	—
MR16-01-1	A	a	44.6	216	2.730	0.1516	18.7	10	0.675	0.260	0.790	0.996	30	0.867	1.00	0.405	0.996	40.0	10.4	3.4
MR16-01-2	A	a	43.2	214	2.730	0.1516	21.3	10	0.620	0.554	0.771	0.998	5	0.921	*0.942*	0.935	0.999	15.7	—	—
MR16-02-1	—	—	42.3	240	2.718	0.1548	20.0	10	0.699	0.499	0.931	0.995	5	0.950	*0.930*	0.927	0.998	20.0	—	—
MR16-02-2	—	—	44.8	231	2.718	0.1548	18.7	10	0.648	0.533	0.773	0.996	5	0.947	0.981	0.929	0.997	15.7	8.37	1.0
MR16-03-2	—	—	46.8	233	2.613	0.1656	18.7	10	0.681	0.979	0.849	0.995	0	0.974	0.954	1.00	0.997	10.0	9.79	2.0
MR16-04-2	—	—	153	248	—	—	17.4	20	0.648	2.52	0.523	*0.984*	0	0.951	0.978	1.00	0.999	10.0	—	—
MR16-05-2	—	—	432	378	—	—	9.1	35	0.817	3.57	0.302	*0.984*	0	0.972	*1.06*	1.00	1.00	10.0	—	—
MR16-06-1	—	—	410	396	—	—	9.9	35	0.833	1.79	0.245	*0.985*	0	0.999	0.984	1.00	1.00	20.0	—	—
MR16-07-1	A	—	279	300	2.754	0.1019	16.0	40	0.667	1.01	0.255	0.995	10	1.02	*0.941*	0.882	1.00	40.0	—	—
MR16-07-2	A	—	428	417	2.754	0.1019	8.3	30	0.741	3.65	0.344	*0.991*	0	1.01	0.987	1.00	1.00	10.0	—	—

Table 2. (*Continued.*)

Sample ID	HT	LT	NRM_0	$ARM0_0$	B_{rc}/B_c	M_{rs}/M_s	LTD (per cent)	First heating H_L	First heating $Slope_A$	First heating $Slope_N$	First heating f_N	First heating r_N	Second heating H_L	Second heating $Slope_A$	Second heating $Slope_T$	Second heating f_T	Second heating r_T	F_L (μT)	F (μT)	ΔAIC
Moorea sequence B (17.50° S, 149.77° W)																				
MR18-07	E	c	—	—	1.869	0.1588	–	—	—	—	—	–	—	—	—	—	—	—	—	—
MR22-07-1	—	—	82.0	251	—	—	17.4	15	1.01	0.327	0.583	0.999	0	0.992	1.01	1.00	0.999	40.0	13.1	0.5
MR23-01-2	—	—	79.4	290	—	—	12.3	15	0.522	1.25	0.661	0.998	0	1.04	*0.921*	1.00	0.997	10.0	—	—
MR23-02-1	B	—	76.4	277	1.953	0.2008	13.8	10	0.600	0.285	0.726	0.998	0	1.02	0.994	1.00	0.999	40.0	11.4	−0.4
MR23-03-1	—	—	81.6	313	1.859	0.2019	10.7	15	0.655	0.487	0.426	0.995	0	0.981	0.959	1.00	1.00	20.0	9.74	−0.6
MR23-04-1	—	—	88.2	209	1.904	0.2686	11.5	10	0.743	0.714	0.931	0.999	0	0.985	1.02	1.00	0.999	20.0	14.3	17.2
MR23-05-1	—	—	79.8	215	1.877	0.2782	16.0	15	0.686	0.696	0.832	0.999	0	1.02	0.963	1.00	0.999	20.0	13.9	20.8
MR23-06-2	—	—	124	317	2.012	0.2650	15.0	20	0.585	1.57	0.749	0.996	0	1.02	0.979	1.00	0.999	10.0	15.7	−1.7
MR23-07-2	—	—	95.0	301	2.058	0.2722	10.7	20	0.609	0.656	0.760	0.995	0	1.02	1.00	1.00	0.999	20.0	13.1	−2.0
MR30-01-2	—	—	61.5	296	—	—	22.5	20	0.119	0.364	*0.108*	*0.950*	25	1.04	*0.881*	0.803	0.998	20.0	—	—
MR30-02-1	—	—	66.3	296	—	—	24.8	10	0.194	0.198	0.275	*0.985*	0	1.03	*0.870*	1.00	0.998	40.0	—	—
MR30-03-2	—	—	43.6	319	—	—	20.6	20	0.160	0.256	0.203	*0.964*	15	1.02	*0.847*	0.917	0.995	20.0	—	—
MR30-06-2	—	—	36.2	289	—	—	24.2	10	0.208	0.281	0.384	*0.984*	25	1.08	*0.866*	0.813	0.998	20.0	—	—
MR30-07-1	B	—	45.6	307	2.096	0.1554	22.5	10	0.231	0.126	0.335	*0.984*	25	1.04	*0.938*	0.829	0.999	40.0	—	—
MR32-01-1	—	—	104	348	1.798	0.3584	7.4	10	0.542	0.266	0.781	0.999	0	1.03	0.979	1.00	0.998	40.0	10.6	−0.4
MR32-02-1	—	—	103	382	1.951	0.3693	4.8	10	0.529	0.537	0.771	0.997	10	1.02	0.980	0.978	0.999	20.0	10.7	−1.1
MR32-03-1	—	—	111	382	1.824	0.3673	7.4	10	0.540	0.575	0.815	0.998	0	1.04	*0.930*	1.00	0.997	20.0	—	—
MR32-03-2	—	—	69.0	223	1.824	0.3673	8.3	15	0.551	1.30	0.827	0.996	0	1.03	1.04	1.00	0.996	10.0	13.0	0.3
MR32-04-2	—	—	159	372	1.828	0.3252	10.7	15	0.548	1.51	0.761	0.996	0	1.01	1.01	1.00	0.999	10.0	15.1	−0.3
MR32-05-2	—	—	172	397	1.928	0.3215	13.0	15	0.502	1.68	0.734	0.999	0	0.994	1.02	1.00	0.998	10.0	16.8	0.9
MR32-06-1	B	a	121	423	2.154	0.3271	11.5	10	0.506	0.296	0.907	0.996	5	1.01	1.05	0.995	0.999	40.0	11.8	−1.5
MR32-07-2	—	—	138	361	1.812	0.3084	12.3	20	0.407	1.47	0.493	0.996	0	1.00	1.00	1.00	0.999	10.0	14.7	6.4
Tahiti sequence A (17.63°S, 149.57°W)																				
PU01-01-2	—	—	132	585	1.617	0.3363	10.7	20	0.852	0.903	0.881	0.996	0	1.04	1.01	1.00	0.997	10.0	9.03	−0.7
PU01-02-1	—	—	122	570	—	—	8.3	20	0.735	0.389	0.865	*0.953*	0	1.03	0.993	1.00	0.998	20.0	—	—
PU01-03-2	—	a	157	596	1.523	0.3647	7.4	30	0.894	1.08	0.844	0.995	0	1.07	1.03	1.00	0.996	10.0	10.8	−0.2
PU01-04-1	A	a	117	568	1.686	0.2986	17.4	15	0.673	0.454	0.895	0.996	0	1.05	0.971	1.00	0.996	20.0	9.08	−0.6
PU01-06-1	—	—	149	480	1.504	0.3736	13.8	15	0.916	0.455	0.982	0.997	0	1.03	1.05	1.00	0.999	20.0	9.10	−1.5
PU01-07-1	—	—	62.8	447	—	—	8.3	30	0.311	0.385	0.727	*0.978*	0	1.00	0.990	1.00	*0.994*	20.0	—	—

Results are listed from top to bottom for each lava sequence. Note that palaeointensities from specimens with suffix ‘m’ are excluded as outliers in the calculation of the flow average.

[a]Not adopted for the calculation of the flow average (because of the possible low temperature oxidation suggested from the M_s–T curve of type E).

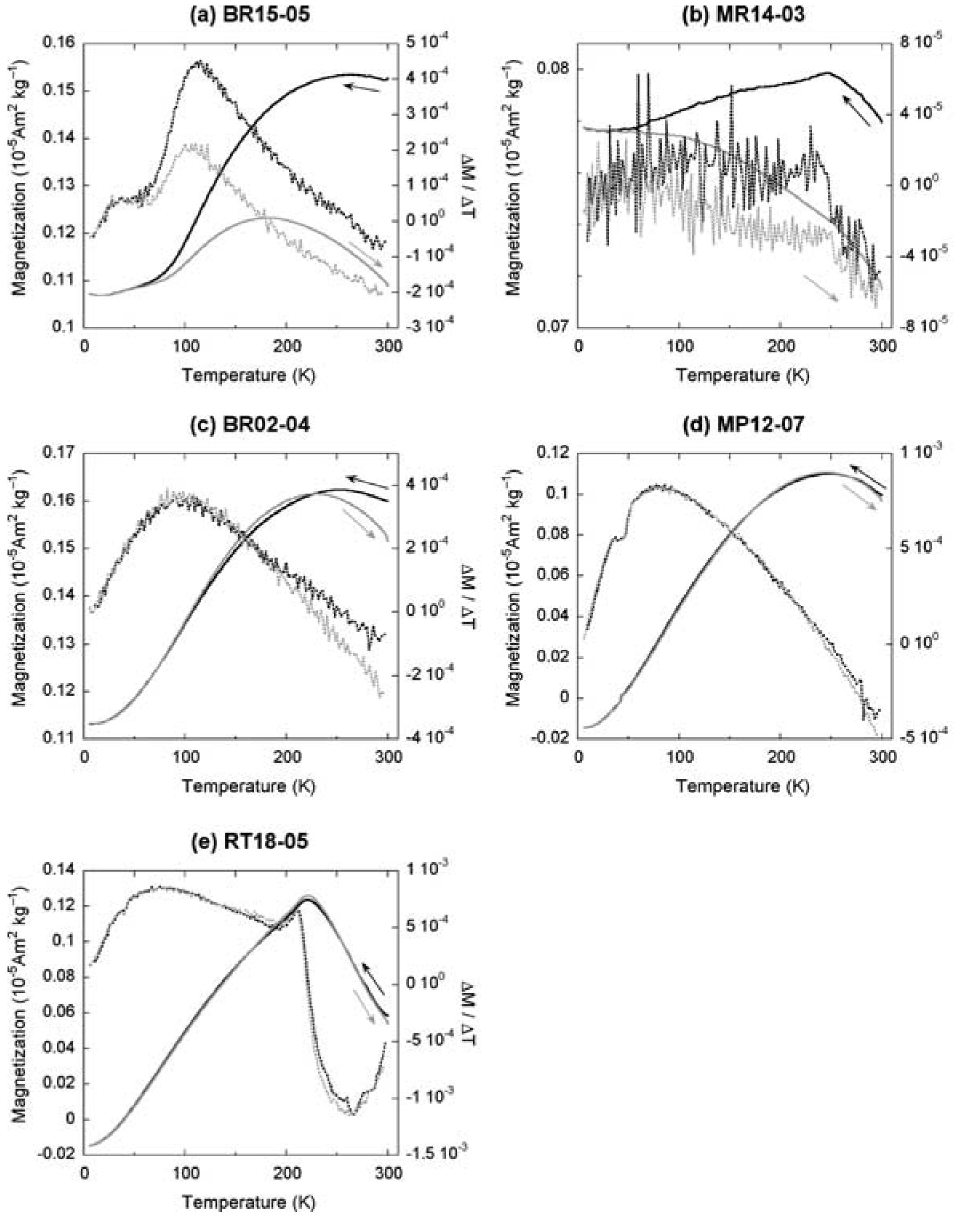

Figure 3. Results of low-temperature magnetometry. Solid and broken curves indicate magnetizations and their derivatives during low-temperature cycling of 300 K SIRM, respectively (black, cooling; grey, warming). The results are grouped into five types.

3.3 Hysteresis properties

Hysteresis parameters of saturation magnetization (M_s), remanent saturation magnetization (M_{rs}), coercivity (B_c) and remanent coercivity (B_{rc}) were measured for 726 small chips from selected palaeomagnetic cores. Measurements were performed on several chips for each core, three on average, by the VSM at room temperature. Core-averaged hysteresis parameters are listed in Tables 1 and 2. The Day plot (Day *et al.* 1977; Dunlop 2002) is also shown in Fig. 4.

Basically, the Day plot was empirically established for titanomagnetite solid solutions (Day *et al.* 1977). The present samples mostly fulfilled this condition (Section 3.1). One might think that some superparamagnetic contributions (e.g. Fig. 2F) would make artificial deviations in hysteresis parameters resulting in non-conformity of the Day plot. However, if theoretical mixing models such as that of Dunlop (2002) are referred to, the deviations can be used for semiquantitative estimation of the superparamagnetic contributions, and the Day plot makes sense. The hysteresis parameters seem to have been used as basic descriptors of samples in recent rock magnetic and palaeomagnetic studies. We think that the parameters determined in this study will be useful for future re-evaluation of palaeointensities.

Fig. 4 shows that data points of the present results are generally distributed between two theoretical mixing lines: SD (single domain)–MD (multidomain) and SP (superparamagnetic)–SD curves (Dunlop 2002). Remanence carriers in the measured samples are considered to consist of various grain sizes, probably an admixture of SD (and/or PSD) and MD. This is also suggested from results of reflected-light microscopy described in the next subsection.

A small number of the data points show $M_{rs}/M_s > 0.5$, indicating the existence of nearly equidimensional titanomagnetites governed by magnetic crystalline anisotropy. However, this may be an experimental artefact, since these data mainly come from samples with

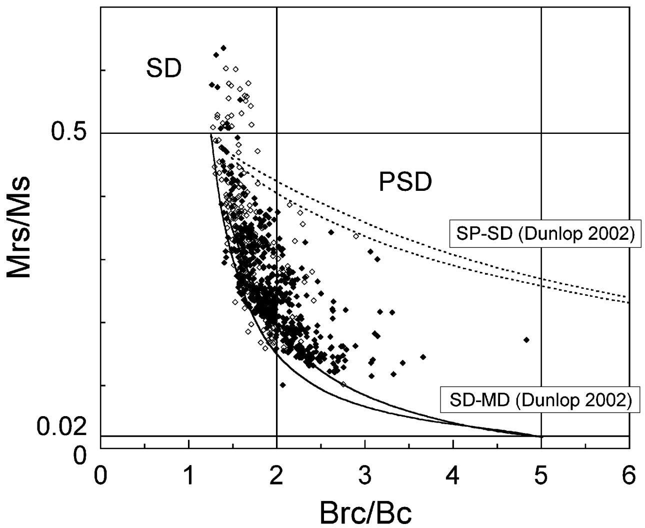

Figure 4. Day plot (Day *et al.* 1977) for the hysteresis parameters of 726 small chips from selected palaeomagnetic cores. Some threshold values are modified following Dunlop (2002). Closed symbols indicate hysteresis parameters for which the parent cores give successful palaeointensities in the LTD-DHT Shaw experiments. Open symbols correspond to the parameters for the unsuccessful ones. It is seen that the data points generally distribute between the theoretical SD–MD and SP–SD curves of Dunlop (2002).

M_s–T curves of type E (Tables 1 and 2), which characterizes the possible existence of a small amount of titanomaghemite. In the hysteresis measurements, a saturation field was set to be 1 T, which might not be sufficient to saturate magnetizations by Ti-poor titanomaghemites. In this case, M_s can be underestimated. Resulting values of M_{rs}/M_s can exceed 0.5 even for samples governed by shape anisotropy.

3.4 Reflected-light microscopy

Recent studies involving reflected-light microscopy have revealed that intermediate high-temperature oxidation states of titanomagnetite grains are related to erroneously high palaeointensities measured by the Thellier method (Yamamoto *et al.* 2003; Mochizuki *et al.* 2004; Oishi *et al.* 2005). Although there are some possible reasons for this relationship, it is important to examine high-temperature oxidation states in checking the quality of palaeointensity results. Therefore, we observed titanomagnetite grains in polished sections from about 50 palaeomagnetic cores.

The titanomagnetite grains in the present samples show a wide range of high-temperature oxidation states. According to the classifications by Haggerty (1991), seven stages are defined as follows:

C1: Optically homogeneous ulvöspinel-rich magnetite solid solutions (ss).

C2: Magnetite-enriched ss with a small number of ‘exsolved’ ilmenite lamellae parallel to $\{111\}$ of the host.

C3: Ti-poor titanomagnetite ss with densely crowded ‘exsolved’ ilmenite lamellae parallel to $\{111\}$.

C4: The first sign of additional oxidation. Optically, an indistinct mottling of the ilmenomagnetite intergrowth is observed.

C5: Rutile and titanohaematite develop extensively within the ‘exsolved’ meta-ilmenite lamellae

C6: Incipient formation of pseudo-brookite (Psb) ss from rutile plus titanohaematite.

C7: Assemblage of Psb ss plus haematite ss. This is the most advanced stage of oxidation of original spinels.

Some sections show both low (C1–C2) and high (C6–C7) oxidation states (e.g. Figs 5A and D), whereas more than half of the sections contained intermediately oxidized (C3–C4) titanomagnetite grains (e.g. Figs 5B and C). According to Yamamoto *et al.* (2003), Mochizuki *et al.* (2004) and Oishi *et al.* (2005), in the Thellier experiments, samples with an intermediate high-temperature oxidation state possibly give anomalously high palaeointensities. Note that these studies employed the oxidation indices of Wilson & Watkins (1967), which are defined as six stages, I–VI. Even for such samples, they confirmed that the LTD-DHT Shaw method was applicable and yielded almost the correct values. In this context, the LTD-DHT Shaw method is preferable for determining palaeointensities from the present samples.

4 PALAEOINTENSITIES BY THE LTD-DHT SHAW METHOD

4.1 Method

As reviewed in Yamamoto *et al.* (2003), the Shaw-type palaeointensity technique has been subject to criticism. We have therefore developed a fairly improved version of the original Shaw method (Shaw 1974), i.e. the LTD-DHT Shaw method (Tsunakawa *et al.* 1997; Yamamoto *et al.* 2003). The main procedures involved in this method are as follows (see Yamamoto *et al.* 2003, for details):

(1) A specimen is subjected to LTD. Then its memory of natural remanent magnetization (NRM) is subjected to the stepwise alternating-field (AF) demagnetization [NRM].

(2) Anhysteretic remanent magnetization (ARM) is given to the specimen and subsequently subjected to stepwise AF demagnetization [ARM00].

(3) ARM is imparted again under the same conditions as ARM00. LTD is conducted on the remanence and its memory is measured with the stepwise AF demagnetization [ARM0].

(4) The specimen is heated for acquisition of the first thermoremanent magnetization (TRM). The same procedures as in steps (1), (2) and (3) are performed for the TRM [TRM1] and ARMs [ARM10 and ARM1].

(5) The specimen is again heated for the second TRM. The same procedures as in steps (1), (2) and (3) are repeated for the TRM [TRM2] and ARMs [ARM20 and ARM2].

This method utilizes individual ARM corrections (Rolph & Shaw 1985), a double heating test (Tsunakawa & Shaw 1994) and low-temperature demagnetization. We can measure palaeointensities from SD-like remanences because the LTD treatment is known to be effective for erasing the MD-like component of Ti-poor titanomagnetites (e.g. Ozima *et al.* 1964; Heider *et al.* 1992). Borradaile *et al.* (2004) recently showed the usefulness of a LTD–AF combined demagnetization technique for isolation of a stable magnetic vector. The validity of the individual ARM corrections was experimentally assessed by Yamamoto *et al.* (2003), Pan *et al.* (2002, 2003) and Mochizuki *et al.* (2004).

The LTD-DHT Shaw method is likely to have following additional advantages:

(1) This method fits well with LTD treatment for the isolation of stable magnetization. Only six (or nine) treatments in total are required for a specimen. If similar procedures are involved in a Thellier-type experiment we have to repeat the treatment at every heating step, at least 20 times for a specimen.

(2) No laboratory CRM (chemical remanent magnetization) contaminates the NRM. This is because full demagnetization of NRM

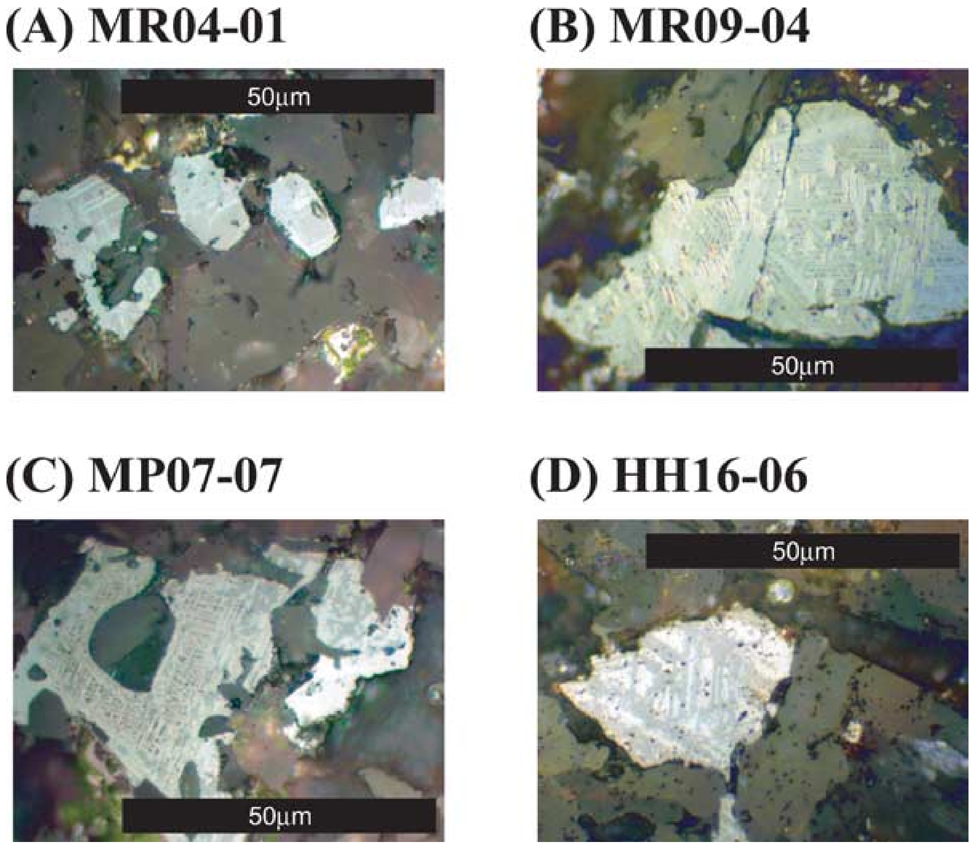

Figure 5. Representative examples of reflected-light microscopy of samples: (A) the core MR04-01, C2–C3 oxidation; (B) MR09-04, C4–C5; (C) MP07-07, C4–C7; (D) HH16-06, C7. These classifications follow Haggerty (1991).

is done prior to the first laboratory heating which produces 'TRM1'. This certifies the fidelity of the palaeodirection if LTD and AF demagnetization can remove secondary components. In Thellier-type experiments, NRM is often contaminated by CRM during progressive laboratory heating (e.g. Mochizuki *et al.* 2004).

(3) The laboratory heating process is thought to be analogous to a natural process (Oishi *et al.* 2005). In contrast to progressive heating in Thellier-type experiments, samples are directly heated above the Curie temperature and cooled down to room temperature.

(4) One of two endpoints for linear segments in NRM–TRM1* diagrams is fixed to steps of maximum AF (TRM1* being the corrected TRM1). This reduces ambiguities in the calculation of palaeointensity. Both endpoints of the linear segments in Arai diagrams are selectable, which allows for more ambiguity in Thellier-type experiments.

(5) A series of measurements can be easily automated since the procedures of the LTD-DHT Shaw method mainly consist of progressive AF demagnetizations. We use an automated spinner magnetometer with an AF demagnetizer (Natsuhara-Giken Dspin-2; Kono *et al.* 1984, 1997). A SQUID magnetometer equipped with an automated AF demagnetizer is also available.

4.2 Experiments and data analysis

In the present study, a total of 361 specimens were used in LTD-DHT Shaw experiments. They were heated in a vacuum (10-10^2 Pa) at a top temperature of 610 °C for 20 and 30 min (first and second heatings, respectively). Laboratory TRM was imparted in a 5.0–50.0 μT DC field while ARM was imparted in a 100 μT field. Progressive AF demagnetization was performed at 5–10 mT intervals up to 160 mT. In the LTD treatment, specimens were soaked in liquid nitrogen in a plastic Dewar for 10 min and then kept outside at room temperature for an hour. This cycle was performed in a magnetically shielded case where the residual field was less than 100 nT. All remanences were measured with an automated spinner magnetometer (Natsuhara-Giken Dspin-2).

For constructions of NRM–TRM1* and TRM1–TRM2* diagrams, TRMs were corrected with the technique of Rolph & Shaw (1985) (corrected TRMs being denoted TRM1* and TRM2*, respectively). This correction is based on the assumption that changes in the TRM coercivity spectra can be followed by those of ARM.

Similar to the previous studies by Yamamoto *et al.* (2003), Mochizuki *et al.* (2004) and Oishi *et al.* (2005), the results are judged by the following quantitative selection criteria:

(1) The primary component is recognized in the Zijderveld diagram.

(2) There should be a linear portion in the NRM–TRM1* diagram. This should not be less than 15 per cent of the original NRM intensity ($f_N \geq 0.15$), and its correlation coefficient should be larger than 0.995 ($r_N \geq 0.995$).

(3) The linear portion ($f_T \geq 0.15$ and $r_T \geq 0.995$) also should exist in the TRM1–TRM2* diagram. Its slope is unity within experimental error ($1.05 \geq \mathrm{Slope}_T \geq 0.95$).

(4) Both linear portions should include the maximum AF demagnetization steps.

Criterion (4) is implicitly involved in the previous studies. A schematic view of the data analysis is illustrated in Fig. 6.

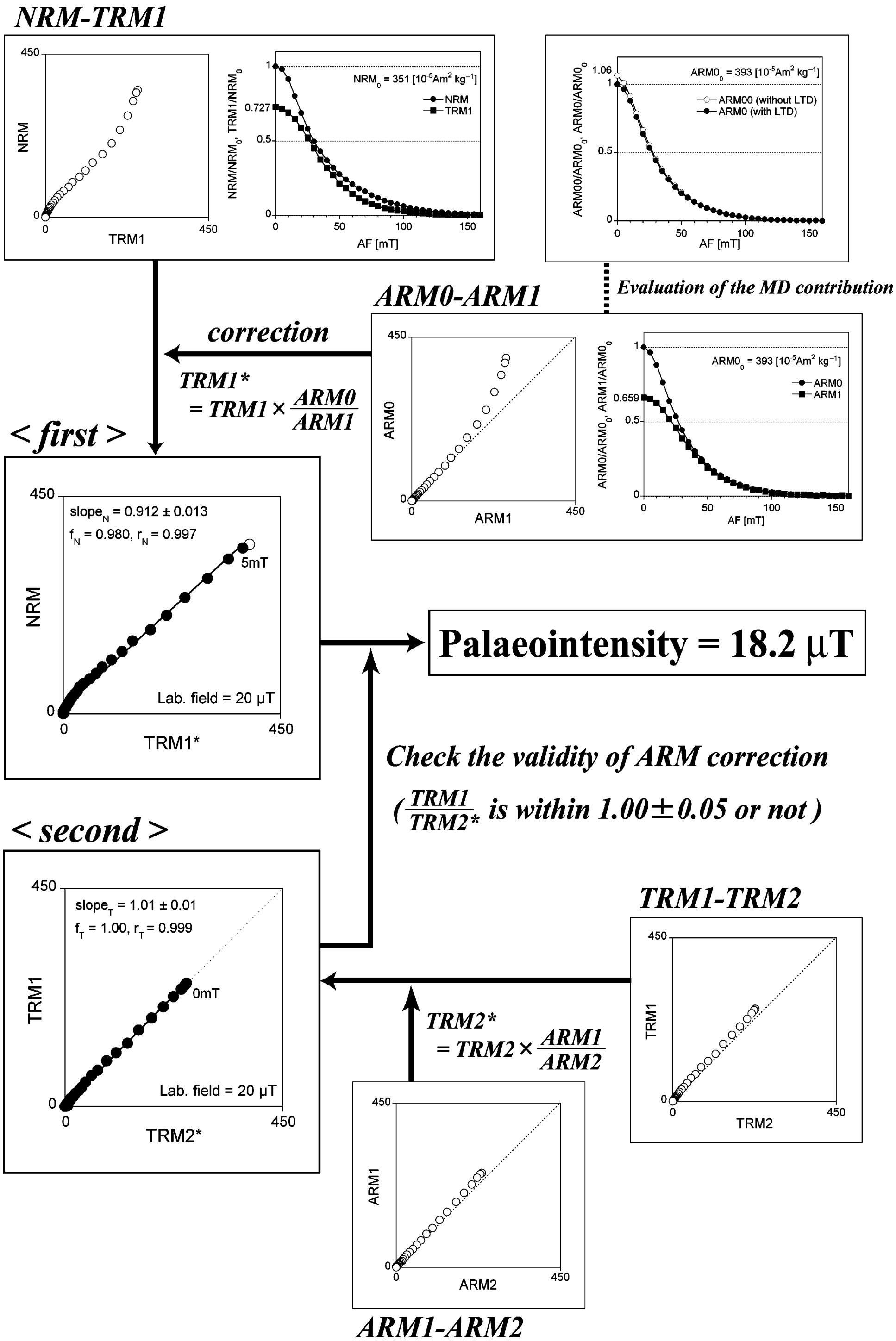

Figure 6. Schematic view of the data analyses for the LTD-DHT Shaw experiments. These figures illustrate example calculations for the results of (A) HH09-04-1 and (B) BR15-05-1 with Types A and B thermomagnetic curves, respectively. Refer to Yamamoto *et al.* (2003) for detailed experimental procedures. Note that the remanences shown in these figures are values after vectorial subtraction of the remanences at 160 mT (maximum AF step). Thus, values of NRM_0 indicated in these figures do not necessarily correspond to those in Tables 1 and 2.

4.3 Results

Comparing magnitudes of ARM0 before and after the LTD treatment, we can roughly estimate the MD contributions for the present samples. Fig. 7 shows a distribution of the LT-demagnetized fractions in ARM0. Since most samples exhibit 0–20 per cent loss of ARM0, the MD contribution should not cause serious problems in the palaeointensity experiments. However, 25 specimens show more than 20 per cent loss up to 31.5 per cent by the LTD treatment, resulting in the effective removals of undesirable remanences.

Applying the quantitative selection criteria described in the previous subsection, we obtained 195 successful results (a success rate of 54 per cent). Representative results are shown in Fig. 8. The remaining 166 results were rejected, mainly because (1) linear

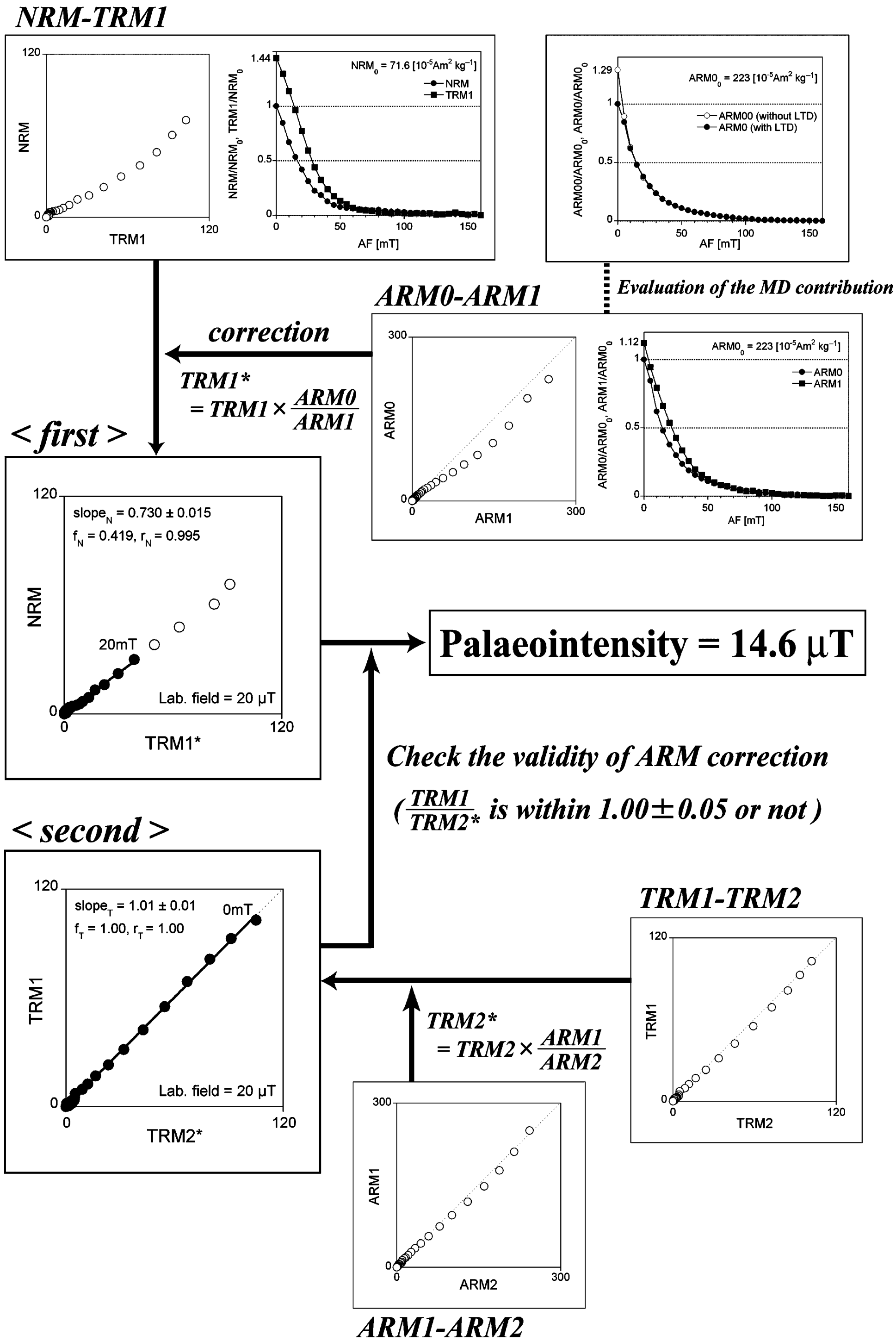

Figure 6. (*Continued*.)

portions were not detected in the NRM–TRM1* diagrams ($r_N < 0.995$; e.g. Figs 9A and C) and (2) slopes of linear portions in the TRM1–TRM2* diagrams were not unity ($\mathrm{Slope_T} < 0.95$ or $1.05 < \mathrm{Slope_T}$; e.g. Figs 9A and B). These results are summarized in Tables 1 and 2.

The successful results exhibit good linearity in both NRM–TRM1* and TRM1–TRM2* diagrams (Fig. 8). As most of their linear portions are associated with $f_N \geq 0.30$ and $f_T \geq 0.90$ (Fig. 10), those palaeointensities are obtained from relatively large fractions of the original NRMs and the ARM correction is fairly applicable for laboratory TRMs. The obtained palaeointensities are thought not to be systematically influenced by the ARM correction because there is no obvious correlation between the measured palaeointensities and the slopes in the corresponding ARM0–ARM1 diagrams (Fig. 11A). The palaeointensities are also independent of the hysteresis properties (Figs 11B and C), suggesting no effect of grain size of magnetic minerals on the present results.

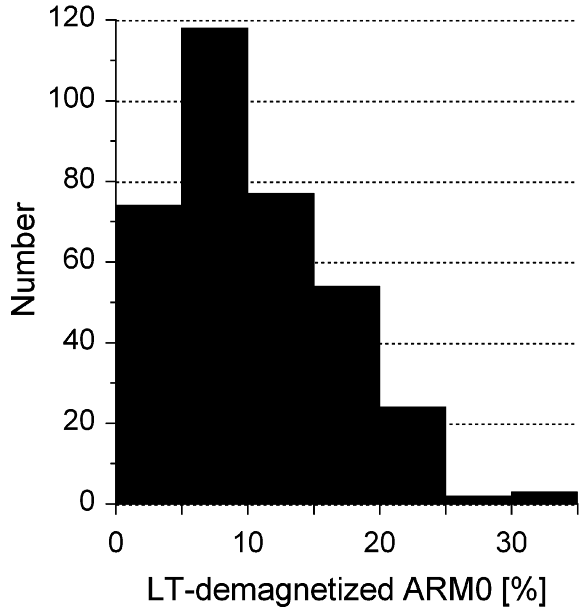

Figure 7. A histogram of LT-demagnetized fractions in ARM0 for the LTD-DHT Shaw experiments. The demagnetized ratios are expressed as remanence decrease after LTD to the original.

A noticeable feature in the present results is that samples collected from site PU06 show similar failures in the LTD-DHT Shaw experiments. Zijderveld diagrams clearly showed the existence of a single component, and TRM1–TRM2* diagrams guaranteed reproducible laboratory TRMs. Slopes of unity in ARM0–ARM1 diagrams indicate little occurrence of laboratory alteration in remanence carriers. In spite of these favourable features, all NRM–TRM diagrams showed convexity (e.g. Fig. 9C). These facts suggest that NRMs of PU06 may not have entirely originated from thermoremanent magnetizations. Other types of remanence, like thermochemical remanent magnetization (TCRM), were possible 'contaminants' during initial cooling in nature (e.g. Yamamoto *et al.* 2003). Indeed, sister specimens subjected to Thellier experiments gave two-sloped Arai diagrams (see Figs 18J and K). This evidence implies that the LTD-DHT Shaw method offers a possible way to discriminate natural TCRM, as suggested by Yamamoto *et al.* (2003). An interesting fact observed in these PU06 specimens is that there are many pseudo-brookite grains (C6–C7 oxidation, e.g. Fig. 12A). The existence of pseudo-brookites has been believed to validate true TRM (Dunlop & Özdemir 1997), but the present study yields an exceptional case. Since C4-class oxidation grains simultaneously occur in the PU06 specimens (e.g. Fig. 12B), they might be a source of the non-ideal behaviour in both the LTD-DHT Shaw and Thellier experiments.

5 PALAEOINTENSITIES BY THE THELLIER METHOD

5.1 Experiments and data analysis

Coe's version of the Thellier method (Coe 1967) was applied to 40 specimens of good thermal stability (Types A and B in Section 3.1; Fig. 2). These results can be compared with the companion LTD-DHT Shaw results because their sister specimens have already given successful palaeointensity results in the LTD-DHT Shaw experiments.

In the Thellier experiments, the specimens were subjected to a series of zero-field and in-field heating cycles at 20–50 °C intervals up to 600 °C. Partial TRM checks were conducted at every other temperature step. Above 200 °C, at least one pTRM-tail check (Riisager & Riisager 2001) step was involved for every 100 °C interval, that is, at least five pTRM-tail checks for each specimen. This check detects a vectorial difference between the pTRM tail of laboratory-produced pTRM and the pTRM tail that is embedded in TRM (e.g. Shcherbakova *et al.* 2000; Riisager *et al.* 2004). The heating cycle was done in air for 1–1.5 hr with a TDS-1 (Natsuhara-Giken) or MMTD-18 (Magnetic Measurements) electric furnace. TRM was imparted in a DC field of 15.0–30.0 μT, which was applied throughout the in-field cycles. All remanent magnetizations were measured by a SMM-85 or ASPIN (Natsuhara-Giken) spinner magnetometer with a resolution better than $\pm 10^{-8}$ A m^2.

Although selection criteria for the Thellier experiments differ in previous studies, we adopted the following:

(1) A stable primary component is recognized in the Zijderveld diagram of zero-field step data (NRM).

(2) A linear portion should be recognized in the Arai diagram. It is composed of the primary component and is not less than 15 per cent of the original NRM ($f \geq 0.15$). This portion should have four or more data points ($N \geq 4$).

(3) The linear portion should exhibit positive pTRM checks. This is judged by an agreement between reproduced pTRM and first TRM at the 2σ level. The error (σ_{pTRM}) is evaluated from experimental uncertainties of remanence measurements (σ_{meas}), heating temperatures (σ_{temp}) and applied DC fields (σ_{DC}), i.e. $\sigma_{\mathrm{pTRM}}{}^2 = \sigma_{\mathrm{meas}}{}^2 + \sigma_{\mathrm{temp}}{}^2 + \sigma_{\mathrm{DC}}{}^2$.

For the pTRM tail checks, accordance between the first and repeated zero-field data was examined at the 2σ level. However, their usefulness is still under debate (e.g. Biggin & Thomas 2003a). Yu *et al.* (2004) showed that a proper pTRM tail check could be made only when a laboratory field was twice as large as an ancient field and was applied parallel to a NRM direction. A laboratory field perpendicular to the NRM results in an overestimated pTRM tail, while a field antiparallel to the NRM causes underestimation. We do not incorporate the results of the pTRM tail checks in the selection criteria.

5.2 Results and discussions

Successful results were obtained for 18 specimens (Table 3). Fifteen results showed quality factors q (Coe *et al.* 1978) of more than 5.0, indicating good Thellier results. The successful results can be classified into following three types.

The first type is characterized by Arai diagrams with a single slope (Figs 13A and B). This type is observed for four specimens, TA15-01-2, MR14-03-2, PU01-03-4 and PU01-06-2. Although the Arai diagram of TA15-01-2 (Fig. 13B) appears to be two-segmented, the low blocking temperature range is probably contaminated by secondary magnetization. These palaeointensities are generally consistent with those of the sister specimens by the LTD-DHT Shaw method.

A feature of the second type of result, from 11 specimens, is two segments in the Arai diagrams (Fig. 13C). Slopes of the low blocking temperature (T_{B}) portion gave high palaeointensities whereas those of the high T_{B} yielded low palaeointensities. The differences in palaeointensities between the two segments are up to about eight times (187 and 22.9 μT in HH16-03-2). It is noted that palaeointensities from the high T_{B} portion are not far from the LTD-DHT Shaw palaeointensities of the sister specimens.

Three specimens resulted in the third type of result, where only a single slope is seen in the Arai diagrams. They show incompatible

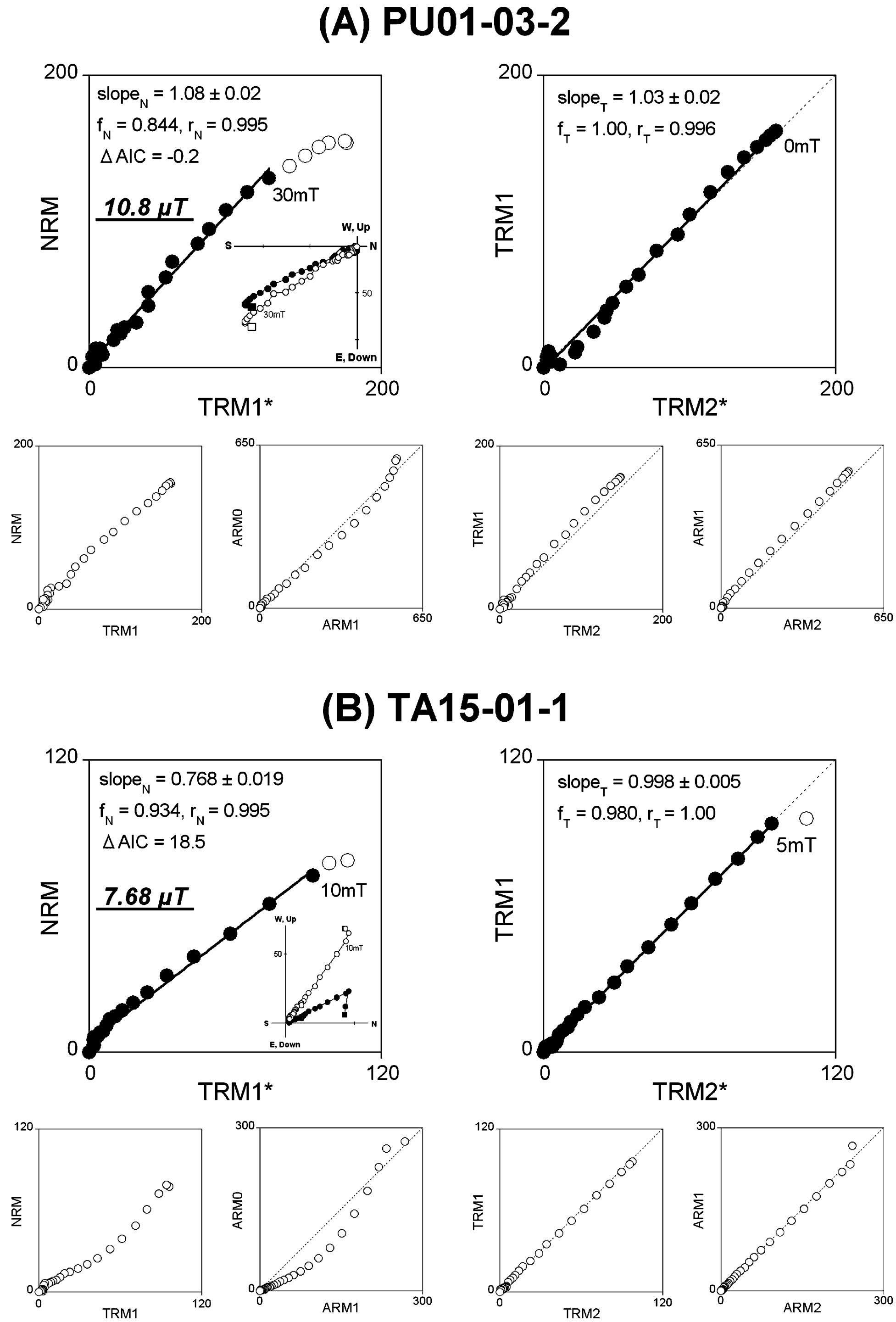

Figure 8. Representative successful results in the LTD-DHT Shaw experiments. (A) PU01-03-2 from Tahiti. (B) TA15-01-1 from Tahaa. (C) HH16-06-1 and (D) HH09-04-1 from Huahine. The left three diagrams indicate results from the first laboratory heating while the right ones are from the second heating. Linear portions consist of closed symbols. Zijderveld diagrams are also shown as insets, where closed and open symbols indicate projections onto horizontal and vertical planes, respectively (squares are NRM before LTD). Units are 10^{-5} A m^2 kg^{-1}. The Thellier results for the sister specimens are shown in Fig. 13.

palaeointensity with the companion LTD-DHT Shaw results. However, if we take alternative slopes in the high T_B portions (e.g. the dotted line in Fig. 13D) with insufficient data points ($N = 3$) they give apparent palaeointensities consistent with the LTD-DHT Shaw results.

In summary, the present Thellier experiments mainly exhibit two-sloped Arai diagrams, which are a possible cause of overestimated palaeointensities (e.g. Yamamoto *et al.* 2003). Overestimations by the Thellier method may also be suggested from the hysteresis parameters of the core-averaged values for the specimens used for palaeointensity determination in the Thellier experiments (Fig. 14). It is obvious that the data points in the Day plot are distributed close to the mixing lines between the SD and MD of Dunlop (2002). Oishi *et al.* (2005) suggest that samples with data points close to SD–MD

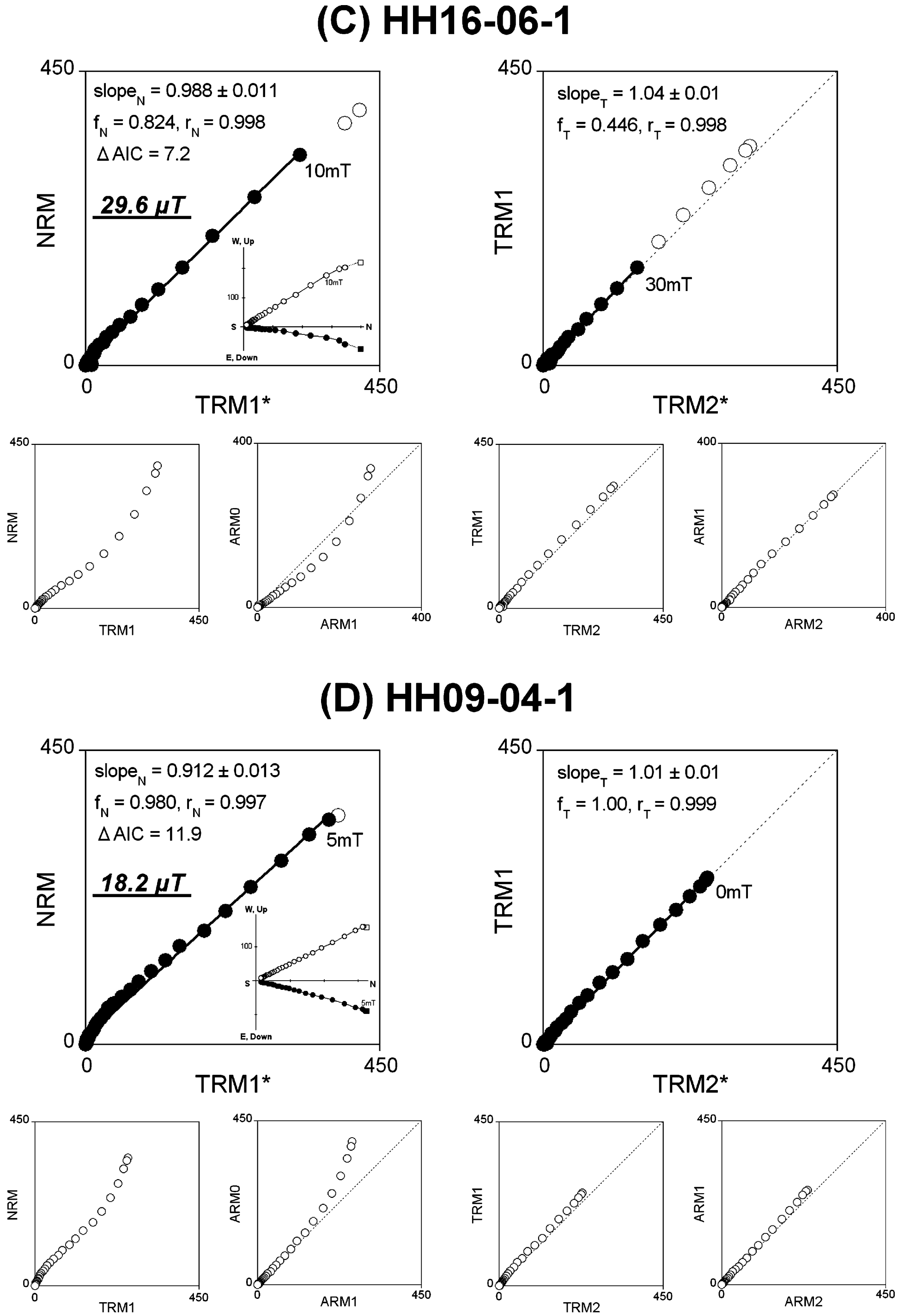

Figure 8. (*Continued*.)

mixing lines tend to give erroneously high palaeointensities by the Thellier method.

However, routine application of the above criteria could not filter out the erroneous results. Anomalously high palaeointensities may be observed especially from the low T_B portion of the second type. A stringent criterion of $q \geq 5.0$, which is often adopted (e.g. Mochizuki *et al.* 2004), could not reject very high palaeointensities (e.g. 145 μT in HH16-06-3 and 167 μT in PU06-04-3). Although the best way to avoid contamination of such anomalous data is probably to discard all the two-segmented results (e.g. Valet 2003), this procedure results in the loss of a large number of the present palaeointensity estimations. Only four results of the first type remain. There is another criterion of $f \geq 0.50$ suggested by Biggin & Thomas (2003a). If we add this criterion, 13 results survive. These palaeointensities, except for BR15-02-2 and HH09-04-2, seem to be improved (closed circles in Fig. 15). Even for BR15-02-2 and HH09-04-2, if their alternative segments of high T_B (discarded due to $f < 0.50$) are adopted, they also become closer to the LTD-DHT Shaw results (open circles in Fig. 15). Discrepancies between the Thellier and the LTD-DHT Shaw data are up to about 40 per cent, which is similar to the results

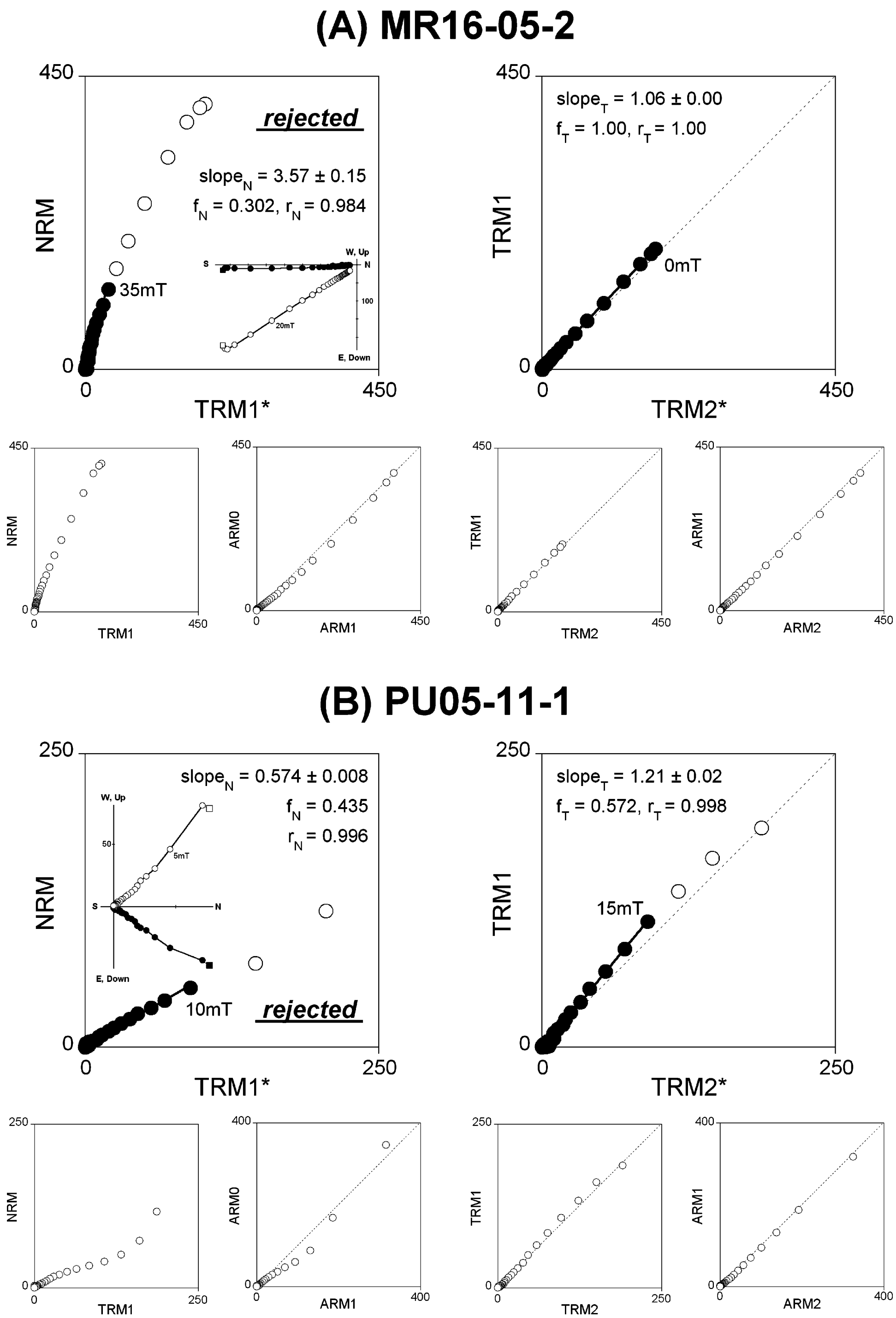

Figure 9. Examples of rejected results in the LTD-DHT Shaw experiments. (A) MR16-05-2 from Moorea. (B) PU05-11-1 and (C) PU06-04-1 from Tahiti. These do not pass the quantitative selection criteria because of (A) a low correlation coefficient ($r_N = 0.984$) in the first heating as well as a non-unity slope ($\mathrm{Slope_T} = 1.06$) in the second heating, (B) a non-unity slope ($\mathrm{Slope_T} = 1.21$) in the second heating and (C) a low correlation coefficient ($r_N = 0.936$) in the first heating.

found for historical lavas by Yamamoto *et al.* (2003), Mochizuki *et al.* (2004) and Oishi *et al.* (2005).

6 EVALUATION OF THE LTD-DHT SHAW PALAEOINTENSITIES

We have obtained 195 successful LTD-DHT Shaw palaeointensities using the quantitative selection criteria (Section 4.3). These criteria seem to be able to reject a majority of the undesirable results, but the reliability of the selected results will be further examined from several aspects.

6.1 Low-temperature oxidation

As discussed in Section 3.1, some samples possibly suffered from low-temperature oxidation. They might give biased

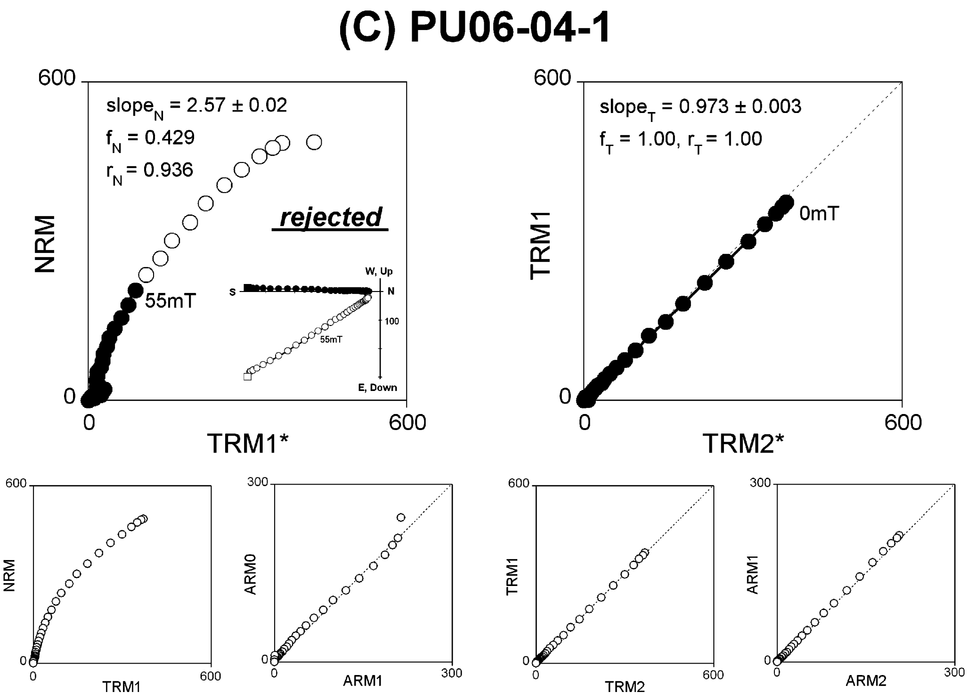

Figure 9. (*Continued*.)

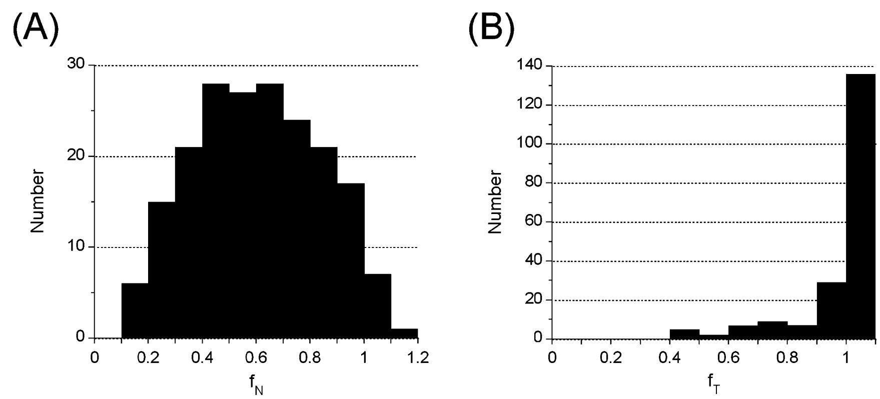

Figure 10. Histograms of (A) NRM fractions (f_N) and (B) TRM fractions (f_T) for the successful LTD-DHT Shaw results.

palaeointensities. Although the thermomagnetic experiments suggest low degrees of low-temperature oxidation (e.g. Fig. 2E), for safety's sake we do not use the 31 palaeointensities from seven flow units (MP19, BR02, HH05, HH06, HH08, HH12, and MP12) in calculations of flow averages.

6.2 Applicability of the ARM correction

Samples from sites BR10 and BR16 show curved NRM–TRM1* diagrams, high B_c portions of which pass the quantitative selection criteria (e.g. Fig. 16). As their Zijderveld diagrams suggested single primary components, their curvature could not be caused by secondary magnetization. For example, in Fig. 16, a NRM–TRM diagram obviously shows a downward concave feature for $B_c \geq 10$ mT (which is sufficient to remove a secondary magnetization), but the corresponding portion in a ARM0–ARM1 diagram gives nearly a straight line. This suggests that ARM changes in the first laboratory heating may not follow TRM changes for some samples. Pan *et al.* (2003) observed similar NRM–TRM* diagrams from samples with heavy laboratory alterations (e.g. C20 in Fig. 1 of Pan *et al.* 2003). If we adopt a possible linear segment from sample C20 in Pan *et al.* (2003), it gives 30 per cent lower palaeointensity than the true field value (50 μT). Therefore, the palaeointensities obtained from sites BR10 and BR16 might be biased, although our specimens did not seem to suffer from such alterations. These nine results are temporarily not used for calculations of flow averages.

6.3 Upward convex features in the NRM–TRM1* diagrams

A number of the successful LTD-DHT Shaw results show some convexity in the NRM–TRM1* diagrams. An evaluation of the convexity is vague regarding the criterion of correlation coefficients. For example, TA15-01-1 and HH09-04-1 passed the criterion, but their high B_c intervals in the NRM–TRM1* diagrams exhibited upward convex features (Figs 8B and C). In the usual Thellier experiments, downward concave features are often observed in Arai diagrams, and there is growing consensus that the palaeofield should not be

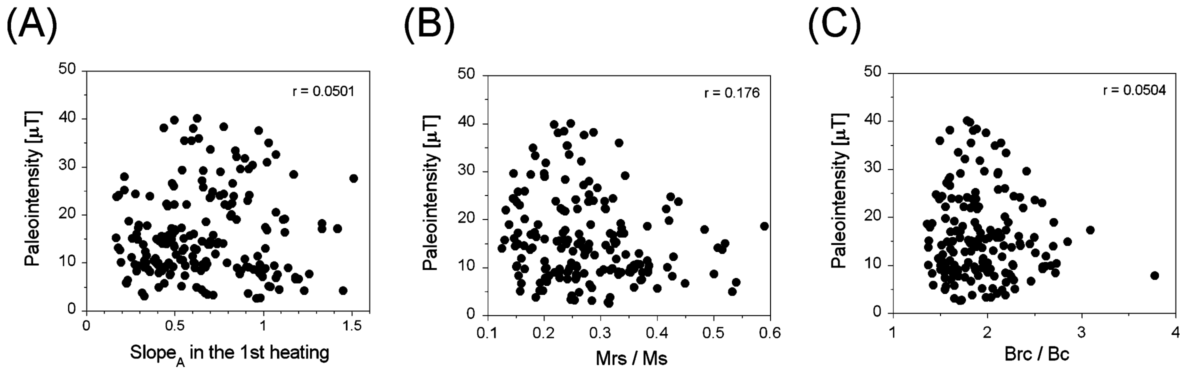

Figure 11. Relation between the LTD-DHT Shaw palaeointensities and (A) slopes in the ARM0–ARM1 diagrams (Slope$_A$ in the first heating), (B) ratios of remanent saturation magnetization to saturation magnetization (M_{rs}/M_s) and (C) ratios of remanent coercivity to coercivity (H_{rc}/H_c). Correlation coefficients (r, absolute values) are shown in each diagram.

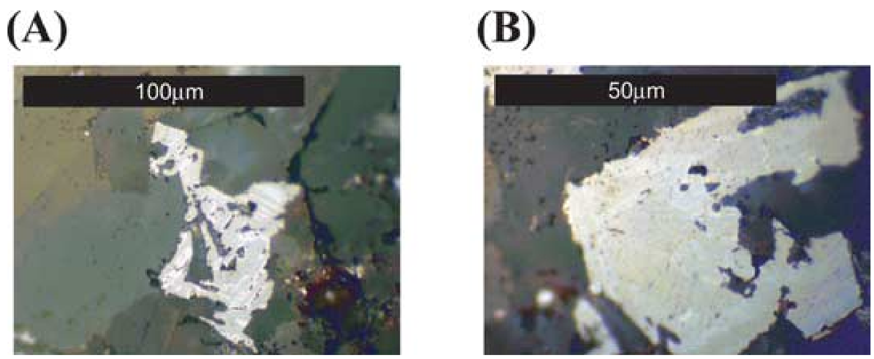

Figure 12. Reflected-light microscopy for the palaeomagnetic core of PU06-04: (A) C7-class oxidation grain, (B) C4-class oxidation grain.

estimated using such diagrams (e.g. Valet 2003). We may apply similar cautions to the present LTD-DHT Shaw results.

6.3.1 Introduction of the Akaike information criterion (AIC)

One of the ways to evaluate the convexity is to introduce the Akaike information criterion (AIC; Akaike 1980). This allows statistical estimation of an optimal model from candidates by a trade-off between goodness of fit data and a number of parameters. The smaller the value of the AIC, the better the model is. If a linear and a quadratic polynomial are introduced as regression functions for the NRM–TRM1* diagrams, their AICs are defined as follows:

$$\mathrm{AIC1} = N \times \left(\ln 2\pi + 1 + \ln \frac{{\chi_1}^2}{N}\right) + 2 \times (1+2), \tag{1}$$

$$\mathrm{AIC2} = N \times \left(\ln 2\pi + 1 + \ln \frac{{\chi_2}^2}{N}\right) + 2 \times (2+2), \tag{2}$$

where N is the number of data points and χ_1 and χ_2 are residuals of the linear and the quadratic fit for the NRM–TRM1* diagrams, respectively. Thus, a difference in the AIC between the linear and quadratic fits (ΔAIC) is

$$\Delta\mathrm{AIC} = \mathrm{AIC1} - \mathrm{AIC2} = N \times \ln \frac{{\chi_1}^2}{{\chi_2}^2} - 2. \tag{3}$$

If $\Delta\mathrm{AIC} \leq 1$, the quadratic fitting is statistically not better than the linear one, suggesting no convexity in the diagram. ΔAICs are calculated for all the NRM–TRM1* diagrams of the successful results (195 specimens). They are listed in Tables 1 and 2, and their distribution is illustrated in Fig. 17. Sixty-nine results show $\Delta\mathrm{AIC} \leq 1.0$, indicating that the quadratic fit is not preferred. The other results seem to prefer the quadratic fit. For instance, ΔAICs of TA15-01-1 and HH09-04-1 were 18.5 and 11.9 (Fig. 8B and C). As stated before, their NRM–TRM1* diagrams appeared to be upward convex especially for the high-B_c portions. On the other hand, PU01-03-2 yielded ΔAIC of −0.2 for its NRM–TRM1* diagram without obvious convexity (Fig. 8A). Possible causes of the convexity are discussed in the following section.

6.3.2 LTD-Thellier experiments

The convexity observed in the NRM–TRM1* diagrams may be analogous to concavity in the Arai diagrams often reported from the usual Thellier experiments. Since LTD-DHT Shaw results cannot be directly compared with Thellier results because of the LTD treatment, we further conducted LTD-Thellier experiments (e.g. Yamamoto *et al.* 2003) on four specimens (MP05-05-3L, MP07-07-3L, HH09-07-4L and PU06-04-4L). All of their sister specimens had already given palaeointensities using the Coe (1967) version of the Thellier method (MP05-05-2, MP07-07-2, HH09-07-3 and PU06-04-3). The LTD-DHT Shaw experiments yielded three successful palaeointensities (MP05-05-1, MP07-07-1 and HH09-07-2). PU06-04-1, which is the sister specimen of PU06-04-4L, unfortunately did not pass the criteria. Fig. 18 illustrates all the results obtained using the Coe (1967) version of the Thellier method with and without LTD, and by the LTD-DHT Shaw method. Noticeable features in these diagrams are that all the Thellier results show two-segmented Arai diagrams (Figs 18B, E, H and K), and also that the LTD-DHT Shaw results give large ΔAICs (45.1, 53.5 and 13.4; Figs 18C, F and I).

In the LTD-Thellier experiments, all the specimens were chilled in liquid nitrogen for 10 min after each of the progressive zero-field

Table 3. Experimental results with the Thellier method.

Sample ID	NRM_0	PTRM	$T_1 - T_2$	N	r	q	f	Slope	F_L (μT)	F (μT)	PTRM tail
MP02-06-2	361	20-300	—	—	—	—	—	—	15.0	—	−
MP05-05-2	241	20-600	400-500	5	0.989	1.94	0.231	1.48 ± 0.13	25.0	37.0[a]	+
			475-540	4	0.999	9.18	0.536	0.839 ± 0.031	25.0	21.0	+
MP06-05-2	277	20-600	300-475	7	0.996	6.97	0.348	2.80 ± 0.12	25.0	70.0[a]	+
			500-580	5	0.999	14.7	0.599	0.925 ± 0.028	25.0	23.1	+
MP07-07-2	296	20-600	300-475	7	0.982	2.82	0.291	3.18 ± 0.27	25.0	79.6[a]	+
			500-580	5	0.996	9.15	0.648	1.05 ± 0.05	25.0	26.1	+
MP12-07-3	134	20-200	—	—	—	—	—	—	15.0	—	−
BR04-05-2	223	20-200	—	—	—	—	—	—	15.0	—	−
BR15-02-2	66.6	20-500	150-450	8	0.985	5.91	0.502	1.97 ± 0.14	15.0	29.2	−
			350-475	5	0.984	2.21	0.336	1.23 ± 0.13	15.0	18.5[a]	−
BR15-05-4	108	20-520	335-425	4	0.989	1.48	0.232	1.94 ± 0.20	20.0	38.8[a]	+
			425-500	4	0.983	1.31	0.256	0.733 ± 0.096	20.0	14.7[a]	−
BR15-07-2	98.1	20-475	—	—	—	—	—	—	15.0	—	−
BR18-02-3	345	20-520	—	—	—	—	—	—	15.0	—	−
TA08-06-3	396	20-200	—	—	—	—	—	—	15.0	—	−
TA11-05-3	423	20-200	—	—	—	—	—	—	15.0	—	−
TA15-01-2	86.4	20-600	500-600	5	0.998	16.2	0.774	0.448 ± 0.016	15.0	6.72	+
TA15-06-2	94.2	20-520	—	—	—	—	—	—	15.0	—	−
TA16-04-2	78.6	20-300	—	—	—	—	—	—	30.0	—	−
TA16-07-2	28.6	20-600	—	—	—	—	—	—	15.0	—	−
HH09-04-2	328	20-560	300-520	9	0.992	9.55	0.510	2.53 ± 0.12	30.0	75.9	+
			520-560	*3*	*0.993*	*1.84*	*0.430*	*0.609 ± 0.071*	*30.0*	*18.3*[a]	+
HH09-07-3	357	20-600	250-500	8	0.991	6.10	0.405	5.74 ± 0.32	15.0	86.1[a]	+
			500-575	4	0.992	4.41	0.609	1.53 ± 0.14	15.0	23.0	+
HH16-03-2	409	20-600	100-475	10	0.956	3.93	0.481	12.4 ± 1.3	15.0	187[a]	−
			475-600	6	0.995	12.8	0.824	1.53 ± 0.08	15.0	22.9	+
HH16-06-3	443	20-560	100-450	10	0.986	6.81	0.456	4.82 ± 0.28	30.0	145[a]	+
			450-560	6	0.995	10.5	0.687	0.971 ± 0.049	30.0	29.1	+
HH20-06-3	599	20-370	—	—	—	—	—	—	20.0	—	−
MR01-02-2	97.8	20-520	335-475	6	0.992	4.18	0.329	1.85 ± 0.12	20.0	36.9[a]	+
			475-520	*3*	*0.998*	*1.70*	*0.231*	*0.705 ± 0.047*	*20.0*	*14.1*[a]	+
MR01-03-2	101	20-300	—	—	—	—	—	—	15.0	—	−
MR01-07-3	84.5	20-425	—	—	—	—	—	—	15.0	—	−
MR02-03-2	89.2	20-520	200-425	7	0.995	4.79	0.270	1.42 ± 0.07	25.0	35.5[a]	+
			450-520	4	0.995	2.24	0.244	0.512 ± 0.037	25.0	12.8[a]	+
MR04-01-2	56.7	20-520	335-475	6	0.998	7.92	0.316	0.773 ± 0.025	25.0	19.3[a]	+
			475-520	*3*	*0.999*	*1.61*	*0.177*	*0.445 ± 0.024*	*25.0*	*11.1*[a]	+
MR06-01-3	86.7	20-520	—	—	—	—	—	—	20.0	—	−
MR06-06-3	57.3	20-520	—	—	—	—	—	—	15.0	—	−
MR09-04-2	300	20-600	370-475	5	0.994	2.61	0.222	1.56 ± 0.10	25.0	38.9[a]	+
			475-560	5	0.999	11.2	0.436	0.690 ± 0.020	25.0	17.3[a]	+
MR12-01-2	142	20-475	—	—	—	—	—	—	15.0	—	−
MR14-03-2	306	20-600	400-520	6	0.999	17.2	0.560	0.948 ± 0.021	25.0	23.7	+
MR23-02-3	58.6	20-520	—	—	—	—	—	—	15.0	—	−
MR23-03-2	36.4	20-300	—	—	—	—	—	—	20.0	—	−
MR32-02-3	122	20-300	—	—	—	—	—	—	15.0	—	−
MR32-06-2	127	20-300	—	—	—	—	—	—	15.0	—	−
PU01-03-4	149	20-500	300-500	7	0.998	21.6	0.822	0.752 ± 0.023	15.0	11.3	−
PU01-06-2	136	20-520	400-520	6	0.997	15.2	0.744	0.513 ± 0.019	20.0	10.3	−
PU01-07-3	45.9	20-370	—	—	—	—	—	—	15.0	—	−
PU06-04-3	547	20-600	300-500	8	0.995	8.22	0.378	6.68 ± 0.26	25.0	167[a]	+
			520-580	4	0.999	15.2	0.597	2.03 ± 0.05	25.0	50.9	+
TR02-04-3	116	20-300	—	—	—	—	—	—	25.0	—	—

NRM_0, initial NRM intensity; PTRM, acceptable temperature interval in the pTRM test; $T_1 - T_2$, N, r, q, f, slope, temperature interval, number of data points, correlation coefficient, quality factor, NRM fraction, and slope of the linear NRM–TRM portion in the Arai diagram; F_L, laboratory-induced DC field for TRM; F, calculated palaeointensity; PTRM tail, positive (+) or negative (−) pTRM tail check for the linear segment. Note that data line indicated in italic is a reference (see text).

[a]Rejected if the criterion of $f \geq 0.50$ is adopted.

and in-field heatings. The LTD treatment was done in a magnetically shielded case and the memories were measured. Except for these points, the experimental procedures were the same as in Section 5.1. We can thus construct Arai diagrams for LT-surviving NRM and TRM components (Figs 18A, D, G and J). The results are examined with the same selection criteria as in Section 5.1, and are listed in Table 4.

As indicated in the Zijderveld diagrams (insets in Fig. 18), LT-demagnetized components are not very large in the present specimens. However, in comparison with the non-LTD-Thellier results,

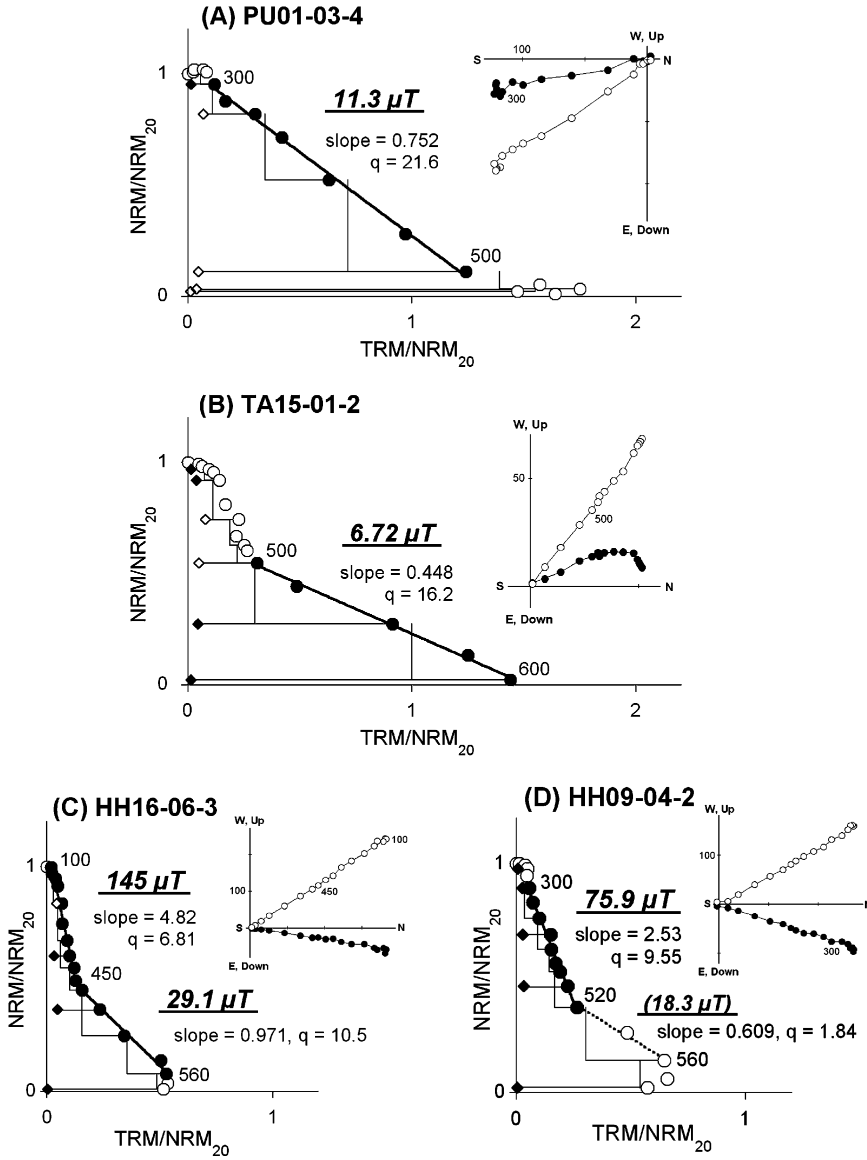

Figure 13. Representative successful results in the Thellier experiments. Linear portions consist of closed circles. Positive and negative pTRM-tail checks are indicated by closed and open diamonds, respectively. Zijderveld diagrams are also shown as insets. The results could be classified into three types: (A) and (B) single-slope type, (C) two-segmented type and (D) quasi two-segmented type. Units are 10^{-5} A m^2 kg^{-1}.

the two-segmented features in the Arai diagrams for the LTD-Thellier results are clearer. This is analogous to the results for the Kilauea, Hawaii, 1960 lava (Yamamoto *et al.* 2003). In their experiments, samples with low and intermediate levels of high-temperature oxidation (corresponding to C1–C3 and C2–C4 oxidations; A-4–4L and B-9–4L in Yamamoto *et al.* 2003) exhibited more concave Arai diagrams in the LTD-Thellier experiments than in the non-LTD-Thellier ones (Figs 5d and e in Yamamoto *et al.* 2003). Although the reason for such a phenomenon is still controversial, they might be evoked by acquisition of thermochemical remanent magnetization (TCRM) during natural cooling of the lava, as suggested by Yamamoto *et al.* (2003). TCRM is contaminated into NRM and it is carried by a number of small domains of Ti-poor titanomagnetites, which are products of moderate high-temperature oxidation and are thought to consist partly of SD-like remanences. It is difficult to regard MD contribution as a main cause because most MD remanences are thought to be erased by LTD treatment.

For specimens of MP05-05-3L and MP07-07-3L, their low $T_{\rm B}$ (43.0 and 59.8 μT) and high $T_{\rm B}$ palaeointensities (20.5 and 20.1 μT) are respectively larger and smaller than the corresponding LTD-DHT Shaw palaeointensities (33.4 μT for MP05-05-1 and 35.0 μT for MP07-07-1). This suggests that the LTD-DHT Shaw palaeointensities obtained from the upward convex NRM–TRM1* diagrams can be weighted-averaged values of the low and high $T_{\rm B}$ LTD-Thellier palaeointensities. PU06-04-4L exhibited a large difference between the low $T_{\rm B}$ (161 μT) and high $T_{\rm B}$ palaeointensities (43.7 μT). PU06-04-1 did not yield a successful palaeointensity in the LTD-DHT Shaw experiment because its NRM–TRM1* diagram showed an excessive upward convexity giving $r_{\rm N} < 0.995$ for a linear fit. It is possible that the difference between the two palaeointensities is so large that their mixture results in excessive convexity in the NRM–TRM1* diagram. HH09-07-4L gave a consistently high $T_{\rm B}$ LTD-Thellier palaeointensity (18.3 μT) with the LTD-DHT Shaw result (17.2 μT).

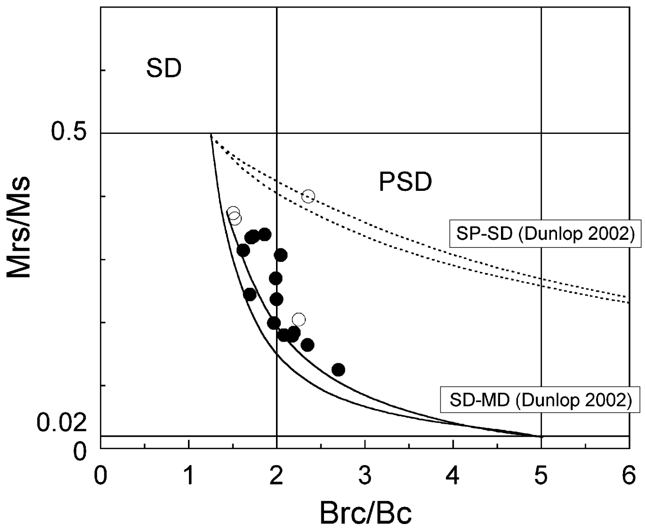

Figure 14. Day plot of the core-averaged hysteresis parameters for the specimens giving palaeointensities in the Thellier experiments. Open and closed symbols indicate the single-slope and two-segmented types, respectively. The parameters are referred from Tables 1 and 2. It is obvious that data points distribute along the mixing lines between SD and MD of Dunlop (2002). This kind of trend is warned against by Oishi *et al.* (2005).

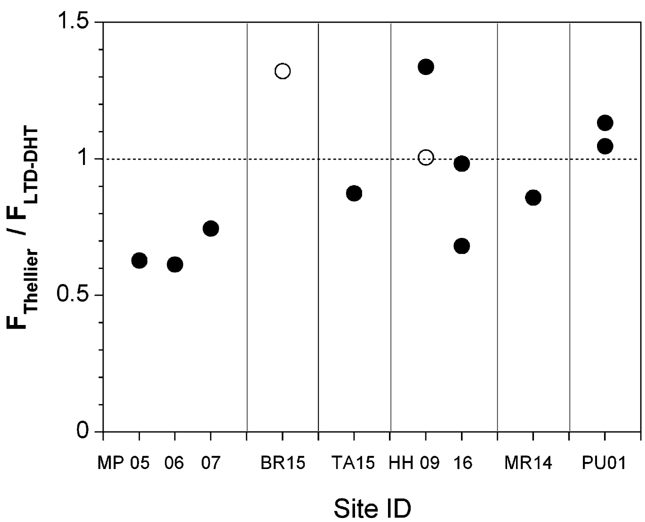

Figure 15. Comparison between the Thellier and the LTD-DHT Shaw palaeointensities for the sister specimens. The vertical axis indicates the normalized Thellier palaeointensity (by the LTD-DHT Shaw palaeointensity) while the horizontal one is the individual site. Closed symbols are the results satisfying the quantitative selection criteria with $f \geq 0.50$. Open symbols are the alternative results (see text).

6.3.3 *Threshold ΔAIC for data selections*

The above discussions suggest that the LTD-DHT Shaw palaeointensities accompanied by large ΔAICs may have equivalent qualities to Thellier palaeointensities with concave Arai diagrams. According to the growing consensus on analysis of Thellier results, it seems better not to adopt such LTD-DHT Shaw palaeointensities for further discussions. It is, however, difficult to define an exact threshold value of ΔAIC at which results should be discarded. In this study, we temporarily determined the threshold value for the present data set based on several concrete examples.

In this section, four LTD-Thellier results were obtained. Three of them were accompanied with the companion LTD-DHT Shaw results. MP05-05-1 and MP07-07-1 gave ΔAICs of 45.1 and 53.5. As discussed before, these LTD-DHT Shaw results are considered to be weighted-averages of the corresponding low and high T_B LTD-Thellier results. On the other hand, HH09-07-2 resulted in ΔAIC of 13.4, and its LTD-DHT Shaw palaeointensity (17.2 μT) is consistent with the companion high T_B LTD-Thellier palaeointensity (18.3 μT, HH09-07-4L).

In Sections 4.3 and 5.2 we can find four pairs of LTD-DHT Shaw and usual Thellier results. Although simple comparison between both results is not straightforward due to a lack of LTD treatment in the usual Thellier results, it may reinforce our ideas. There are three LTD-DHT Shaw results showing relatively large ΔAICs. TA15-01-1 gave ΔAIC of 18.5. The LTD-DHT Shaw palaeointensity (7.68 μT) is concordant with the companion Thellier one (6.72 μT, TA15-01-2). Also, HH16-06-1 and HH09-04-1 yielded ΔAICs of 7.2 and 11.9. Their LTD-DHT Shaw results (29.6 and 18.2 μT) agree well with the companion high T_B Thellier palaeointensities (29.1 and 18.3 μT; note that the latter is the reference, see Section 5.2).

If the agreements between the LTD-DHT Shaw and the high T_B Thellier palaeointensities are tentatively permitted when the Thellier experiments yield two-sloped Arai diagrams, the quality of the LTD-DHT Shaw palaeointensities with ΔAIC $\leq$ 18.5 does not seem to be too bad. Therefore, we temporarily take a threshold ΔAIC of 15, which is set to be slightly on the safe side. ΔAIC exceeding ∼15 is possibly a sign of an undesirable LTD-DHT Shaw palaeointensity. There are 49 results with ΔAIC > 15 among the present successful results (Fig. 17). It is, however, emphasized that this threshold is limited to the present data set.

7 GEOMAGNETIC FIELD INTENSITY DURING THE LAST 5 MYR

7.1 New data set from the LTD-DHT Shaw palaeointensities

Discussions in Sections 6.1 and 6.2 discriminated 151 LTD-DHT Shaw palaeointensities. Their statistical results are summarized in Table 5. In this table it is noted that site means of RT12, RT18 and HH11 are calculated excluding four outliers because they are statistically distinguishable from the site means at the 2σ level. Yamamoto *et al.* (2003) observed the same phenomena from the Kilauea, Hawaii, 1960 lava, and obtained a true palaeointensity after excluding outliers.

From these data, we can choose 24 reliable site-mean LTD-DHT Shaw palaeointensities by the following criteria:

(1) Each mean is determined from no fewer than three individual results ($N \geq 3$).

(2) The standard deviation is within 20 per cent ($\sigma \leq$ 20 per cent).

(3) The minimum value of ΔAIC among the results for each site is no larger than 15 (ΔAIC $\leq$ 15).

Criterion (3) is based on the discussion in Section 6.3. The result for sample MP01 is considered to be a record of a transitional geomagnetic field because the corresponding VGP locates at 18.7°N. However, we intend to include this record. Transitional data are usually excluded from discussions about long-term variations in the geomagnetic dipole moments. We think such omissions may cause some artefact in statistical analyses since volcanic data are random readings of the ancient geomagnetic field.

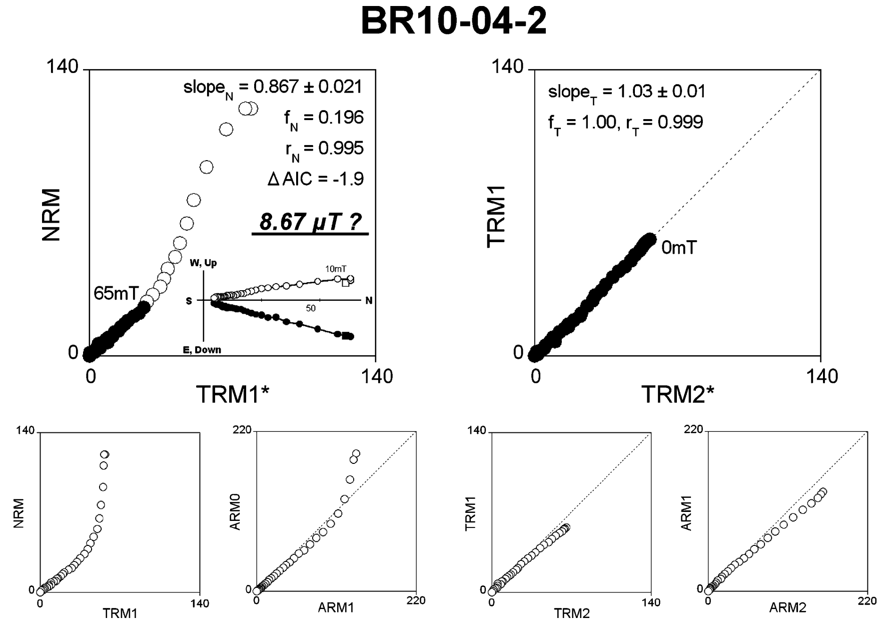

Figure 16. Example of the results with the curved NRM–TRM1* diagram passing the quantitative selection criteria. Since the Zijderveld diagram suggests a single primary component, the curvature would not be caused by secondary magnetization. This palaeointensity may be a biased estimate (see the text).

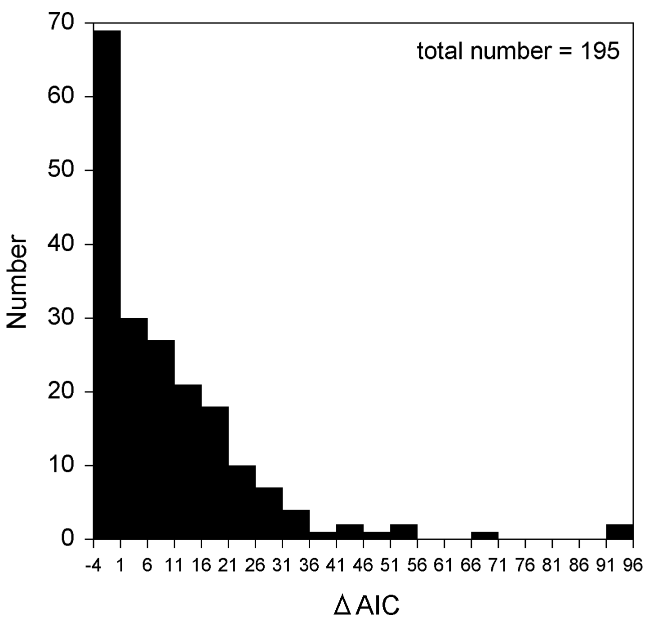

Figure 17. Distribution of the ΔAICs for the NRM–TRM1* diagrams passing the quantitative selection criteria (195 specimens).

The present data set will help in studies of the time-averaged field (TAF) and palaeosecular variations (PSV). Most of the analyses (e.g. Gubbins & Kelly 1993; Johnson & Constable 1995, 1997; Kelly & Gubbins 1997; Hatakeyama & Kono 2002) only use palaeodirectional data because of the small number of existing absolute palaeointensity data (Hatakeyama & Kono 2002). Only Kono *et al.* (2000) incorporated absolute palaeointensities.

7.2 Comparison with the Thellier data set

The LTD-DHT Shaw data set obtained in Section 7.1 can be compared with an available Thellier data set having the similar quality. From the latest palaeointensity database (Perrin & Schnepp 2004), Thellier data are selected using the following criteria:

(1) Ages range between 0 and 5 Ma.
(2) Palaeointensities are obtained by the Thellier method with a pTRM check (T+).
(3) The average palaeointensity for each cooling unit is calculated from no fewer than three individual determinations ($N \geq 3$).
(4) The standard deviation of each average is within 20 per cent ($\sigma \leq 20$ per cent).

Note that we do not limit the palaeomagnetic polarities, similarly to the LTD-DHT Shaw data set. Except for this point, these criteria are almost the same as those used in the previous studies with palaeointensity databases (e.g. Juarez & Tauxe 2000; Selkin & Tauxe 2000; Heller *et al.* 2002; Biggin & Thomas 2003b). Criterion (4) seems to be reasonable because Valet (2003) reviewed numerous palaeointensity results reported from the Kilauea, Hawaii, 1960 lava, and concluded that the present palaeointensity techniques could not determine the field with a precision of better than 20 per cent. The total number of selected Thellier data is 458, about half of which comprise data from the Hawaiian Islands.

The selected LTD-DHT Shaw and the Thellier data are presented in Fig. 19 with their ages. This figure indicates that there is no systematic bias in age distributions between the LTD-DHT Shaw and the Thellier data set prior to ~0.9 Ma. Most Thellier data belong to the Brunhes chron, but their VADMs do not differ significantly from those of older ages. Average VADMs are calculated for each data set: $(3.64 \pm 2.10) \times 10^{22}$ A m^2 for the LTD-DHT Shaw data ($N = 24$) and $(7.46 \pm 3.10) \times 10^{22}$ A m^2 for the Thellier data ($N = 458$). Although the reliability of palaeointensity determination from submarine basaltic glass is still under debate (e.g. Heller *et al.* 2002; Smirnov & Tarduno 2003), their contributions are too small to affect the present Thellier data set: if the submarine basaltic glass data are excluded, the average is $(7.49 \pm 3.15) \times 10^{22}$ A m^2 ($N = 434$). Histograms of both data set are illustrated in Fig. 20. The average of the LTD-DHT Shaw data set is nearly half

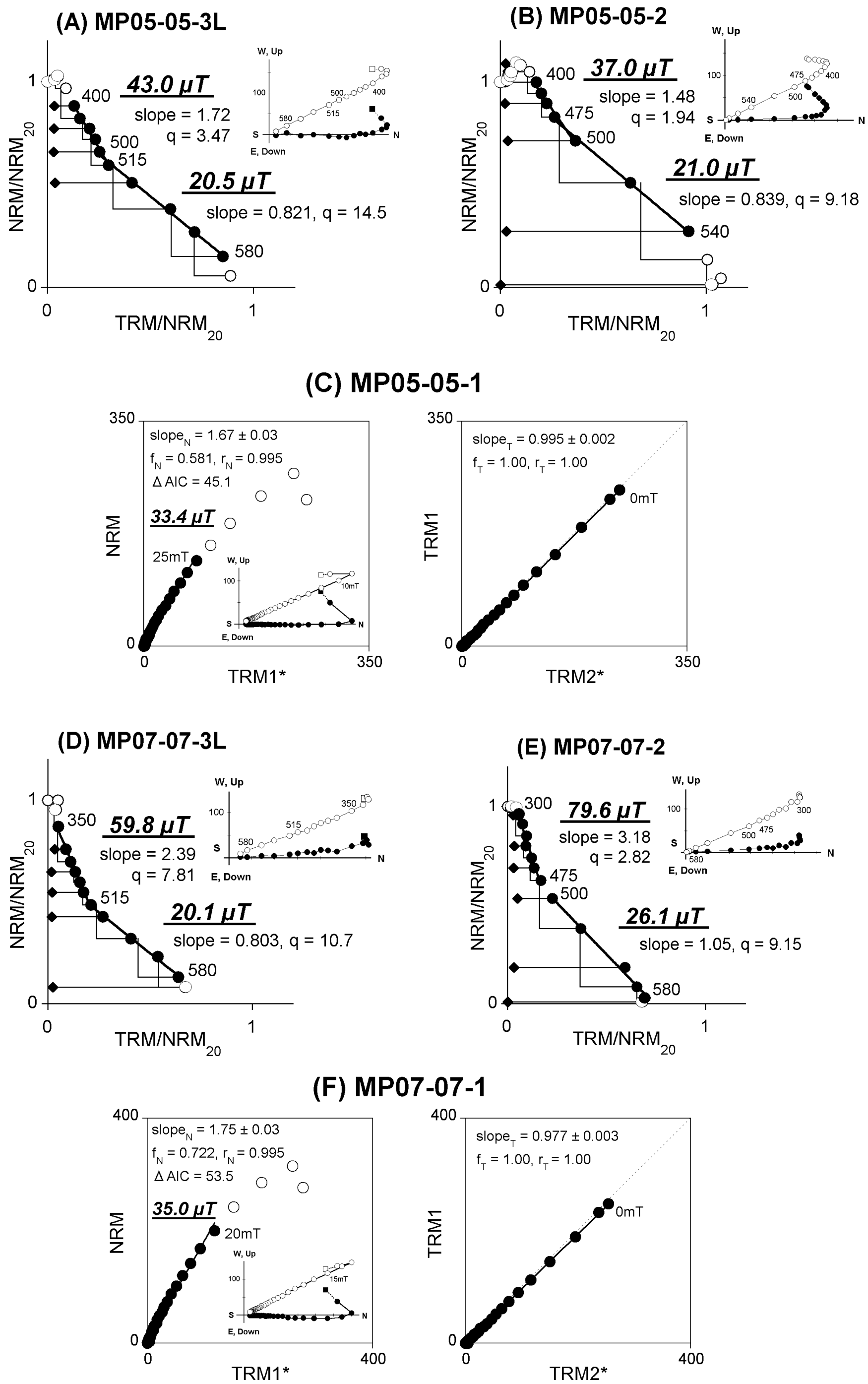

Figure 18. Results of the LTD-Thellier (A, D, G and J), Thellier (B, E, H and K) and LTD-DHT Shaw (C, F, I and L) experiments for the sister specimens. The suffix 'L' in the specimen name indicates the result of a Thellier experiment with LTD treatment. Zijderveld diagrams are also shown as insets, where closed and open symbols indicate projections onto horizontal and vertical planes, respectively (squares are NRM before LTD).

of the mean of the Thellier data set as well as the present dipole moment.

The large discrepancy between the two data sets is probably due to the different methods of palaeointensity determination. This is because the mean VGP positions calculated from the two data set almost coincide with each other (Fig. 21), suggesting that the palaeodirections are of equivalent quality. In the calculation, the Thellier data set is split into two data sets—Hawaiian and non-Hawaiian data—since 64 per cent of the Hawaiian data ($N = 148$) are inclination only. Ninety-eight per cent of the non-Hawaiian data have both inclination and declination. For the LTD-DHT Shaw data set, the mean locates at 83.2°N, 353.4°E with $\alpha_{31} = 5.9°$ and $\alpha_{32} = 8.4°$ (α_{31} and α_{32} are 95 per cent confidence limits along minor and major axes). Regarding the Thellier data set, the Hawaiian mean is expressed as a great circle with variable declinations (D). We calculated the mean inclination following McFadden & Reid (1982) and it was converted to VGP for 10° intervals of declination. The location of the non-Hawaiian mean is 83.9°N, 46.2°E with $\alpha_{31} = 3.0°$ and

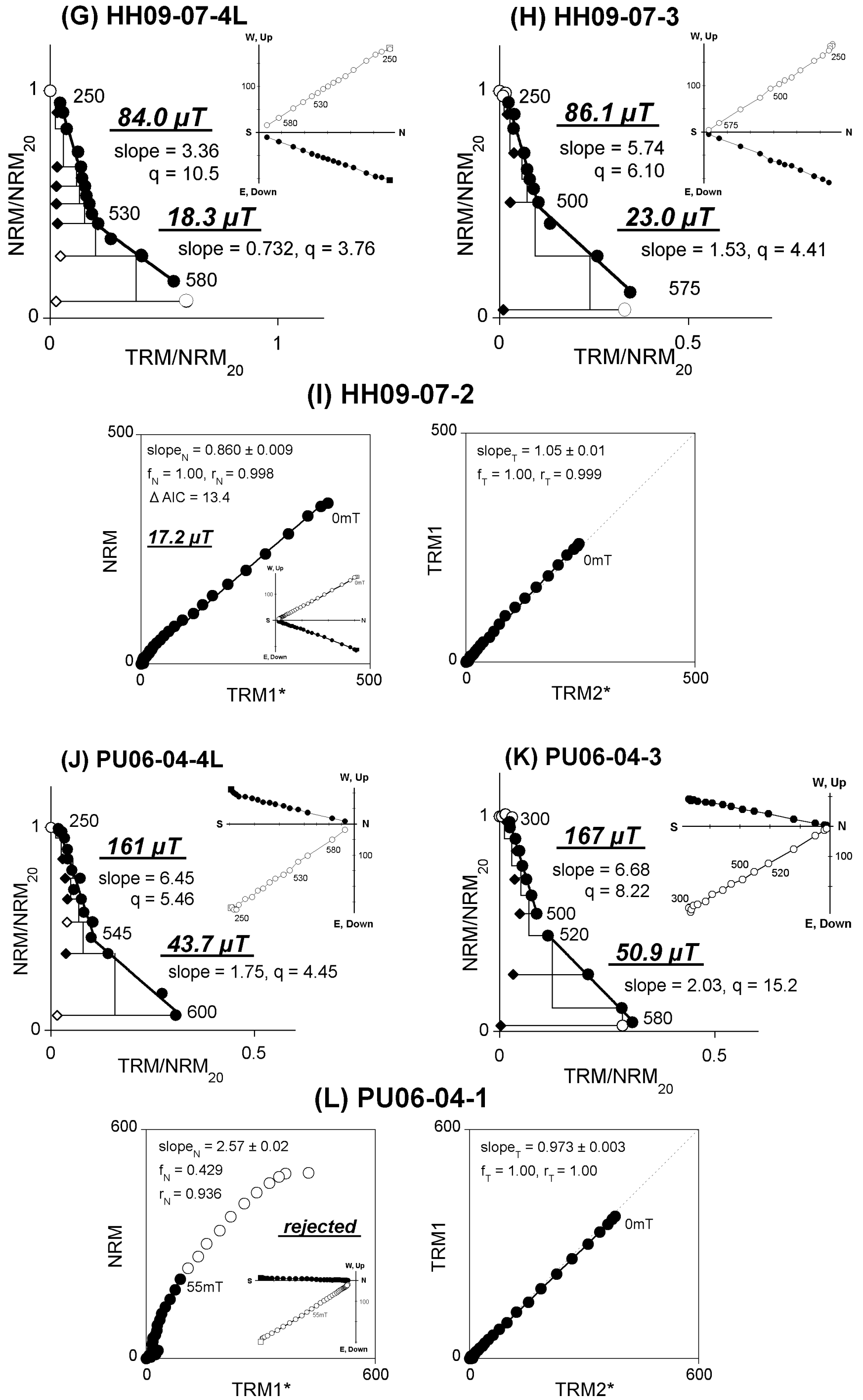

Figure 18. (*Continued*.)

Table 4. Experimental results with the LTD-Thellier method.

Sample ID	NRM_0	PTRM	$T_1 - T_2$	N	r	q	f	Slope	F_L (μT)	F (μT)	PTRM tail
MP05-05-3L	313	20-600	400-515	6	0.993	3.47	0.261	1.72 ± 0.10	25.0	43.0	+
			500-580	6	0.998	14.5	0.596	0.821 ± 0.027	25.0	20.5	+
MP07-07-3L	333	20-600	350-515	7	0.996	7.81	0.395	2.39 ± 0.10	25.0	59.8	+
			515-580	5	0.998	10.7	0.547	0.803 ± 0.030	25.0	20.1	+
HH09-07-4L	353	20-600	250-530	11	0.993	10.5	0.484	3.36 ± 0.14	25.0	84.0	+
			530-580	4	0.994	3.76	0.453	0.732 ± 0.057	25.0	18.3	−
PU06-04-4L	567	20-600	250-545	12	0.969	5.46	0.474	6.45 ± 0.50	25.0	161	+
			545-600	4	0.993	4.45	0.607	1.75 ± 0.15	25.0	43.7	+

NRM_0, initial NRM intensity after the first LTD treatment.

Table 5. Statistical results of the palaeodirections and LTD-DHT Shaw palaeointensities.

Site	K–Ar age (Ma)	N_d	Dec. (°)	Inc. (°)	α_{95} (°)	P_{Lat} (°)	P_{Long} (°)	N_F	F (μT)	VDM (10^{22} A m ^{2})	VADM (10^{22} A m ^{2})	ΔAIC_{min}
Dykes and single lavas												
MP01	—	5	−80.4	−79.7	4.4	18.7	48.6	4	4.17 ± 0.32	0.566 ± 0.043	0.971 ± 0.075	−2.0
(TA13)	3.11 ± 0.04	9	158.6	37.3	6.3	−69.3	−76.6	1	10.2	2.25	2.37	21.3
(RT03)	2.65 ± 0.03	6	1.3	−26.4	4.6	86.8	−127.8	2	16.1 ± 1.7	3.85 ± 0.41	3.73 ± 0.39	5.0
(RA01)	2.45 ± 0.05	4	6.0	−24.7	3.2	83.0	−94.1	1	12.6	3.04	2.92	6.3
PU04	0.92 ± 0.03	6	20.3	−62.3	4.1	58.9	1.4	5	22.4 ± 0.8	3.74 ± 0.14	5.15 ± 0.19	−0.5
PU05	1.03 ± 0.02	7	19.9	−33.4	6.1	71.1	−54.7	5	15.1 ± 1.8	3.44 ± 0.41	3.47 ± 0.41	4.2
TR02	—	6	−8.0	−23.8	5.1	80.6	154.6	4	9.21 ± 0.93	2.24 ± 0.23	2.11 ± 0.21	−1.0
(TH02)	0.72 ± 0.11	4	12.5	−29.4	4.7	77.9	−66.3	2	27.7 ± 2.4	6.51 ± 0.57	6.38 ± 0.56	−0.4
TH03	—	4	4.7	−18.3	7.7	80.7	−119.6	3	4.71 ± 0.77	1.18 ± 0.19	1.08 ± 0.18	1.0
(TH04)	0.51 ± 0.10	4	7.4	−18.6	3.7	79.1	−106.9	1	9.24	2.30	2.12	25.5
Lava sequences												
(MP13)	4.61 ± 0.05	5	−3.8	−20.2	5.3	82.9	175.5	2	25.3 ± 1.8	6.26 ± 0.46	5.89 ± 0.43	10.1
(MP11)	—	5	2.4	−24.5	3.6	85.7	−118.5	1	24.8	6.00	5.78	16.7
(MP10)	—	5	0.3	−29.4	7.9	89.2	−129.9	1	19.0	4.45	4.42	7.4
(MP07)	—	5	−4.8	−25.3	7.7	84.4	151.1	2	33.0 ± 2.8	7.95 ± 0.68	7.69 ± 0.66	34.0
(MP06)	—	5	−2.0	−27.6	6.5	87.4	161.2	2	35.1 ± 3.5	8.34 ± 0.84	8.18 ± 0.82	42.6
(MP05)	—	5	−1.0	−25.6	2.3	86.9	−169.8	2	31.9 ± 2.1	7.67 ± 0.51	7.43 ± 0.49	16.8
(MP04)	—	5	−4.7	−28.0	2.5	85.2	136.1	1	27.2	6.45	6.34	−0.6
(MP03)	—	5	0.0	−25.3	2.4	86.9	−153.0	1	32.2	7.76	7.50	18.9
MP02	4.52 ± 0.05	5	3.3	−25.0	3.7	85.4	−107.9	3	21.9 ± 2.0	5.30 ± 0.49	5.11 ± 0.47	−1.7
(BR07)	3.67 ± 0.05	7	−176.9	24.6	4.2	−85.3	67.6	3	23.4 ± 12.3	5.65 ± 2.97	5.44 ± 2.85	6.3
BR04	3.75 ± 0.05	7	−160.4	29.6	4.2	−71.2	118.9	4	26.5 ± 3.3	6.22 ± 0.77	6.18 ± 0.77	−1.9
BR15	3.43 ± 0.06	7	−159.2	42.2	2.8	−69.0	143.9	6	14.5 ± 1.5	3.06 ± 0.32	3.37 ± 0.35	−0.9
(BR14)	—	5	−160.2	37.6	3.1	−70.7	135.1	1	20.1	4.43	4.69	0.9
BR18	3.51 ± 0.05	8	15.0	−45.8	3.2	72.4	−21.5	4	17.4 ± 1.1	3.54 ± 0.23	4.05 ± 0.27	−0.1
(TA07)	3.24 ± 0.05	5	−67.4	70.3	5.3	−1.1	176.0	1	4.46	0.670	1.04	9.3
TA11	2.57 ± 0.13	7	173.4	22.6	12.4	−81.9	−25.1	3	23.1 ± 0.8	5.65 ± 0.18	5.37 ± 0.18	−1.8
TA08	3.14 ± 0.06	7	179.1	17.8	7.5	−82.4	21.7	5	23.8 ± 3.9	5.96 ± 0.97	5.54 ± 0.90	7.4
(TA19)	—	5	−12.9	−54.3	9.2	68.5	58.4	1	8.96	1.65	2.08	1.5
(TA17)	2.99 ± 0.04	7	−16.8	−59.0	6.0	62.6	57.4	2	5.68 ± 1.17	0.986 ± 0.203	1.32 ± 0.27	−0.7
TA16	2.97 ± 0.04	5	−5.9	−60.9	7.7	64.2	38.7	4	3.02 ± 0.40	0.512 ± 0.068	0.701 ± 0.093	−2.0
(TA15)	2.90 ± 0.05	7	−23.0	−49.2	2.0	65.1	81.8	5	7.36 ± 0.71	1.44 ± 0.14	1.71 ± 0.17	18.5
(RT05)	—	6	2.7	51.7	3.0	40.7	−148.4	1	5.20	0.989	1.21	14.4
(RT10)	2.76 ± 0.03	7	−41.4	−28.3	9.3	50.2	115.2	3	4.23 ± 1.39	1.00 ± 0.33	0.981 ± 0.322	−1.3
RT12m	2.61 ± 0.03	7	7.3	−39.2	2.0	81.3	−22.3	6	8.67 ± 1.03	1.88 ± 0.22	2.01 ± 0.24	−1.9
RT18m	2.67 ± 0.03	6	14.3	−24.7	4.9	75.6	−75.2	4	9.03 ± 1.08	2.18 ± 0.26	2.09 ± 0.25	5.5
(HH01)	2.72 ± 0.03	7	3.1	−22.8	1.8	84.2	−119.0	1	38.4	9.39	8.91	28.8
HH11m	3.09 ± 0.04	6	7.0	−26.8	4.4	82.7	−81.3	4	15.1 ± 1.5	3.60 ± 0.36	3.50 ± 0.35	9.7
HH09	—	7	22.3	−31.1	3.4	68.7	−57.8	5	17.8 ± 1.0	4.12 ± 0.22	4.12 ± 0.22	0.0
HH16	—	7	9.9	−34.6	2.1	80.3	−45.8	5	33.9 ± 3.4	7.65 ± 0.76	7.86 ± 0.79	4.1
HH20	2.83 ± 0.09	7	1.3	−40.8	1.7	83.3	18.7	4	38.4 ± 2.1	8.21 ± 0.46	8.91 ± 0.49	−1.2
MR01	1.58 ± 0.04	7	170.4	31.0	2.4	−80.8	−56.0	5	15.0 ± 1.0	3.49 ± 0.23	3.45 ± 0.22	−1.8
(MR02)	—	5	172.6	29.5	3.9	−82.6	−46.6	1	7.55	1.77	1.74	20.4
(MR04)	—	5	172.3	37.9	0.9	−81.9	−88.3	1	11.4	2.50	2.62	11.4
MR06	1.62 ± 0.08	7	173.5	30.5	4.8	−83.7	−50.0	5	8.72 ± 0.64	2.03 ± 0.15	2.00 ± 0.15	−1.9
(MR09)	—	5	163.6	34.1	4.6	−74.4	−66.4	1	26.6	6.04	6.11	−1.2
(MR12)	—	5	174.9	29.3	3.3	−84.7	−39.6	1	20.6	4.84	4.74	−0.3
(MR14)	—	5	174.1	25.4	4.8	−82.9	−24.2	1	27.6	6.65	6.34	1.3
MR16	1.51 ± 0.04	7	174.1	32.8	3.0	−84.4	−63.2	3	9.52 ± 1.03	2.18 ± 0.24	2.19 ± 0.24	1.0
(MR22)	—	5	168.0	56.4	4.4	−67.9	−123.6	1	13.1	2.35	3.01	0.5
MR23	1.55 ± 0.06	7	181.8	61.4	6.0	−64.9	−153.0	6	13.0 ± 2.1	2.20 ± 0.36	3.00 ± 0.49	−2.0
MR32	1.50 ± 0.04	7	185.7	68.0	3.6	−56.2	−156.2	7	13.3 ± 2.4	2.05 ± 0.36	3.05 ± 0.54	−1.5
PU01	1.12 ± 0.02	7	160.8	33.1	4.6	−71.8	−63.9	4	9.50 ± 0.87	2.17 ± 0.20	2.18 ± 0.20	−1.5

Site, site ID; N_d, number of the specimens used for the calculation of palaeodirection; Dec., Inc., α_{95}, palaeodirection and its 95 per cent confidence circle; P_{Lat}, P_{Long}, latitude and longitude of the virtual geomagnetic pole; N_F, number of the specimens used for the calculation of mean palaeointensity; F, VDM, VADM, mean palaeointensity, virtual dipole moment and virtual axial dipole moment with their standard deviations; ΔAIC_{min}, minimum ΔAIC values for the individual sites. Note that the mean palaeointensity is calculated without the outliers (multispecimen test) for the site ID with suffix of ‘m’. K–Ar ages and palaeodirections are referred from Uto *et al.* (submitted) and Yamamoto *et al.* (2002).

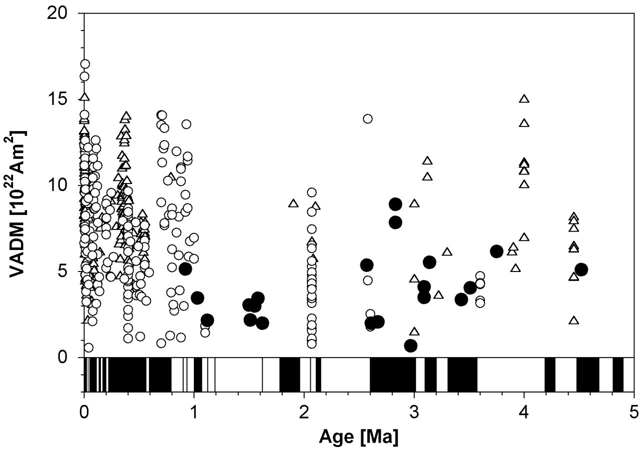

Figure 19. VADM variations for the period of the last 5 Myr. Open symbols indicate the selected Thellier data ($N = 458$) while closed ones correspond to the LTD-DHT Shaw palaeointensities ($N = 21$; note that VADMs of the sites MP01, TR02 and TH03 are not indicated because of undetermined K–Ar ages). The selections are mainly based on the criteria of $N \geq 3$ and $\sigma \leq$ 20 per cent (see text). About half of the Thellier data are Hawaiian data ($N =$ 232, triangles). The geomagnetic polarity timescale (radiometric timescale) is from Singer *et al.* (2002) and Uto *et al.* (submitted).

$\alpha_{32} = 4.2°$. Note that the means except for the Hawaiian data are evaluated by the Bingham statistics because their elongation parameters (α_{32}/α_{31}; Tanaka 1999) are large (1.41 and 1.39).

We consider that the average calculated from the present LTD-DHT Shaw data set is more appropriate for the mean VADM of the last 5 Myr. As mentioned in Section 1, the Thellier method occasionally fails in accurate determinations of palaeointensity from historical lavas. Fig. 22 (A) summarizes the intensities reported from historical lavas (Tanaka & Kono 1991; Tanaka *et al.* 1995a; Hill & Shaw 2000; Calvo *et al.* 2002; Böhnel *et al.* 2003; Yamamoto *et al.* 2003; Mochizuki *et al.* 2004; Oishi *et al.* 2005). Almost all the reported Thellier palaeointensities are overestimates, which are as high as 200 per cent of the expected value. On the other hand, LTD-DHT Shaw palaeointensities from the same lavas (Yamamoto *et al.* 2003; Mochizuki *et al.* 2004; Oishi *et al.* 2005) are clustered around the expected value except for some outliers (Fig. 22B). These observations can explain the large discrepancy in the 0–5 Ma mean VADMs between the LTD-DHT Shaw and the Thellier data set.

7.3 Overestimated palaeointensities in the Hawaiian Thellier data set

The overestimated palaeointensities might be especially accumulated in the Hawaiian data set. If average VADMs are calculated separately for the Hawaiian and non-Hawaiian Thellier data sets, they give $(8.10 \pm 2.62) \times 10^{22}$ A m^2 ($N = 232$) and $(6.80 \pm 3.41) \times 10^{22}$ A m^2 ($N = 226$), respectively (Fig. 20). The F-test and t-test for these values gave an F value of 1.69 and a t value of 4.60, both of which correspond to probabilities of <0.0001. This situation is almost unchanged even if the submarine basaltic glass data are excluded: average VADMs are calculated to be $(8.21 \pm 2.71) \times 10^{22}$ A m^2 ($N = 211$, Hawaiian data) and $(6.80 \pm 3.39) \times 10^{22}$ A m^2 ($N = 223$, non-Hawaiian data).The Hawaiian and non-Hawaiian data set are statistically distinguishable from each other. As discussed in the previous subsection, the mean VGP positions from the two data set do not significantly differ from each other (Fig. 21). Thus, the difference could be solely attributed to quality of the reported palaeointensities.

The high palaeointensities in the Hawaiian data set possibly originate from ancient lavas with NRMs of non-TRM origin. For example, the data set includes 10 results from 2.1–3.9 Ma lavas in Oahu, Hawaii (Laj *et al.* 2000). One of their Arai diagrams (KO26–146B; Fig. 5 of Laj *et al.* 2000) appears to be two-segmented. Seventy-three results came from the Hawaiian Scientific Drilling Program (HSDP) cores studied by Laj & Kissel (1999). Thermomagnetic analyses indicated the presence of low-Ti titanomagnetites in ~85 per cent of their samples. Recently, Kontny *et al.* (2003) have extensively studied the thermomagnetic properties of samples from the subaerial part of the HSDP2 cores and classified the properties into three types. Two of them resulted in Curie temperatures of 480–600 °C. They reported that the ore mineral textures of these two types were characterized by titanomagnetites with ilmenite lamellae. These features resemble those of the Kilauea 1960 lava which yields a number of anomalously high palaeointensities with the Thellier method (Yamamoto *et al.* 2003). They suggested that its main cause was NRM of non-TRM origin.

The possibility of biased palaeointensities in the Hawaiian data set is also supported from recently reported Thellier results from submarine basaltic glass of HSDP2 cores (Tauxe & Love 2003). Although the reliability of palaeointensity determination on submarine basaltic glass is still under debate, as stated before, Tauxe & Love (2003) carefully examined the rock magnetic properties of their

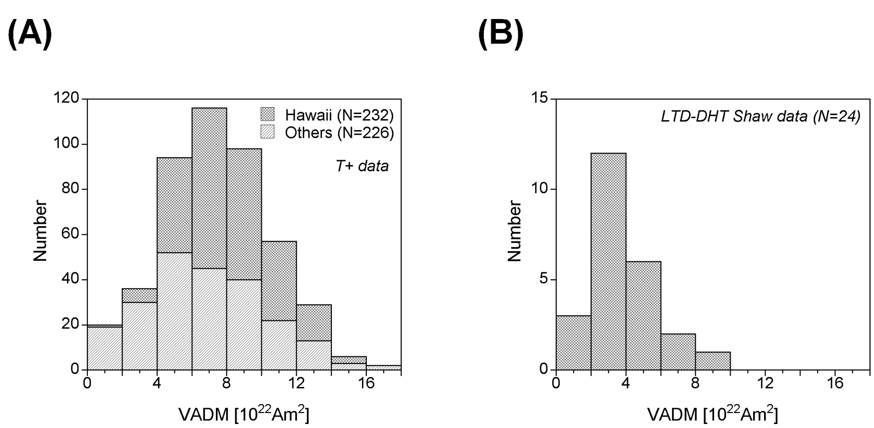

Figure 20. Histograms of the VADMs for (A) the Thellier and (B) the LTD-DHT Shaw data set. Average VADMs are calculated to be $(7.46 \pm 3.10) \times 10^{22}$ A m^2 ($N = 458$, Thellier) and $(3.64 \pm 2.10) \times 10^{22}$ A m^2 ($N = 24$, LTD-DHT Shaw) for each data set. If the Thellier data set is split into two data sets—Hawaiian and non-Hawaiian—they result in average VADMs of $(8.10 \pm 2.62) \times 10^{22}$ A m^2 ($N = 232$) and $(6.80 \pm 3.41) \times 10^{22}$ A m^2 ($N = 226$), respectively. They are statistically distinguishable by both the t-test and the F-test at >99.9999 per cent confidence (see text).

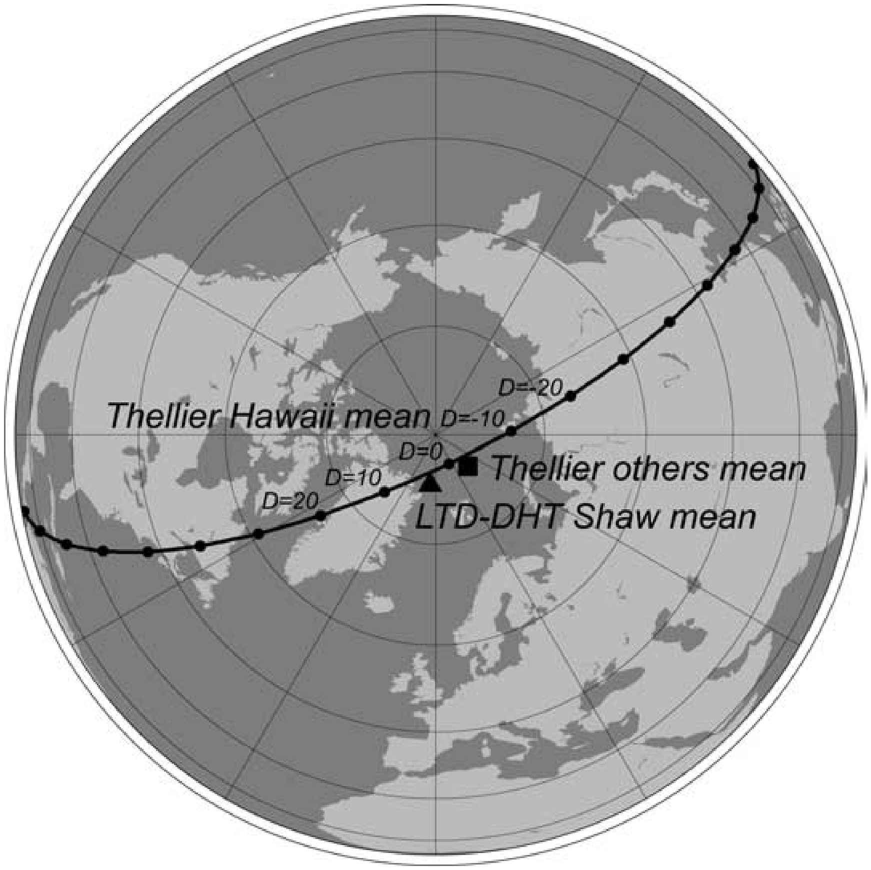

Figure 21. Mean VGP positions of the LTD-DHT Shaw and Thellier data set. The former mean locates at 83.2°N, 353.4°E with $\alpha_{31} = 5.9°$ and $\alpha_{32} = 8.4°$ (closed triangle). As for the latter, the data set is split into Hawaiian and non-Hawaiian data. The position of the Hawaiian data is expressed as a great circle with variable declination (*D*) indicated by closed circles. The mean of the non-Hawaiian data locates at 83.9°N, 46.2°E with $\alpha_{31} = 3.0°$ and $\alpha_{32} = 4.2°$ (closed square).

samples and showed their robustness to Thellier palaeointensity determinations. As a result, they obtained Thellier palaeointensities spanning 440–550 kyr from 34 cooling units. If these data are subjected to the same statistical criteria as described in the previous subsection ($N \geq 3$ and $\sigma \leq 20$ per cent), 21 site means can be selected (note that these data are already included in the Hawaiian Thellier data set). They give an average VADM of $(7.02 \pm 0.87) \times 10^{22}$ A m^2. This is almost the same as the average VADM of the non-Hawaiian data set [$(6.80 \pm 3.41) \times 10^{22}$ A m^2, $N = 226$]. Although the time coverage of the data of Tauxe & Love (2003) is very short, the duration of ~100 kyr is thought to be sufficient to represent the palaeosecular variation (Tanaka & Kobayashi 2003). Also, in the Brunhes chron, a VADM of ~100 kyr scale average does not appear to show significant variations in relative palaeointensities from sediments (e.g. Guyodo & Valet 1999; Yamazaki 2002) and deep-tow magnetic anomalies (e.g. Gee *et al.* 2000). This feature is unchanged prior to the Matuyama chron (e.g. Kok & Tauxe 1999; Pouliquen *et al.* 2001; Yamazaki & Oda 2002). Thus, the two average VADMs seem to be comparable. Submarine basaltic glass is generally believed not to suffer from deuteric oxidation. Its rock magnetic properties are thought to be different from those of subaerial lavas such as the Kilauea 1960 lava. The coincidence between the two average VADMs suggests a relatively smaller probability of biased palaeointensities in the non-Hawaiian data set. However, it is emphasized that the non-Hawaiian data set still gives an average VADM twice as large as that obtained with the LTD-DHT Shaw data set.

8 CONCLUSIONS

We have performed various rock magnetic measurements and palaeointensity determinations on 0.5–4.6 Ma volcanic rocks collected from the Society Islands, French Polynesia.

(1) Based on the thermomagnetic analyses, low-temperature magnetometry and hysteresis measurements, the main remanence carriers are identified to be titanomagnetites with different Ti contents. Some samples additionally contain a minor amount of Ti-rich titanomaghemites. They are considered to be an admixture of SD (and/or PSD) and MD, and the MD content is not too large. Reflected-light microscopy suggests that many of the present samples contain intermediately high-temperature-oxidized titanomagnetite grains (C3–C4). They are possible candidates for giving anomalously high palaeointensities in Thellier experiments but not in LTD-DHT Shaw experiments.

(2) LTD-DHT Shaw experiments gave 195 out of 361 successful palaeointensity determinations with the quantitative selection criteria. They are independent of the hysteresis properties and not thought to be systematically influenced by the ARM correction.

(3) Thellier experiments were conducted on 40 selected specimens with good thermal stability. Their sister specimens had already given successful results in the LTD-DHT Shaw experiments. The selection criteria admit 18 palaeointensities, but they contain a number of anomalous results. Many of them are characterized by two-segmented Arai diagrams. If we add a criterion of $f \geq 0.50$, 13 results survive and these palaeointensities seem to be improved.

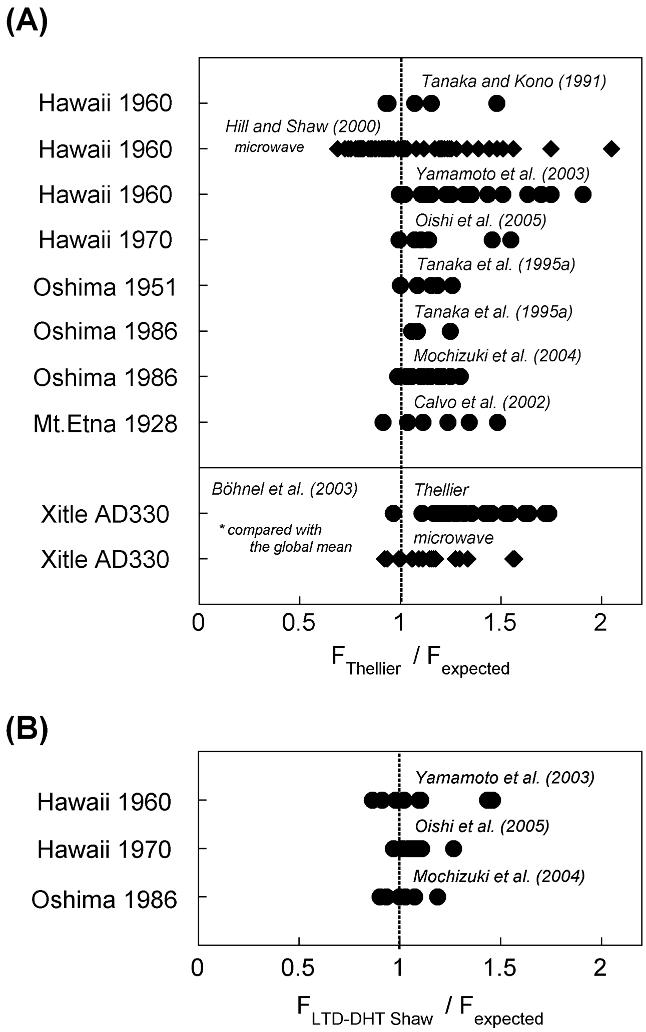

Figure 22. Compilation of the reported palaeointensities from historical lavas. The Thellier and LTD-DHT Shaw data (Tanaka & Kono 1991; Tanaka *et al.* 1995a; Hill & Shaw 2000; Calvo *et al.* 2002; Böhnel *et al.* 2003; Yamamoto *et al.* 2003; Mochizuki *et al.* 2004; Oishi *et al.* 2005) are separately illustrated in (A) and (B), respectively. The abscissa indicates normalized palaeointensities divided by the expected field intensity while the ordinate shows each reference. Note that the microwave Thellier palaeointensities of Hill & Shaw (2000) are adopted from the first slopes when corresponding specimens yielded two-segmented Arai diagrams. The palaeointensities of Böhnel *et al.* (2003) are compared with the contemporaneous global mean of Yang *et al.* (2000).

Discrepancies between the Thellier and the LTD-DHT Shaw palaeointensities are up to about 40 per cent for the sister specimens, which is similar to the results from the historical lavas by Yamamoto *et al.* (2003), Mochizuki *et al.* (2004) and Oishi *et al.* (2005).

(4) The reliability of the successful LTD-DHT Shaw results was further examined from several aspects. Possible low-temperature oxidation and inapplicability of the ARM corrections were suggested for 40 specimens. These may be sources of biased palaeointensities. Some part of the successful results also showed upward convexity in the NRM–TRM1* diagrams, which may have equivalent qualities to Thellier palaeointensity results with concave Arai diagrams. According to the growing consensus on analyses of Thellier results, it seems better not to use such LTD-DHT Shaw palaeointensities. This convexity could be evaluated by ΔAIC. Although it is difficult to define an exact threshold ΔAIC, we temporarily take a threshold value of 15 in this study. There are 49 results with $\Delta\mathrm{AIC} > 15$ among the present successful results.

(5) We can pick up 24 reliable site-mean palaeointensities from the newly obtained LTD-DHT Shaw data set. They give the average VADM of $(3.64 \pm 2.10) \times 10^{22}$ A m^2 for the last 5 Myr. This is nearly half of the mean of the 0–5 Ma Thellier data selected from the latest palaeointensity database [$(7.46 \pm 3.10) \times 10^{22}$ A m^2, $N = 458$]. The large discrepancy between the two averages originates from the difference in the palaeointensity techniques.

(6) We consider that the average VADM by the present LTD-DHT Shaw data set is more appropriate for the mean of the last 5 Myr. This is because the Thellier method occasionally gives overestimated palaeointensities as high as 200 per cent of the true value while the LTD-DHT Shaw method does not. In particular, overestimated palaeointensities might be accumulated in the Hawaiian data set. Many results in this data set might suffer from NRMs of non-TRM origin. The newly determined LTD-DHT Shaw palaeointensities indicate that the present dipole moment ($\sim 8 \times 10^{22}$ A m^2) is about twice the time average for the last 5 Myr. The characteristics of the present field may not be typical of the geomagnetic field. We have to be careful when extending the characteristics of the present-day field to the ancient field.

ACKNOWLEDGMENTS

The authors thank Koichiro Shimura, Tetsu Kogiso, Kozo Uto, Hirokuni Oda, Toshitsugu Yamazaki, Hans G. Barsczus and Eiichi Kikawa for their intensive work in collecting samples. T. Yamazaki and H. Oda are also grateful for their critical reading of the manuscript. We also appreciate insightful comments by Yongjae Yu and Avto Goguitchaichvili. Fruitful discussions with D. J. Dunlop and Ö. Özdemir are also acknowledged. This study was funded by the 'Super Plume' project by the Science and Technology Agency of Japan. Y. Yamamoto is supported by Research Fellowships of the Japan Society for the Promotion of Science for Young Scientists.

REFERENCES

Akaike, H., 1980. Likelihood and the Bayes procedure, in *Bayesian Statistics*, pp. 143–166, University Press, Valencia.

Alva-Valdivia, L.M., Goguitchaichvili, A. & Urrutia-Fucugauchi, J., 2001. Further constraints for the Plio-Pleistocene geomagnetic field strength: new results from the Los Tuxtlas volcanic field (Mexico), *Earth Planets Space,* **53,** 873–881.

Bando, Y., Kiyama, M., Yamamoto, N., Takada, T., Shinjo, T. & Takaki, H., 1965. Magnetic properties of $\alpha - Fe_2O_3$ fine particles, *J. Phys. Soc. Japan,* **20,** 2086.

Biggin, A.J. & Thomas, D.N., 2003a. The application of acceptance criteria to results of Thellier palaeointensity experiments performed on samples with pseudo-single-domain-like characteristics, *Phys. Earth planet. Int.,* **138,** 279–287.

Biggin, A.J. & Thomas, D.N., 2003b. Analysis of long-term variations in the geomagnetic poloidal field intensity and evaluation of their relationship with global geodynamics, *Geophys. J. Int.,* **152,** 392–415.

Blais, S., Guille, G., Maury, R.C., Guillou, H., Miau, D. & Cotten, J., 1997. Geology and petrology of Raiatea Island (Society Islands, French Polynesia), *C. R. Acad. Sci. Paris, Ser. IIa,* **324,** 435–442.

Blais, S., Guille, G., Guillou, H., Chauvel, C., Maury, R.C. & Caroff, M., 2000. Geology, geochemistry and geochronology of Borabora island (Society Islands, French Polynesia), *C. R. Acad. Sci. Paris, Earth Planet. Sci.,* **331,** 579–585.

Bogue, S.W., 2001. Geomagnetic field behaviour before and after the Kauai reverse-normal polarity transition, *J. geophys. Res.,* **106,** 447–461.

Böhnel, H., Biggin, A.J., Walton, D., Shaw, J. & Share, J.A., 2003. Microwave palaeointensities from a recent Mexican lava flow, baked sediments and reheated pottery, *Earth planet. Sci. Lett.,* **214,** 221–236.

Borradaile, G.J., Lucas, K. & Middleton, R.S., 2004. Low-temperature demagnetization isolates stable magnetic vector components in magnetite-bearing diabase, *Geophys. J. Int.,* **157,** 526–536.

Calvo, M., Prevot, M., Perrin, M. & Riisager, J., 2002. Investigating the reasons for the failure of paleointensity experiments: a study on historic lava flows from Mt Etna (Italy), *Geophys. J. Int.,* **149,** 44–63.

Chauvin, A., Roperch, P. & Duncan, R.A., 1990. Records of geomagnetic reversals from volcanic islands of French Polynesia 2. Paleomagnetic study of flow sequence (1.2–0.6 Ma) from the Island of Tahiti and discussion of reversal models, *J. geophys. Res.,* **95,** 2727–2752.

Coe, R.S., 1967. Paleointensities of the Earth's magnetic field determined from Tertiary and Quaternary rocks, *J. geophys. Res.,* **72,** 3247–3262.

Coe, R.S., Gromme, S. & Mankinen, E.A., 1978. Geomagnetic paleointensities from radiocarbon-dated lava flows on Hawaii and the question of the Pacific nondipole low, *J. geophys. Res.,* **83,** 1740–1756.

Day, R., Fuller, M. & Schmidt, V.A., 1977. Hysteresis properties of titanomagnetites: grain-size and compositional dependence, *Phys. Earth planet. Int.,* **13,** 260–267.

Diraison, C., 1991. Le volcanisme aerien des archipels Polynesiens de la Societe, des Marquises et des Australes-Cook, *PhD thesis*, Universite de Bretagne Occidentale, France.

Duncan, R.A., 1975. Paleosecular variation at the Society Islands, French Polynesia, *Geophys. J. R. astr. Soc.,* **41,** 245–254.

Duncan, R.A. & McDougall, I., 1976. Linear volcanism in French Polynesia, *J. Volc. Geotherm. Res.,* **1,** 197–227.

Duncan, R.A., Fisk, M.R., White, W.M. & Nielsen, R.L., 1994. Tahiti: geochemical evolution of a French Polynesian volcano, *J. geophys. Res.,* **99,** 24 341–24 357.

Dunlop, D.J., 2002. Theory and application of the Day plot (Mrs/Ms versus Hcr/Hc) 1. Theoretical curves and tests using titanomagnetite data, *J. geophys. Res.,* **107,** 3, doi:10.1029/2001JB000486.

Dunlop, D.J. & Özdemir, Ö., 1997. *Rock Magnetism: Fundamentals and Frontiers,* Cambridge University Press, Cambridge.

Dymond, J., 1975. K–Ar ages of Tahiti and Moorea, Society Islands, and implications for the hot-spot model, *Geology,* **3,** 236–240.

Gee, J., Cande, S., Hildebrand, J., Donnelly, K. & Parker, R., 2000. Geomagnetic intensity variations over the past 780 kyr obtained from near-seafloor magnetic anomalies, *Nature,* **408,** 827–832.

Goguitchaichvili, A., Urrutia-Fucugauch, J., Alva-Valdivia, L. M., Morales, J., Riisager, J. & Riisager, P., 2004. Long-term variation of geomagnetic field strength: a cautionary note, *EOS, Trans. Am. geophys. Un.,* **85,** 209–212.

Gripp, A.E. & Gordon, R.G., 1990. Current plate velocities relative to the hotspots incorporating the NUVEL-1 global plate motion model, *Geophys. Res. Lett.,* **17,** 1109–1112.

Grommé, C.S., Wright, T.L. & Peak, D.L., 1969. Magnetic properties and oxidation of iron-titanium oxide minerals in Alae and Makaopulhi lava lakes, Hawaii, *J. geophys. Res.,* **74,** 5277–5293.

Gubbins, D. & Kelly, P., 1993. Persistent patterns in the geomagnetic field over the last 2.5 Myr, *Nature,* **365,** 829–832.

Guillou, H., Blais, S., Guille, G., Maury, R.C., Le Dez, A. & Cotten, J., 1998. Age (K-Ar) and duration of the subaerial build-up of Moorea, Raiatea and Maupiti (Society Islands, French Polynesia), *Géol. France,* **3,** 29–36.

Guyodo, Y. & Valet, J.P., 1999. Global changes in intensity of the Earth's magnetic field during the past 800 kyr, *Nature,* **36,** 234–238.

Haggerty, S.E., 1991. Oxide textures—a mini-atlas. Oxide minerals: petrologic and magnetic significance, *Rev. Mineral.,* **25,** 129–219.

Hatakeyama, T. & Kono, M., 2002. Geomagnetic field model for the last 5 My: time-averaged field and secular variation, *Phys. Earth planet. Inter.,* **133,** 181–215.

Heider, F., Dunlop, D.J. & Soffel, H.C., 1992. Low-temperature and alternating field demagnetization of saturation remanence and thermoremanence in magnetite grains (0.037 μm to 5 mm), *J. geophys. Res.,* **97,** 9371–9381.

Heller, R., Merrill, R.T. & McFadden, P.L., 2002. The variation of intensity of earths magnetic field with time, *Phys. Earth planet. Inter.,* **131,** 237–249.

Hill, M.J. & Shaw, J., 2000. Magnetic field intensity study of the 1960 Kilauea lava flow, Hawaii, using the microwave paleointensity technique, *Geophys. J. Int.,* **142,** 487–504.

Johnson, C. & Constable, C.G., 1995. The time averaged field as recorded by lava flows over the past 5 Myr, *Geophys. J. Int.,* **122,** 489–519.

Johnson, C. & Constable, C.G., 1997. The time averaged geomagnetic field: global and regional biases for 0–5 Ma, *Geophys. J. Int.,* **131,** 643–666.

Juarez, M.T. & Tauxe, L., 2000. The intensity of the time-averaged geomagnetic field: the last 5 Myr, *Earth planet. Sci. Lett.,* **175,** 169–180.

Kelly, P. & Gubbins, D., 1997. The geomagnetic field over the past 5 million years, *Geophys. J. Int.,* **128,** 315–330.

Kogiso, T., Tatsumi, Y., Shimoda, G. & Barsczus, H.G., 1997. High mu (HIMU) ocean island basalts in southern Polynesia: new evidence for whole mantle scale recycling of subducted oceanic crust, *J. geophys. Res.,* **102,** 8085–8103.

Kok, Y.S. & Tauxe, L., 1999. A relative geomagnetic paleointensity stack from Ontong-Java Plateau sediments for the Matuyama, *J. geophys. Res.,* **104,** 25 401–25 413.

Kono, M., Kitagawa, H. & Tanaka, H., 1997. Use of automatic spinner magnetometer–AF demagnetizer system for magnetostratigraphy and paleosecular variation studies (abstract), in *Proc. 8th Scientific Assembly IAGA, 1997 Abstract book, pp. 66, Uppsala*.

Kono, M., Hamano, Y., Nishitani, T. & Tosha, T., 1984. A new spinner magnetometer: principles and techniques, *Geophys. J. R. astr. Soc.,* **67,** 217–227.

Kono, M., Tanaka, H. & Tsunakawa, H., 2000. Spherical harmonic analysis of paleomagnetic data: the case of linear mapping, *J. geophys. Res.,* **105,** 5817–5833.

Kontny, A., Vahle, C. & de Wall, H., 2003. Characteristic magnetic behavior of subaerial and submarine lava units from the Hawaiian Scientific Drilling Project (HSDP-2) *Geochem. Geophys. Geosyst.,* **4**(2), 8703, doi:10.1029/2002GC000304.

Laj, C. & Kissel, C., 1999. Geomagnetic field intensity at Hawaii for the last 420 kyr from the Hawaii Scientific Drilling Project core, Big Island, Hawaii, *J. geophys. Res.,* **104,** 15 317–15 338.

Laj, C., Szeremeta, N., Kissel, C. & Guillou, H., 2000. Geomagnetic paleointensities at Hawaii between 3.9 and 2.1 Ma: preliminary results, *Earth planet. Sci. Lett.,* **179,** 191–204.

Leonhardt, R., Matzka, J. & Menor, E.A., 2003. Absolute paleointensities and paleodirections of Miocene and Pliocene lavas from Fernando de Noronha, Brazil, *Phys. Earth planet. Inter.,* **139,** 285–303.

McFadden, P.L. & McElhinny, M.W., 1982. Variations in the geomagnetic dipole. 2. Statistical analysis of VDMs for the past 5 million years, *J. Geomag. Geoelectr.,* **34,** 163–189.

McFadden, P.L. & Reid, A.B., 1982. Analysis of paleomagnetic inclination data, *Geophys. J. R. astr. Soc.,* **69,** 307–319.

Mochizuki, N., Tsunakawa, H., Oishi, Y., Wakai, S., Wakabayashi, K. & Yamamoto, Y., 2004. Palaeointensity study of the Oshima 1986 lava in Japan: implications for the reliability of the Thellier and LTD-DHT Shaw methods, *Phys. Earth planet. Inter.,* **146,** 395–416.

Oishi, Y., Tsunakawa, H., Mochizuki, N., Yamamoto, Y., Wakabayashi, K. & Shibuya, H., 2005. Validity of the LTD-DHT Shaw and Thellier paleointensity methods: a case study of the Kilauea 1970 lava, *Phys. Earth planet. Inter.,* **149,** 243–257.

Ozima, M., Ozima, M. & Akimoto, S., 1964. Low temperature characteristics of remanent magnetization of magnetite—self-reversal and recovery phenomena of remanent magnetization, *J. Geomag. Geoelectr.,* **16,** 165–177.

Pan, Y., Shaw, J., Zhu, R. & Hill, M.J., 2002. Experimental reassessment of the Shaw paleointensity method using laboratory-induced thermal remanent magnetization, *J. geophys. Res.,* **107,** doi:10.1029/2001JB000620.

Pan, Y., Shaw, J., Zhu, R. & Hill, M.J., 2003. Reply to comment by Y. Yamamoto on 'Experimental reassessment of the Shaw paleointensity method using laboratory-induced thermal remanent magnetization', *J. geophys. Res.,* **108,** 2279, doi:10.1029/2002JB002355, 2003.

Perrin, M. & Schnepp, E., 2004. IAGA paleointensity database: distribution and quality of the data set, *Phys. Earth planet. Inter.,* **147,** 255–267.

Perrin, M., Schnepp, E. & Shcherbakov, V., 1998. Update of the paleointensity database, *EOS, Trans. Am. geophys. Un.,* **79,** 198.

Pouliquen, G., Gallet, Y., Patriat, P., Dyment, J. & Tamura, C., 2001. A geomagnetic record over the last 3.5 million years from deep-tow magnetic anomaly profiles across the Central Indian Ridge, *J. geophys. Res.,* **106,** 10 941–10 960.

Riisager, P. & Riisager, J., 2001. Detecting multidomain magnetic grains in Thellier palaeointensity experiments, *Phys. Earth planet. Int.,* **125,** 111–117.

Riisager, J., Riisager, P., Zhao, X., Coe, R.S. & Pedersen, A.K., 2004. Paleointensity during a chron C26r excursion recorded in west Greenland lava flows, *J. geophys. Res.,* **109,** B04107, doi:10.1029/2003JB002887.

Rolph, T.C. & Shaw, J., 1985. A new method of paleofield magnitude correction for thermally altered samples and its application to Lower Carboniferous lavas, *Geophys. J. R. astr. Soc.,* **80,** 773–781.

Roperch, P. & Duncan, R.A., 1990. Records of geomagnetic reversals from volcanic islands of French Polynesia 1. Paleomagnetic study of a polarity transition in a lava sequence from the island of Huahine, *J. geophys. Res.,* **95,** 2713–2726.

Selkin, P.A. & Tauxe, L., 2000. Long-term variations in paleointensity, *Phil. Trans. R. Soc. Lond.,* A. **358,** 1065–1088.

Senanayake, W.E., McElhinny, M.W. & McFadden, P.L., 1982. Comparison between the Thelliers' and Shaw's paleointensity methods using basalts less than 5 million years old, *J. Geomag. Geoelectr.,* **34,** 141–161.

Shaw, J., 1974. A new method of determining the magnitude of the paleomagnetic field. Application to five historic lavas and five archaeological samples, *Geophys. J. R. astr. Soc.,* **76,** 637–651.

Shcherbakova, V.V., Shcerbakov, V.P. & Heider, F., 2000. Properties of partial thermoremanent magnetization in pseudosingle domain and multidomain magnetite grains, *J. geophys. Res.,* **105,** 767–781.

Singer, B.S., Hoffman, K.A., Chauvin, A., Coe, R.S. & Pringle, M.S., 1999. Dating transitionally magnetized lavas of the late Matuyama Chron: toward a new $^{40}Ar/^{39}Ar$ timescale of reversals and events, *J. geophys. Res.,* **104,** 679–693.

Singer, B.S., Relle, M.K., Hoffman, K.A., Battle, A., Laj, C., Guillou, H. & Carracedo, J.C., 2002. Ar/Ar ages from transitionally magnetized lavas on La Palma, Canary Islands, and the geomagnetic instability timescale, *J. geophys. Res.,* **107,** 2307, doi:10.1029/2001JB001613.

Smirnov, A.V. & Tarduno, J.A., 2003. Magnetic hysteresis monitoring of Cretaceous submarine basaltic glass during Thellier paleointensity experiments: evidence for alteration and attendant low field bias, *Earth planet. Sci., Lett.*, **206,** 571–585.

Tanaka, H., 1999. Circular asymmetry of the paleomagnetic directions observed at low latitude volcanic sites, *Earth Planets Space,* **51,** 1279–1286.

Tanaka, H. & Kobayashi, T., 2003. Paleomagnetism of the late Quaternary Ontake Volcano, Japan: directions, intensities, and excursions, *Earth Planets Space,* **55,** 189–202.

Tanaka, H. & Kono, M., 1991. Preliminary results and reliability of paleointensity studies on historical and ^{14}C dated Hawaiian lavas, *J. Geomag. Geoelectr.,* **43,** 375–388.

Tanaka, H. & Kono, M., 1994. Paleointensity database provides new resource, *EOS, Trans. Am. geophys. Un.,* **75,** 498.

Tanaka, H., Kono, M. & Kaneko, S., 1995a. Paleosecular variation of direction and intensity from two Pliocene–Pleistocene lava sections in southwestern Iceland, *J. Geomag. Geoelectr.,* **47,** 89–102.

Tanaka, H., Kono, M. & Uchimura, H., 1995b. Some global features of paleointensity in geological time, *Geophys. J. Int.,* **120,** 97–102.

Tauxe, L. & Love, J.J., 2003. Paleointensity in Hawaiian Scientific Drilling Project hole (HSDP2): results from submarine basaltic glass, *Geochem., Geophys., Geosyst.,* **4,** 8702, doi:10.1029/2001GC000276.

Thellier, E. & Thellier, O., 1959. Sur l'intensite du champ magnetique terrestre dans le passe historique et geologique, *Ann. Geophys.,* **15,** 285–376.

Tsunakawa, H. & Shaw, J., 1994. The Shaw method of paleointensity determinations and its application to recent volcanic rocks, *Geophys. J. Int.,* **118,** 781–787.

Tsunakawa, H., Shimura, K. & Yamamoto, Y., 1997. Application of double heating technique of the Shaw method to the Brunhes epoch volcanic rocks (abstract), in *Proc. 8th Scientific Assembly IAGA, 1997 Abstract book, pp. 85, Uppsala*.

Uto, K., Yamamoto, Y., Sudo, M., Uchiumi, S., Ishizuka, O., Kogiso, T. & Tsunakawa, H., submitted, K-Ar ages and magnetostratigraphy of the Society Islands, French Polynesia, *Earth Planets Space*.

Valet, J.P., 2003. Time variations in geomagnetic intensity, *Rev. Geophys.,* **41,** 1004, doi:10.1029/2001RG000104.

White, W.M. & Duncan, R.A., 1996. Geochemistry and Geochronology of the Society Islands: new evidence for deep mantle recycling, in *Earth Processes: Reading the Isotopic Code,* American Geophysical Union Geophysical Monograph 95, pp. 183–206, eds Basu, A. & Hart, S., American Geophysical Union, Washington, DC.

Wilson, R.L. & Watkins, N.D., 1967. Correlation of petrology and natural magnetic polarity in Columbia Plateau basalts, *Geophys. J. R. astr. Soc.,* **12,** 405–424.

Yamamoto, Y. *et al.*, 2002. Geomagnetic paleosecular variation for the past 5 Ma in the Society Islands, French Polynesia, *Earth Planets Space,* **54,** 797–802.

Yamamoto, Y., Tsunakawa, H. & Shibuya, H., 2003. Paleointensity study of the Hawaiian 1960 lava: implications for possible causes of erroneously high intensities, *Geophys. J. Int.,* **153,** 263–276.

Yamazaki T., 2002. Long-term secular variation in geomagnetic field inclination during Brunhes Chron recorded in sediment cores from Ontong-Java Plateau, *Phys. Earth planet. Inter.,* **133,** 57–72.

Yamazaki, T. & Oda, H., 2002. Orbital influence on earth's magnetic field: 100,000-year periodicity in inclination, *Science,* **295,** 2435–2438.

Yamazaki, T., Abdeldayem, A.L. & Ikehara, K., 2003. Rock-magnetic changes with reduction diagenesis in Japan Sea sediments and preservation of geomagnetic secular variation in inclination during the last 30,000 years, *Earth Planets Space,* **53,** 327–340.

Yang, S., Odah, H. & Shaw, J., 2000. Variations in the geomagnetic dipole moment over the last 12 000 years, *Geophys. J. Int.,* **140,** 158–162.

Yu, Y., Tauxe, L. & Genevey, A., 2004. Toward an optimal geomagnetic field intensity determination technique, *Geochem. Geophys. Geosyst.,* **5,** Q02H07, doi:10.1029/2003GC000630.